Project Report
CMT-57

Measured Spectral Extent of L- and X-Band Radar Reflections from Wind-Blown Trees

J.B. Billingsley
J.F. Larrabee

6 February 1987

Lincoln Laboratory
MASSACHUSETTS INSTITUTE OF TECHNOLOGY
LEXINGTON, MASSACHUSETTS

Prepared for the Defense Advanced Research Projects Agency and the Department of the Air Force under Electronic Systems Division Contract F19628-85-C-0002.

The work reported in this document was performed at Lincoln Laboratory, a center for research operated by Massachusetts Institute of Technology. This work was sponsored by the Defense Advanced Research Projects Agency and the Department of the Air Force under Air Force Contract F19628-85-C-0002 (ARPA Order 3724).

This technical report has been reviewed and is approved for publication.

FOR THE COMMANDER

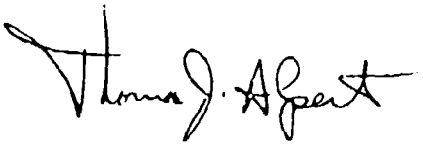

Thomas J. Alpert, Major, USAF
Chief, ESD Lincoln Laboratory Project Office

MASSACHUSETTS INSTITUTE OF TECHNOLOGY
LINCOLN LABORATORY

MEASURED SPECTRAL EXTENT OF L- AND X-BAND RADAR REFLECTIONS FROM WIND-BLOWN TREES

J.B. BILLINGSLEY
Group 45

J.F. LARRABEE
Ford Aerospace and Communications Corporation

PROJECT REPORT CMT-57

6 FEBRUARY 1987

LEXINGTON MASSACHUSETTS

ABSTRACT

Measurements of the spectral content of L- and X-band radar reflections from several resolution cells containing wind-blown trees are examined under a wide variety of typical wind conditions. Most of the discernible energy (i.e., within 60 dB of the peak zero-Doppler level) occurs in the spectra at Doppler velocities usually less than 1.0 m/s, or at most 2.0 m/s on very windy days. The rates of decay of energy with increasing Doppler velocity in the tails of the spectral distributions at spectral off-sets well removed from zero often appear to be approximately exponential. Estimates of rates of exponential decay in the spectral tails as a function of windspeed are provided in three regimes of windspeed.

TABLE OF CONTENTS

LIST OF FIGURES

LIST OF FIGURES (Continued)

LIST OF TABLES

1. INTRODUCTION

During the period of time from late 1984 to mid-1985, radar ground reflections from hilly tree-covered terrain were measured on a nominal once-a-week basis from Katahdin Hill in eastern Massachusetts. These reflections were measured as relatively long (e.g., 5 min) pulse sequences on specific resolution cells. The purpose of this measurement program was to establish a multi-frequency data base from which temporal and seasonal variations of ground clutter could be examined.

In this report, we examine the spectral content of reflections from wind-blown tree foliage in selected cells from this data base, over a wide variety of wind conditions. That is, wind-induced motion of the trees causes Doppler-shifted energy in the power spectra of the received temporal signals. We illustrate here the sorts of spectra that result from typical wind conditions as they routinely vary with weather and season. We are interested in how wide these spectra usually become at the limits at which we can easily discern energy in their tails, and the approximate rates of decay of energy with increasing Doppler velocity in these tails well removed from zero-Doppler velocity. Most of the spectral data presented are at L-band, although a few examples of X-band spectra are also presented. Two of the X-band examples are from sites other than Katahdin Hill. Some brief multifrequency information on temporal autocorrelation properties of radar returns from wind-blown trees is included to complement the spectral data.

2. CLUTTER MEASUREMENTS AT KATAHDIN HILL

For the purpose of obtaining a set of temporal ground clutter measurements, our mobile five-frequency ground clutter measurement radar was set up on Katahdin Hill at Lincoln Laboratory. Lincoln Laboratory is located on Hanscom Air Force Base in Lexington, Massachusetts. We refer to this radar as Phase One, to distinguish it from an earlier, X-band only, clutter measurement radar which we call Phase Zero. The Phase One radar is a modern, computer controlled, pulsed instrumentation radar with high data rate recording capability (i.e., linear receiver with 13 bit A/D converters in I and Q channels), and maintains coherence and stability sufficient for 60 dB two-pulse-canceler clutter attenuation in post-processing. The Phase One antenna beams are fixed at zero degrees in elevation, and are steerable in azimuth. The Phase One waveform is uncoded. A photograph of the Phase One equipment set up on Katahdin Hill is shown in Figure 1. Important Phase One measurement parameters are shown in Table 1.

In these temporal measurements, long time dwells of backscatter data were recorded from a number of contiguous range gates in a fixed azimuth beam position looking out to the southwest (i.e., 235°) from Katahdin Hill across hilly wooded terrain in the suburban town of Lincoln. Lincoln is located 12 miles northwest of Boston. The Phase One L-band antenna mast height on Katahdin Hill was 94'3". We refer to each long time dwell of contiguous pulses as a data collection experiment. Experiments were usually collected one day per week from March through June, 1985, and at less frequent intervals before (i.e., late November/early December, 1984) and after (i.e., early August 1985) this time. In much of the L-band data discussed in this report, experiments consisted of 30,720 contiguous pulses

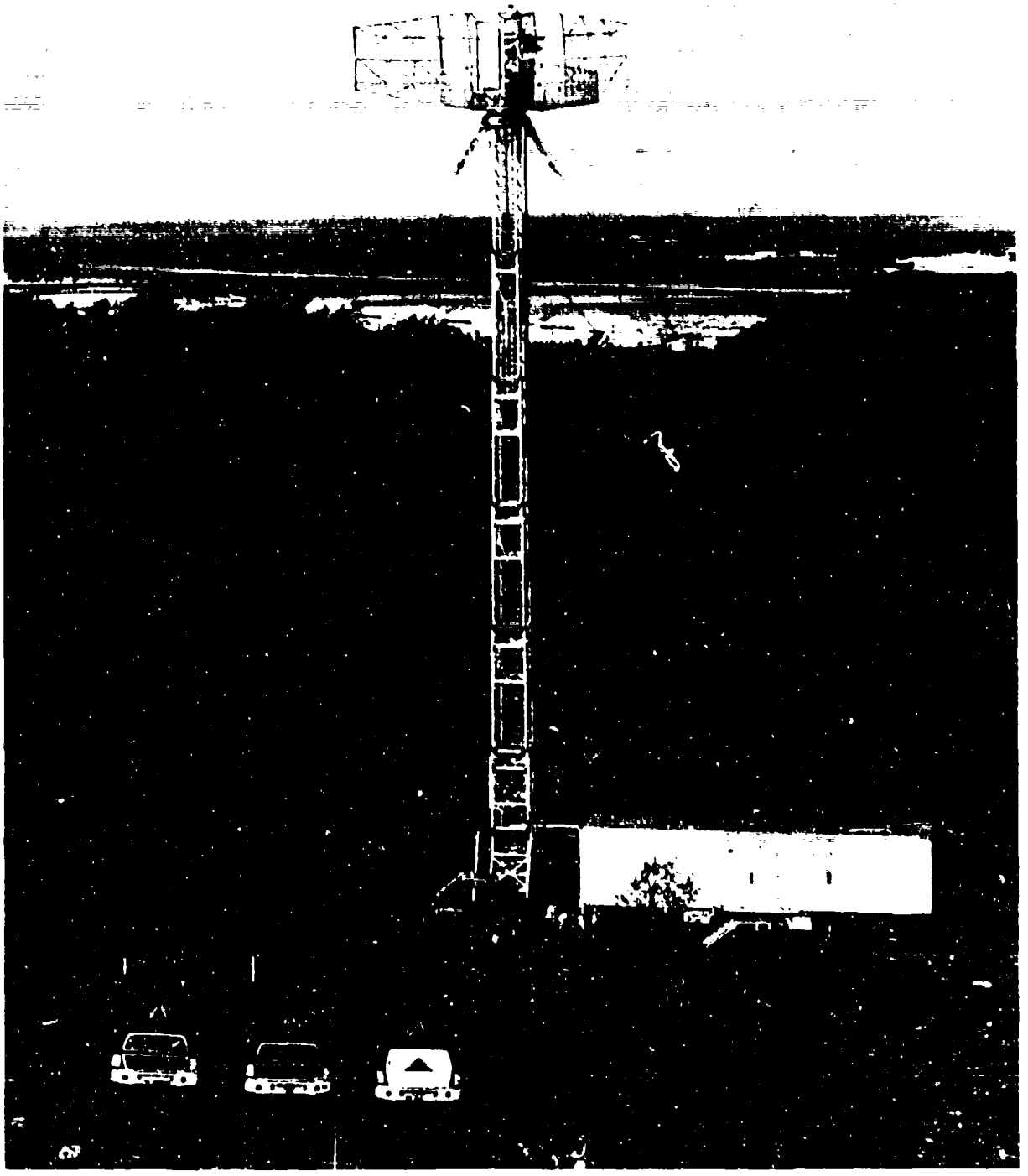

FIG. 1. PHASE ONE EQUIPMENT AT KATAHDIN HILL, MASS. Camera viewing direction is northwest. Antenna tower is erected to 95 feet.

TABLE 1

PHASE ONE SYSTEM PARAMETERS*

FREQUENCY					
BAND	VHF	UHF	L-BAND	S-BAND	X-BAND
MHz	169	435	1230	3230	9100
POLARIZATION	VV OR HH				
RESOLUTION					
RANGE	15, 36, 150m				
AZIMUTH	13°	5°	3°	1°	1°
ELEVATION BEAMWIDTH	39°	15°	10°	4°	3°
PEAK POWER	10 kW (50 kW AT X-BAND)				
10 km SENSITIVITY	$\sigma^{\circ}F^{4}$ = -60 dB				
A/D SAMPLING RATE	1, 2, 5, OR 10 MHz				
A/D NUMBER OF BITS	13				
DATA RECORDING RATE	625K BYTES/SEC				
OUTPUT DATA	I and Q				
RCS ACCURACY	2 dB rms				
MINIMUM RANGE	1 km				
DYNAMIC RANGE					
INSTANTANEOUS	60 dB				
ATTENUATOR CONTROLLED	40 dB				
DATA COLLECTION MODES	BEAM SCAN PARKED BEAM BEAM STEP				
AZIMUTH SCAN RATE	0 TO 3 DEG/SEC				
TOWER HEIGHT	95'				

*The specific frequencies and tower height employed at Katahdin Hill are listed here; the other measurement parameters were used at all sites.

collected over a 5 minute interval at a 10 ms pulse repetition interval. Occasionally, the data were collected faster (see Table 2, p. 24). On each data collection day, the recording sequence involved collecting long time dwell experiments both from forested clutter cells at 235° azimuth, as well as from a cell at 68.5° azimuth containing a large water tower as a system reference target, across our five Phase One frequency bands. The period of time over which we conducted these experiments spanned winter, spring, and summer seasons. During this period in eastern Massachusetts, deciduous trees begin to show the emergence of new leaves in early May, and are essentially fully leaved out by the end of May.

Phase One L-band range resolution may be selected to be either 150 m (i.e., 1.0 μs) or 15 m (i.e., 0.1 μs). In each experiment with range resolution set to 150 m, we recorded data from 16 contiguous range gates located from 1.5 km to 3.9 km in range from Phase One. In each experiment with range resolution set to 15 m, we recorded data from 76 contiguous range gates located from 2.0 km to 3.1 km. For the results presented in this report, we emphasize 15 m data taken from the range gate between 2756 m and 2771 m, and 150 m data taken from the range gate between 2786 and 2936 m. Both of these range gates lie on the south side of Jupiter Ridge, where the terrain abruptly drops 100 feet in elevation over a distance of about 500 feet (i.e., approximately 11° terrain slope). This south face of the ridge is directly visible from Phase One at oblique incidence. Thus Jupiter Ridge produced strong ground clutter for Phase One, at L-band σ° levels of between -17 and -23 dB, where σ° represents radar cross section per unit area in the resolution cell. Jupiter Ridge is tree covered, primarily with mixed deciduous trees (e.g., oak, maple, beech, birch, locust), but with occasional pine and cedar as well, all to an approximate height

of 60 or 70 feet. Jupiter Ridge is settled with occasional suburban houses located within the trees and back from the front of the ridge. However, at the low depression angle of about 0.65° at which the ridge was viewed from the Phase One antenna, it was essentially solid tree foliage that was under direct illumination along the relatively steeply dropping front face of the ridge. Three photographs of the terrain along Jupiter Ridge are shown in Figure 2. For the computations of clutter spectra presented in this report, we carefully selected cells from along the ridge with strong signal-to-noise ratio, and in which the measured temporally varying clutter amplitude statistics were close to Rayleigh distributed, to ensure that only tree foliage was under illumination and that there were no strong stationary discrete scatterers in the cells as would be indicated by strongly Ricean amplitude statistics.

Our focus of interest is in the sorts of general spectral variation that can occur under wind conditions broadly characterizable as strong (i.e., "windy"), moderate (i.e., "breezy"), or light (i.e., "light air"). We took our measure of wind conditions from the weather information continuously being broadcast from Hanscom airfield, 1-1/2 miles from our principal clutter cells. We believe this information to be a reasonable indication of general free-space wind conditions in the neighborhood in which we conducted our measurements. For every experiment, we recorded mean windspeed and wind direction as they were being broadcast at that time, as well as gust velocity when conditions were gusty. When possible, we attempted to select a relatively windy day during the week as our clutter measurement day.

Figure 3 shows a 1:40,000 scale aerial photograph of the terrain surroundings in which we conducted our Katahdin Hill measurements. The Phase One position on Katahdin Hill, Jupiter Ridge, and Hanscom airfield are all indicated in this air photo, as are Route 128, Route 2, and Lincoln Laboratory.

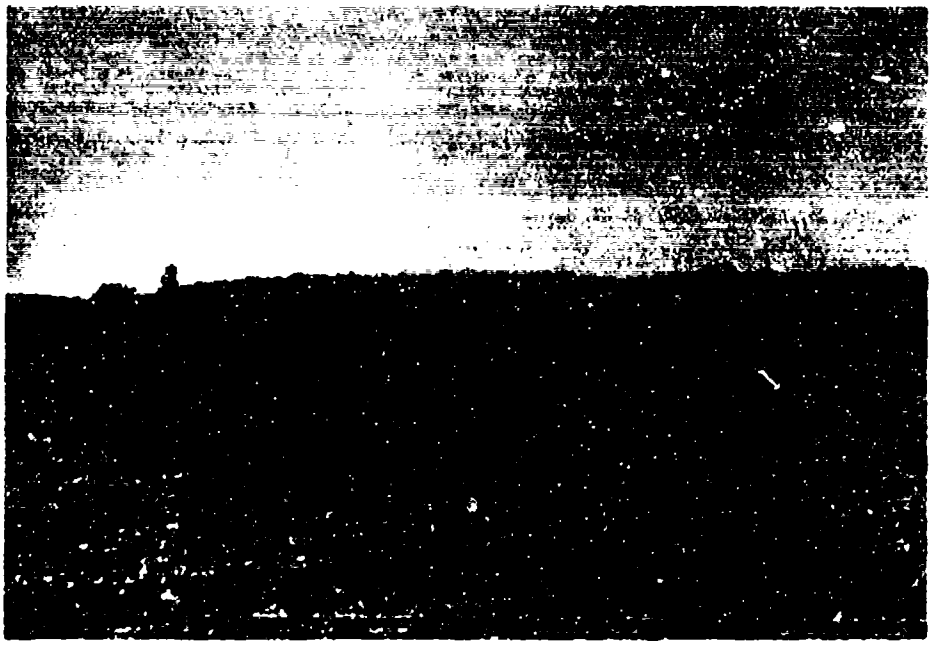

a) Looking southwest up the side of Jupiter Ridge from across a plowed field

FIG. 2. PHOTOGRAPHS OF JUPITER RIDGE TERRAIN.

Continued...

b) Looking upslope from the bottom of Jupiter Ridge

FIG. 2. PHOTOGRAPHS OF JUPITER RIDGE TERRAIN.

Continued...

c) Trees atop Jupiter Ridge

FIG. 2. PHOTOGRAPHS OF JUPITER RIDGE TERRAIN.

Concluded.

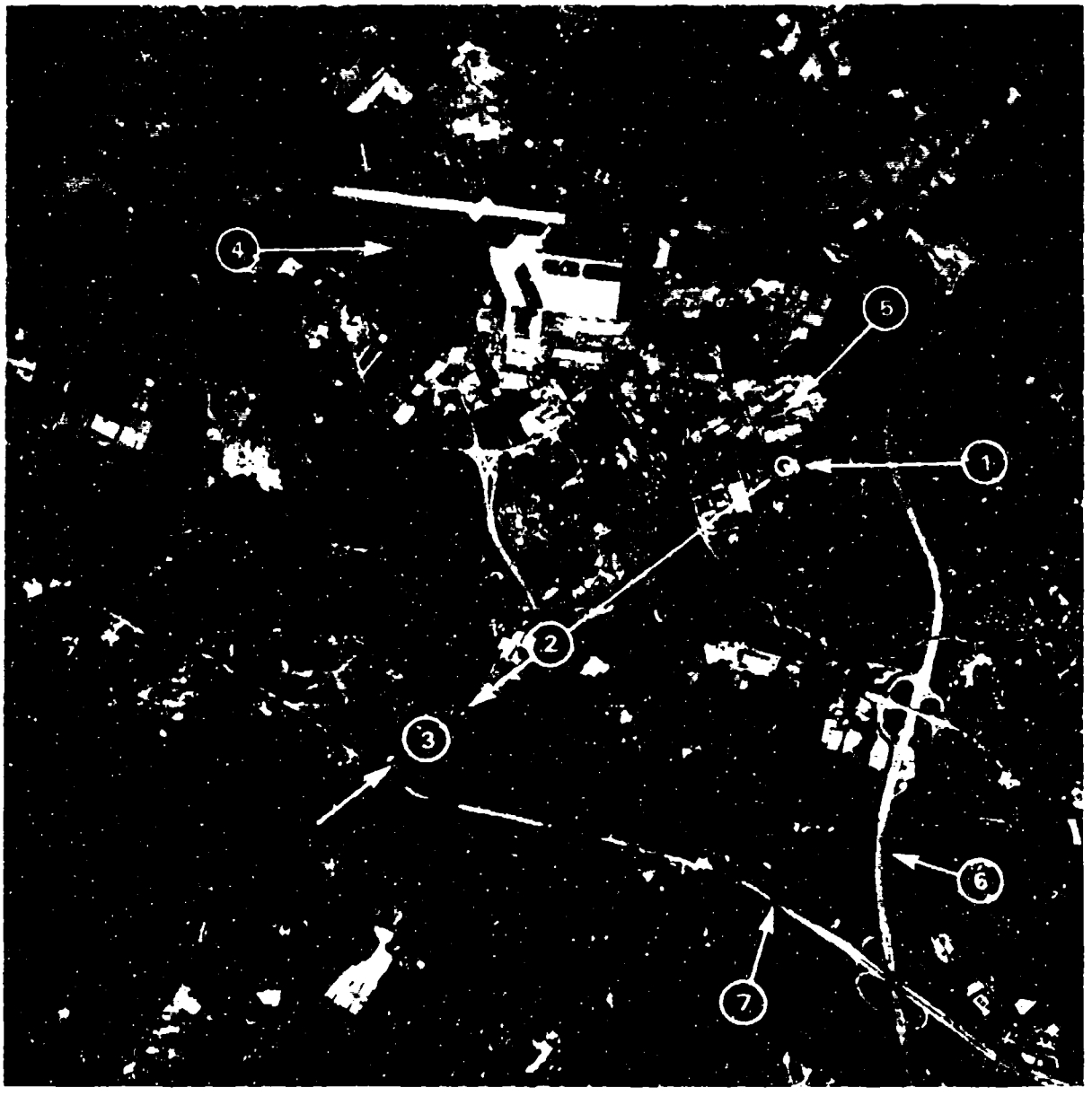

FIG. 3. AERIAL PHOTOGRAPH OF KATAHDIN HILL MEASUREMENT AREA. Scale = 1:40,000. The numbered circles are: (1) Phase One position on Katahdin Hill; (2) 235° azimuth from Phase One; (3) Jupiter Ridge; (4) Hanscom Field; (5) Lincoln Laboratory; (6) Route 128; and (7) Route 2.

3. CLUTTER SPECTRA

Prior to the Katahdin Hill measurement program, which provided the L-band spectral information which is the main subject of interest in this present report, the Phase One equipment was involved in making measurements at many sites, primarily in western Canada. Early spectral investigations of these data were conducted at X-band. In Section 3.1, we present some of these early spectral X-band data from two different Canadian sites, Neepawa, Manitoba, and Woking, Alberta, as well as more recent X-band spectral data from Katahdin Hill. This allows us to bring into consideration from the outset and show how our thinking evolved as we observed in these early results the effect of windspeed on spectral width and approximate exponential decay of spectral tails. It also allows us to broaden our Katahdin Hill L-band data to another frequency and other sites. The results suggest that there is no strong frequency dependency in power spectra from wind-blown foliage between L-band and X-band (beyond the basic Doppler dependency which is linear with frequency), and that the Katahdin Hill data are not particularly specific to site or tree type. In Sections 3.2 and 3.3 we go on and discuss our much more comprehensive L-band spectral data base from Katahdin Hill.

3.1 Preliminary X-Band Results

In our earliest computations of clutter spectra from wind-blown trees, it was apparent that windspeed was of dominant influence on spectral width, and that frequently the rate of decay of the spectrum with increasing Doppler velocity in the tail of the spectrum was approximatly exponential. Figure 4 shows two examples of early spectral results obtained from Phase One X-band measurements at two sites in western Canada. Both of these measurements were conducted from cells containing deciduous aspen trees in winter season when the trees were bare of leaves.

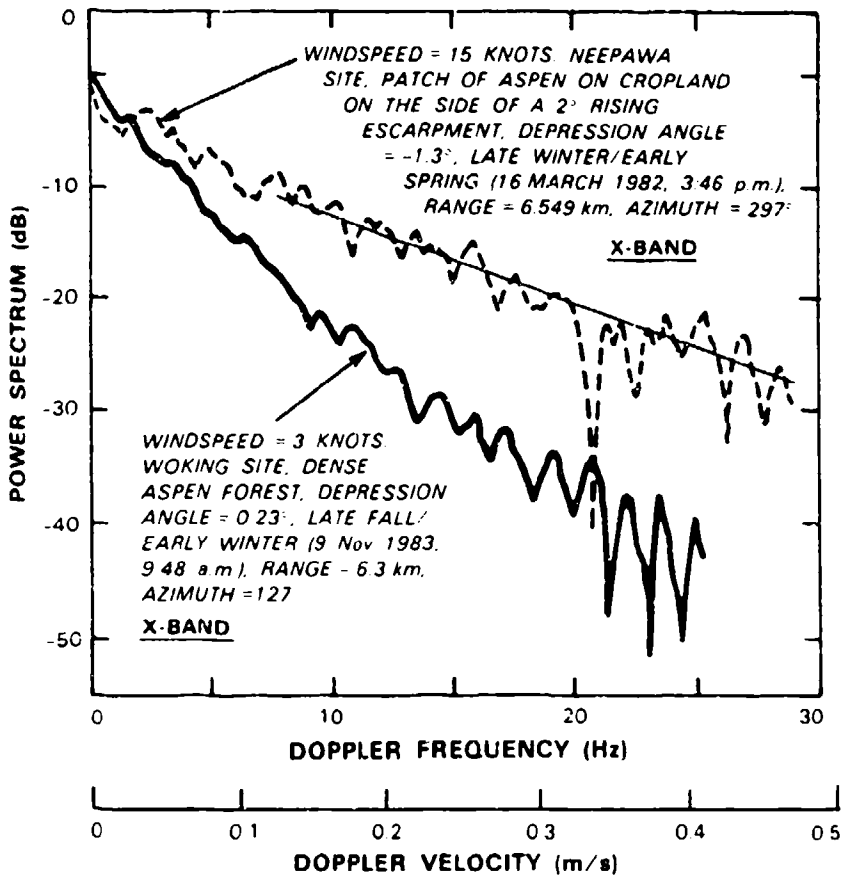

FIG. 4 POWER SPECTRA OF X-BAND RADAR RETURNS FROM WIND-BLOWN TREES, MEASURED AT TWO CANADIAN SITES. Range res. = 150 m, pol. = vertical, 7680 samples, pri = 8 ms, record duration = 1.024 min, 512 point FFT, Blackman-Harris window.

Otherwise these two sites were quite different and far removed from one another, Woking being a densely forested site in northern Alberta, whereas Neepawa was a farmland site in southern Manitoba. These early spectral data from Canadian sites were obtained by first computing the autocorrelation function over the full 1.024 min duration of the temporal record (i.e., 7680 pulses with pulse repetition interval = 8 ms), and subsequently computing the power spectrum as the Fourier transform of the autocorrelation function.[1] In Figure 4, what we mean by approximate exponential spectral decay is illustrated by the straight-line approximation drawn through the Neepawa data. Exponential decay of clutter spectra from wind-blown trees has been observed previously.[2] In the Woking data of Figure 4, of considerably lower windspeed than the Neepawa data, the spectrum is considerably narrower and an exponential approximation is somewhat less valid.

Figure 5 shows two examples of X-band spectral results from a forested cell at Katahdin Hill measured on two different days, 17 April 1985 and 25 April 1985. The cell measured, at 2582 m to 2597 m range and at 235° azimuth, lies on the south side of Jupiter Ridge, but at slightly closer range than the cells for which we show L-band data in Section 3.2. On 17 April the winds were quite strong; at the time of this X-band experiment, windspeed was recorded to be 10 knots gusting to 20 knots. In contrast, 25 April was a very still day and the winds were recorded as "calm" at the time of our experiment.

The spectra of Figure 5 are computed directly as Fast Fourier Transforms (FFT's) of the temporal pulse-by-pulse return including the dc component calibrated in RCS units of m^2. The spectral content is displayed in decibels with respect to 1 m^2 (i.e., in dBsm). The method used in generating these spectra is the method of modified periodograms,[3] where the temporal record

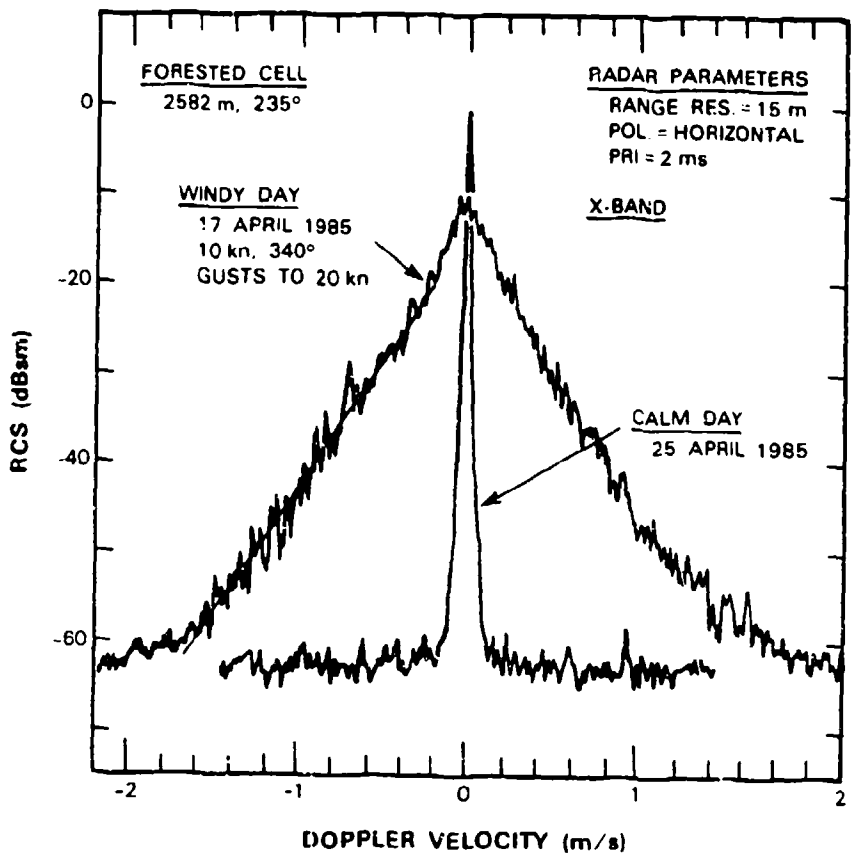

FIG. 5 POWER SPECTRA OF X-BAND RADAR RETURNS FROM WIND-BLOWN TREES, MEASURED FROM KATAHDIN HILL, MASS., ON A WINDY DAY AND ON A CALM DAY. 30,720 samples, pri = 2 ms, record duration = 1.024 min, 1024 point FFT, Blackman-Harris window.

of 30,720 pulses is divided into contiguous groups of 1024 samples, a 1024 point complex FFT is generated for each group, and the amplitudes of the resultant set of FFT's are arithmetically averaged together in each Doppler cell to provide the spectrum illustrated. Thus, in Figure 5, each spectrum shown is the result of averaging 30 individual spectra from an overall RCS record of 1.024 min duration and 2 ms pulse repetition interval (pri). In the generation of each spectrum, a 4-sample Blackman-Harris window or weighting function is utilized, with highest sidelobe level at -74 dB and with -6 dB per octave falloff.[4] All of the L-band spectral results in Section 3.2 are computed similarly. Appendix A illustrates this process of computation of spectra much more thoroughly.

The results in Figure 5 illustrate the differences in spectral content of the X-band reflections from this cell between when the tree branches are relatively motionless and when they are undergoing relatively strong, wind-induced, random motion. It is graphically apparent in these results how much of the dc or zero-Doppler return on the calm day is converted to ac return distributed over Doppler velocities up to 2 m/s on the windy day. The windy day spectrum shown in Figure 5 is one of the widest spectra we have so far found in our clutter data base. As in the Neepawa data of Figure 4, again we observe in this windy day Katahdin Hill data that the rate of decay of spectral energy with increasing Doppler velocity in the tail of the spectrum is approximately exponential as indicated by the straight line drawn through the left side of the spectrum. The exponential approximation is slightly less valid on the right side of this spectrum. The Phase One system noise levels are evident in both the calm and windy day results of Figure 5 at a level of about -64 dBsm. It is evident that on the windy day there is

essentially no observable energy above this noise floor for Doppler velocities greater than about 2 m/s. A physical velocity of 2 m/s would seem reasonable to attribute as a near-maximum velocity to expect for components of tree branches that might be acting as scattering centers causing direct phase modulation at our X-band RF wavelength of 1.3 inches under windy conditions. However, we made no measurements of tree motion.

The calm day spectrum in Figure 5 is one of the narrowest spectra we have so far found in our clutter data base. In contrast to the windy day spectrum of Figure 5, which is somewhat wider but at least comparable to the Neepawa data of Figure 4, the calm day spectrum of Figure 5 is much narrower than the Woking data of Figure 4. Although very narrow, this calm day spectrum is slightly wider than the corresponding X-band spectrum from our water tower reference target measured on the same day, indicating that there is some slight motion of the tree branches even on this very calm day. In this regard, we mention that during actual Phase One data collection, where we have a live instantaneous A-scope showing the returns being recorded, we have noticed that the display of X-band returns from forested cells, although usually exhibiting rapidly varying dynamic scintillation, very infrequently and only under the stillest air conditions does occasionally settle down and become almost stationary. Together, then, the two spectra illustrated in Figure 5 may be thought of as representing extreme or bounding conditions on X-band spectral extent from wind-blown trees, at least as determined by the Phase One data thus far examined.

In following discussions, we expand on these preliminary X-band observations from Figures 4 and 5, as follows:

a) higher windspeed causes wider spectra (even when windspeed is just grossly applicable to the general neighborhood and not measured specifically in the treed clutter cell);

b) approximate exponential decay of spectral tails;

c) exponential approximation better for higher windspeeds and wider spectra;

d) gross similarity in spectra from site-to-site and between X- and L-band.

3.2. L-Band Results from Katahdin Hill

As was mentioned in Section 2, for system reference data on each clutter measurement day, we recorded long time dwell experiments on a cell containing a large cylindrical municipal water tower. Figure 6 shows the power spectrum computed from the water tower L-band returns that were measured on the relatively calm day of 15 May. As expected, most of the energy from this stationary tower is at zero-Doppler velocity. The slight spectral spreading just above noise level in these data is attributable to ground clutter (i.e., trees) in the same cell at the base of the water tower. In other L-band measurements of this same water tower on windier days, the spectral width 55 to 65 dB below the peak increases to as much as $\pm$ 0.15 m/s to $\pm$ 0.4 m/s, respectively. The theoretical spectral response ot Blackman-Harris weighting of a constant signal is also shown in Figure 6. It is clear from Figure 6 that we are limited in providing measured 1024-point FFT clutter spectra by the Phase One system noise level rather than by the theoretical window function response. It is also clear, however, that our Phase One system maintains the theoretical Blackman-Harris spectral resolution over more than 50 dB of dynamic range. The data of Figure 6 define the instrumentation and processing limitations in the L-band spectral data presented subsequently.

With our system limits established, we now go on and show L-band clutter spectra from wind-blown trees. Similarly as we did in Figure 5 for X-band data, Figure 7 shows two examples of L-band spectra from wind-blown trees on a day of light winds and

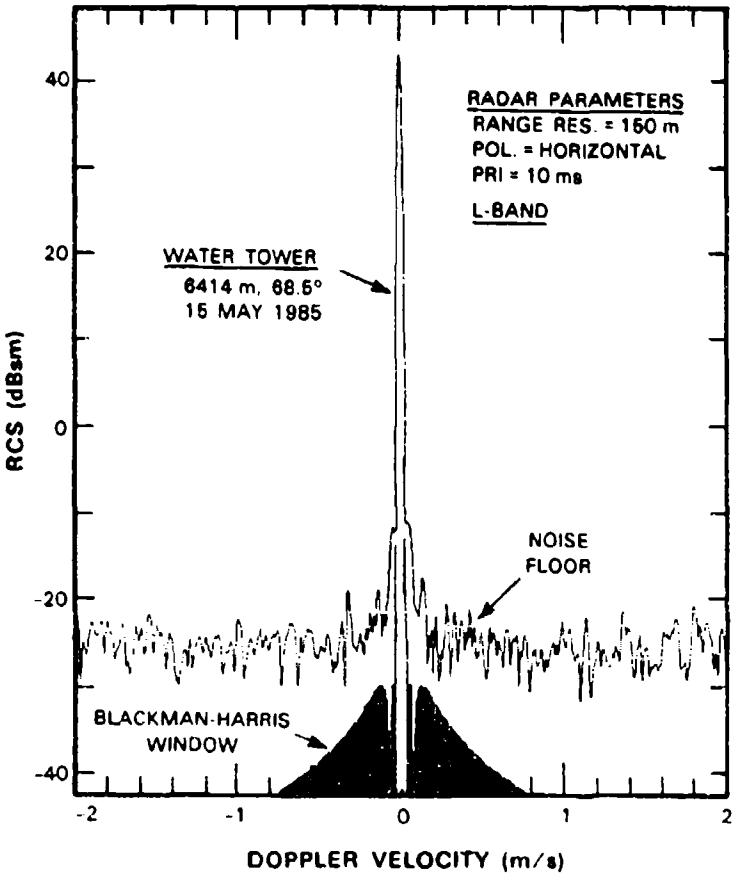

FIG. 6 POWER SPECTRUM OF L-BAND RADAR RETURNS FROM A WATER TOWER, MEASURED FROM KATAHDIN HILL. 6144 samples, pri = 10 ms, record duration = 1.024 min, 1024 point FFT, Blackman-Harris window.

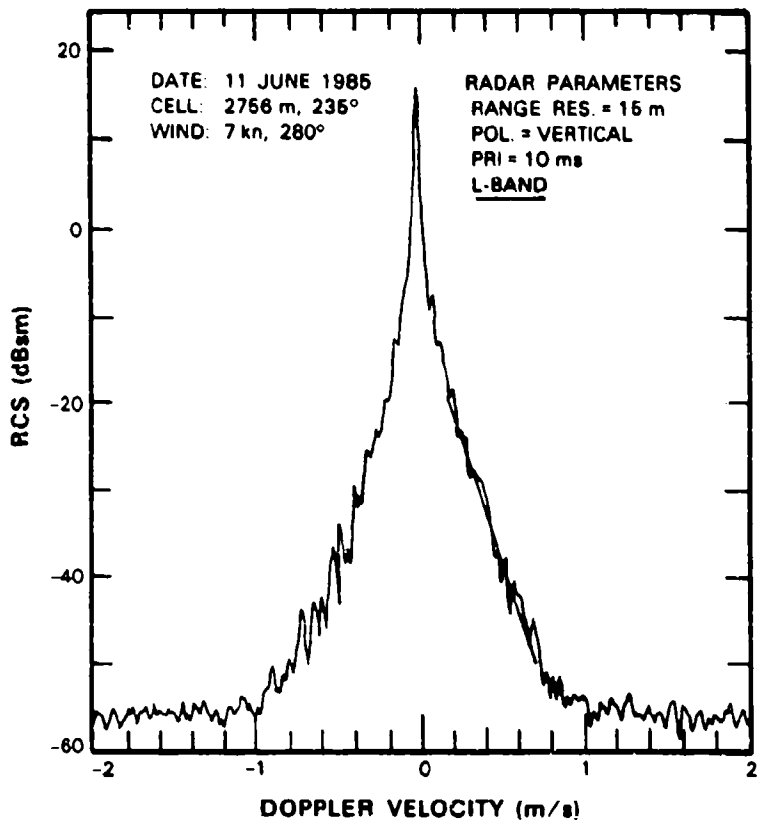

a)

FIG. 7 POWER SPECTRA OF L-BAND RADAR RETURNS FROM WIND-BLOWN TREES, MEASURED FROM KATAHDIN HILL ON A DAY OF a) LIGHT WINDS = 7kn AND ON A DAY OF b) STRONG WINDS = 17 kn. 30,720 samples, pri = 10 ms, record duration = 5.120 min, 1024 point FFT, Blackman-Harris window.

Continued...

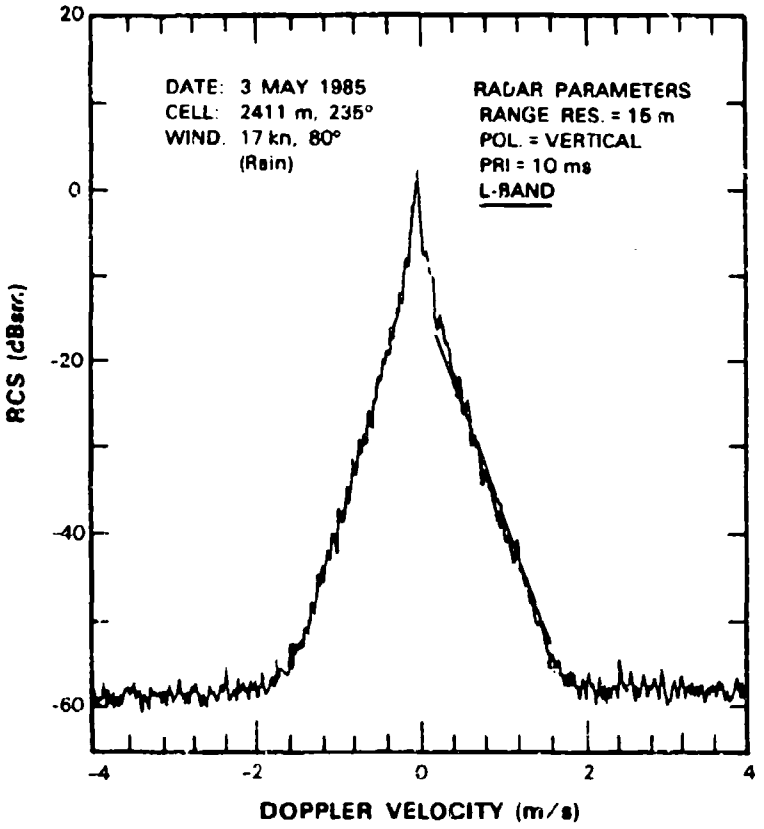

b)

FIG 7 POWER SPECTRA OF L-BAND RADAR RETURNS FROM WIND-BLOWN TREES, MEASURED FROM MEYAHDIN HILL ON A DAY OF a) LIGHT WINDS = 7kn AND ON A DAY OF b) STRONG WINDS = 17 kn. 30,720 samples, pri = 10 ms, record duration = 5.120 min, 1024 point FFT, Blackman-Harris window.

Concluded.

on a day of strong winds. Note that these two results in Figure 7 are from different cells, although both lie along the south side of Jupiter Ridge at 235° azimuth. Further note that the abscissa scales differ by a factor of two. In contrast to the X-band calm day spectrum of Figure 5, the L-band light wind spectral data of Figure 7(a) do not apply to absolutely still air conditions. Therefore the spectral extent is greater in the light-wind L-band spectrum of Figure 7 than in the calm day X-band spectrum of Figure 5. Nevertheless, as in the X-band data of Figure 5, we continue to see in the L-band data of Figure 7 that spectral extent increases significantly with windspeed. Furthermore, we continue to observe in the L-band data of Figure 7 that the rate of decay of spectral energy with increasing Doppler velocity is approximately exponential. As before at X-band in Figures 4 and 5, we illustrate what we mean by approximately exponential by straight-line fits drawn through the right sides of the L-band spectra in Figure 7. As in the X-band data, the fit is very good for the strong winds data of Figure 7(b) and not as good for the light winds data of Figure 7(a).

The spectrum shown in Figure 7(b) is the widest L-band spectrum that we have found so far in our measurement data base. It is interesting to observe that our widest examples of very windy day X- and L-band spectra in Figures 5 and 7(b) are very similar, even though these measurements apply to different days and different cells. Both of them are well-approximated by exponential fall-offs that decay at nearly equal rates with increasing Doppler velocity until the minimum discernible energy above the system noise level in the measurement is reached, which in each case occurs at a maximum Doppler velocity of about 1.8 or 2.0 m/s. On the basis of these widest windy day spectra shown in

Figures 5 and 7(b), there does not appear to be any marked dependence with RF frequency on spectral shape or extent on windy days. The data in Figure 7(b) are described in much greater detail in Appendix A.

We now go on from discussions of individual spectra to consideration of many spectra grouped within broad categories of windspeed. Before we consider these groups of spectral data, we pause to clarify our focus of interest in this regard. As mentioned previously, we did not measure windspeed in the clutter cell. Neither did we make any effort to record tree motion (e.g., via movies). It is not that we lack interest in these matters, but that the ground truth tail can quickly begin wagging the radar measurement dog. In the end, our interest is in how spectral widening can influence radar system performance, not in the random motion of trees in winds. In fact, if our interest were directly in the latter, we could think of no more useful device to investigate the phenomenon than Doppler radar measurements. Rather than a deterministic association between directly observed windspeed, tree motion, and recorded spectrum, we are more interested in the range of spectra that occur under broad nominal assessment of general wind conditions at a gross overall level of information such as might be available for a typical radar operating in the field. For such a radar, continuous detailed information on wind condition in every clutter cell can never be available, even if we were to devise a spectral model based on such information. Thus, our Hanscom airfield wind condition information serves our interests very well in providing a general indication of free-space wind conditions in the neighborhood of our clutter cells. This information allows us to follow our line of interest and see the extent of variation that occurs in clutter spectra within groups of similar wind conditions, and the separation of the spectral data between such groups.

Table 2 lists parameters of 23 long time dwell L-band experiments in which backscatter from Jupiter Ridge forested clutter cells was measured at Katahdin Hill during the period of time from November 1984 to August 1985. These 23 experiments are ordered in three groups by nominal wind condition, as a) light air (5 to 8 kn), b) breezy (10 to 11 kn), and c) windy (15 to 25 kn). Our wind terminology is not that of the meteorological Beaufort scale. Thus, for us "light air" covers Beaufort light-to-gentle breezes, "breezy" covers Beaufort gentle-to-moderate breezes, and "windy" covers Beaufort moderate-to-strong breezes.

Figure 8 shows L-band power spectra for the 23 experiments listed in Table 2, ordered within the same three groups by nominal wind condition (viz., light air, breezy, or windy) as are shown in Table 2. In Figure 8, the number in the key to the upper right in each part of the figure is the spectrum number in Table 2. We observe in Figure 8 that there is reasonably good clustering within the three groups of results by windspeed, and reasonably good separation between the three groups. As would be expected when using the Hanscom broadcast information as a general indication of wind conditions in the Phase One neighborhood, within the three groups of spectra there are a few examples when the local wind conditions in the clutter cell itself did not appear to match the wind conditions being broadcast during the 5 minute interval when the measurement data were being acquired. Thus, for example, under the nominal breezy conditions of Fig. 8(b), spectrum number 2 and, to a lesser extent, spectrum number 6, are narrower than the rest of the spectra in the group. And under the nominal windy conditions of Fig. 8(c), spectrum number 7 is narrower and spectrum number 4 is wider than the rest of the spectra in the group. Except for these few examples, the remainder of the spectra in Fig. 8 cluster

TABLE 2.
TWENTY-THREE TEMPORAL RECORDS OF L-BAND REFLECTIONS FROM WIND-BLOWN TREES

Spectrum Number	Measurement Date and Time-of-Day (h:min)	Range Resolution (m)†	Polarization	Pulse Repetition Interval (ms)††	Windspeed Mean (kn)	Windspeed Peak Gust (kn)	Wind Direction (deg)	Rain (R)
Light Air (5 to 8 kn)								
11	9 May 85 11:09	15	V	10	6		280	
13	22 May 85 13:39	15	V	10	6		10	
14	22 May 85 13:51	15	H	10	6		10	
16	5 Jun 85 14:00	15	V	10	8		100	R
17	5 Jun 85 14:16	150	V	10	8		100	R
18	11 Jun 85 10:41	15	V	10	7		270	
19	11 Jun 85 10:52	150	H	10	7		270	
20	11 Jun 85 11:01	15	H	10	7		270	
22	12 Aug 85 15:05	15	V	10	5		290	
23	12 Aug 85 16:45	15	V	10	8		320	
Breezy (10 to 11 kn)								
1	30 Nov 84 11:01	15	V	2	10		310	
2	30 Nov 84 13:40	15	V	8	10		280	
6	10 Apr 85 11:26	150	H	2	11		280	
12	15 May 85 14:57	15	V	10	10		260	
15	29 May 85 16:48	15	V	10	10		110	
21	19 Jun 85 16:27	15	V	10	10		300	
Windy (15 to 25 kn)								
3	7 Dec 84 10:44	15	H	2	15		310	
4	4 Apr 85 10:24	150	H	2	10	20	310	
5	4 Apr 85 15:18	15	H	10	10	20	290	
7	17 Apr 85 14:12	150	H	10	15	25	350	
8	17 Apr 85 16:36	15	V	10	15	25	310	
9	3 May 85 11:07	15	V	10	17		80	R
10	3 May 85 14:31	15	H	10	15		70	R

† Azimuth was 235°; the 15 m cell started at 2756 m range; the 150 m cell started at 2786 m.

†† In every case (except spectrum #2), 30 successive 1024 point complex FFT's were computed and averaged, covering dwells of 1.024 and 5.120 min at 2 and 10 ms pri, respectively. For spectrum #2, 10 successive 1024 point FFT's were computed and averaged over a 1.365 min dwell.

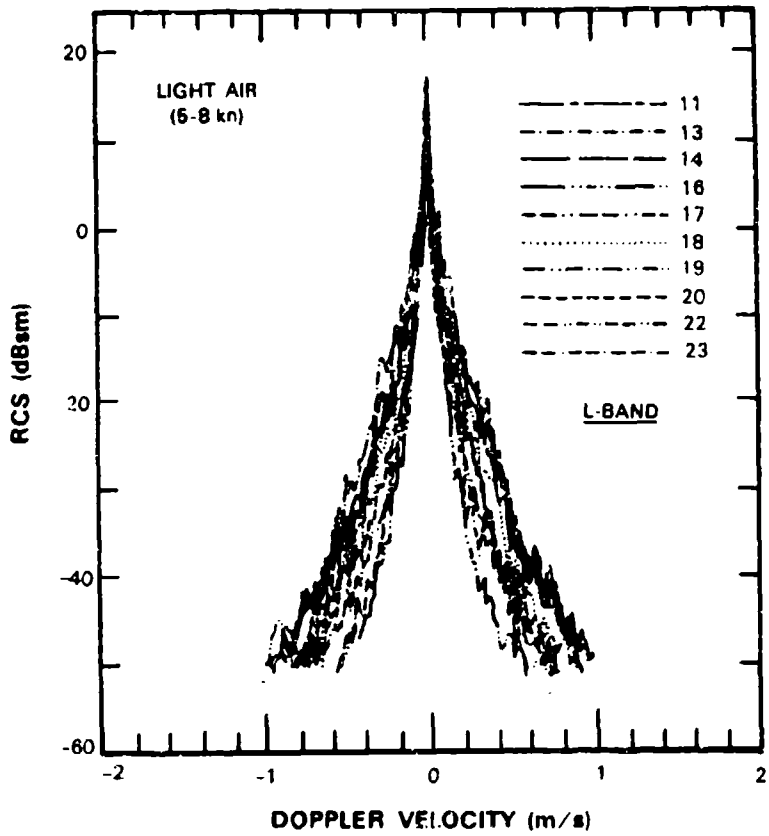

a)

FIG. 8 POWER SPECTRA OF L-BAND RADAR RETURNS FROM WIND-BLOWN TREES, MEASURED FROM KATAHDIN HILL FOR a) LIGHT AIR DAYS, b) BREEZY DAYS AND c) WINDY DAYS. See Table 2.

Continued...

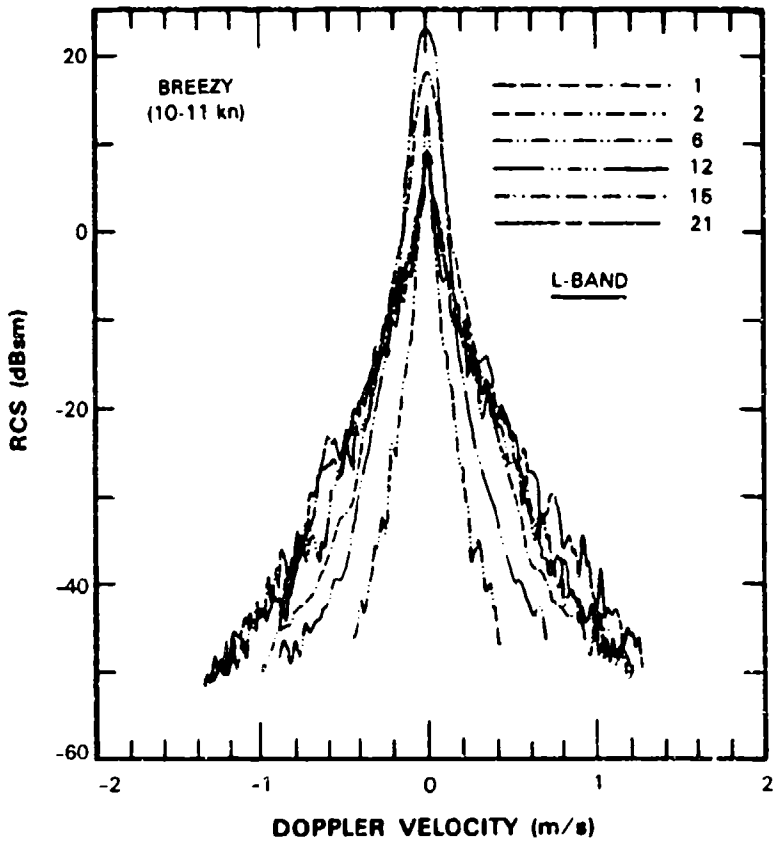

b)

FIG. 8 POWER SPECTRA OF L-BAND RADAR RETURNS FROM WIND-BLOWN TREES, MEASURED FROM KATAHDIN HILL FOR a) LIGHT AIR DAYS, b) BREEZY DAYS AND c) WINDY DAYS. See Table 2.

Continued...

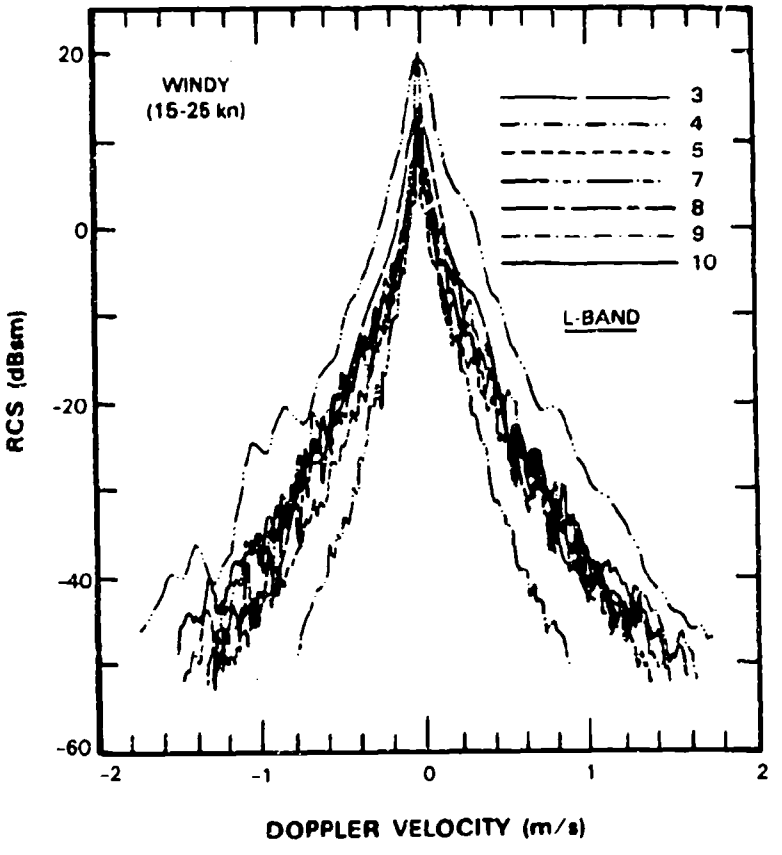

c)

FIG. 8 POWER SPECTRA OF L-BAND RADAR RETURNS FROM WIND-BLOWN TREES, MEASURED FROM KATAHDIN HILL FOR a) LIGHT AIR DAYS, b) BREEZY DAYS AND c) WINDY DAYS. See Table 2.

Concluded.

remarkably tightly in three groups by nominal neighborhood windspeed. The three groups of results in Figure 8 may be regarded as being indicative of probability of occurrence of spectral width of radar returns from cells containing wind-blown trees for radars operating in forest ground clutter, in three broad regimes of general windspeed in the neighborhood of the radar.

In absolute terms, the spectral widths in all three groups are narrow, with most of the discernible energy occurring at Doppler velocities usually less than 1.0 m/s or at most 2.0 m/s. Such narrow spectral extents are commensurate with what might be expected from direct phase modulation of the radar returns by the physical velocities of individual wind-driven tree elements.

Also, except for the few examples mentioned above, there is good separation between the three groups of results in Figure 8. For example, if we consider the -40 dBsm level in the spectra and neglect the few examples just mentioned, we observe that at this level the light air spectra in Fig. 8(a) have Doppler velocities between 0.35 and 0.65 m/s, the breezy day spectra in Fig. 8(b) have Doppler velocities between 0.65 and 1.0 m/s, and the windy day spectra in Fig. 8(c) have Doppler velocities between 0.9 and 1.2 m/s. Or, if we consider the -20 dBsm level in the spectra, we observe that at this level the light air spectra have Doppler velocities between 0.1 and 0.35 m/s, the breezy day spectra have Doppler velocities between 0.35 and 0.45 m/s, and the windy day spectra have Doppler velocities between 0.4 and 0.6 m/s.

Except for this correlation of spectral width with nominal neighborhood windspeed, there appear to be no strong trends with other measurement parameters in the spectral results of Figure 8. That is, such ground truth parameters as time-of-year (i.e., leaves on or off), prevailing wind direction, or whether there was rain in the neighborhood during the measurement, all have little observable effect on spectral shape. Similarly, whether the polarization of the radar was vertical or horizontal

also has little observable effect in the measured spectra. The range resolution of the radar does affect the dc level of the measured spectra, in that the 150 m pulse has larger zero-Doppler RCS levels in the results of Figure 8; but beyond this expected result (viz., larger cells have greater RCS) there is little observable effect on the spectral shape at non-zero Doppler velocities. The shorter dwell times of experiments with pri < 10 ms do lead to less spectral resolution, as is theoretically required, which careful examination of the results in Figure 8 does reveal.

We now select one representative spectrum from each of the three groups in Figure 8. That is, from within the central region of each group where most of the data clusters together, we select the single spectrum which appears to most closely exist at the center of the cluster over its full spectral extent. These "most representative" spectra are spectra numbers 18, 12, and 10 in Table 2, for light air, breezy, and windy conditions, respectively. These three spectra are plotted together in Figure 9, and clearly illustrate the effect of windspeed on spectral extent. Also plotted in Figure 9 are the thinnest L-band spectrum we have found so far in our data base (viz., spectrum number 16, Table 2), and the widest L-band spectrum we have found so far in our data base (viz., the spectrum of Fig. 7(b), for the 2411 m range cell). In terms of probability of occurrence, these latter two results may be thought of as approximations to limiting situations for spectral extent of radar returns from cells containing wind-blown trees, whereas the former three results may be thought of as representative of typical situations in three regimes of windspeed. Altogether, Figure 9 constitutes the beginning of a model, although it shows data by individual example only, whereas a general model is better if based on statistical combination of many similar measurements. Note that the dc component has been removed from the spectra shown in

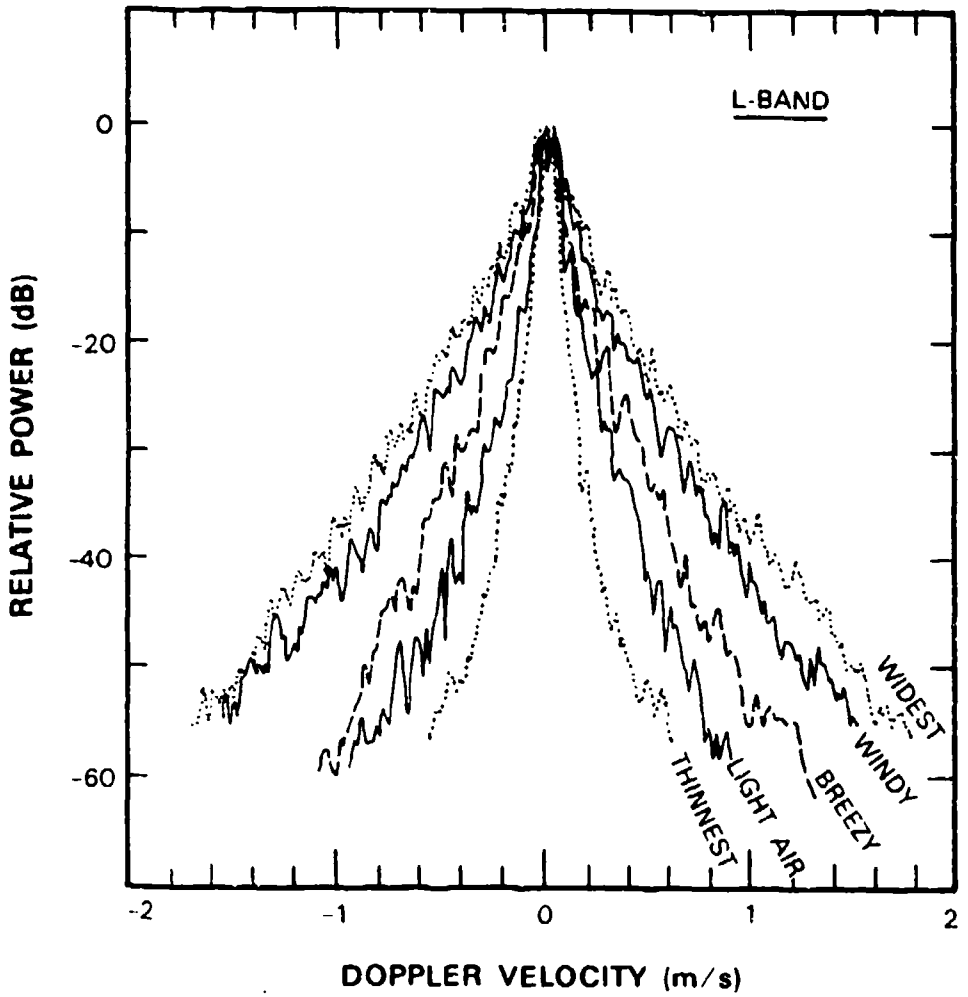

FIG. 9 FIVE POWER SPECTRA OF L-BAND RADAR RETURNS FROM WIND-BLOWN TREES, MEASURED FROM KATAHDIN HILL, SHOWING THE RANGE OF VARIATION OCCURRING IN SPECTRAL WIDTH WITH DIFFERENT WIND CONDITIONS. The spectra labelled "thinnest", "light air", "breezy", and "windy" are spectra numbers 16, 18, 12 and 10, respectively, in Table 2. The spectrum labelled "widest" is that shown in Fig. 7(b). The dc component is removed in these data.

Figure 9 in order to facilitate the comparison of data from the different range cells.

3.3 Exponential Model

We have observed earlier in this report that the rates of decay of spectral energy with increasing Doppler velocity in radar returns from wind-blown trees are often reasonably well approximated as exponential in the tails of the spectral distributions well removed from the zero-Doppler region. That is, the rates of decay in the spectral tails are often fairly linear as plotted in our standard logarithmic power (y-axis) versus linear Doppler velocity (x-axis) spectral plots, especially for the wider spectra that occur at higher windspeeds. However, in many cases, especially for narrower spectra that occur at lower windspeeds, if a slight degree of curvature is allowed in approximating spectral decay in our standard plots, a slightly better power-law fit can be obtained, in which the energy decays slightly less rapidly (never more rapidly) than exponential. We believe this reflects the fact that nature does not always obey some simple analytic law in this matter. Rather, we would expect that the distributions of radial velocities of blowing branches acting to directly phase modulate radar returns to be very complexly related to wind conditions and tree species. In any event, in the cases where spectral decay is less rapid than exponential, the degree of departure from exponential is usually rather slight and different from case to case. For our purposes, it is more useful to deal with the approximating exponential representaion for the simplicity, uniformity, and generality it introduces.

Therefore, we now set out to gain the obvious general modeling benefit of having observed frequent quasi-exponential decay in the tails of spectra from wind-blown trees. To do so we

proceed as follows. In the tail region of the power spectrum where the exponential approximation is valid, we represent the spectrum as

$$P(v) = A\, e^{-\beta|v|}, \quad v \geq 0.2 \text{ m/s},$$

where

P = power spectral density (w/Hz);
v = Doppler velocity (m/s);
β = exponential decay factor;
A = arbitrary constant.

For each of the 23 experiments for which measurement parameters are shown in Table 2, the best exponential approximation to the spectral tail is determined, and the corresponding decay factor β is noted. Then these 23 values of β are separated into three groups by windspeed as are shown in Table 2, and the mean β within each group determined. The resulting values of β and corresponding rates of exponential decay of spectral tails in three regimes of windspeed are shown in Table 3 and Figure 10. As is indicated in Figure 10, these exponential decay factors apply only in the tail regions of spectra for Doppler velocities $v \geq 0.2$ m/s, well removed from zero-Doppler velocity. The spectral modeling information of Figure 10 has the advantage of statistical generality, obtained by averaging over a number of like-classified measurements.

Let us briefly review our modeling position with respect to the information shown in Table 3 and Figure 10. We are interested in Doppler spectra of radar returns from wind-blown trees, and particularly the rates of decay in the tails of such spectra at spectral offsets well removed from zero. We believe that the information of Table 3 and Figure 10 is reasonably representative of our measurements. However, we do not make a strong case here for the advancement of a rigorous exponential

TABLE 3

EXPONENTIAL DECAY FACTORS† IN THE TAILS†† OF L-BAND SPECTRA FROM WIND-BLOWN TREES IN THREE REGIMES OF WINDSPEED

Windspeed	Exponential Decay Factor, β
Light Air (5 to 8 kn)	23.5
Breezy (10 to 11 kn)	17.5
Windy (15 to 25 kn)	10.7

---

† $P(v) = Ae^{-\beta|v|}$,

where $P(v)$ = power spectrum (w/Hz),
v = Doppler velocity (m/s),
β = exponential decay factor
A = arbitrary constant

†† $v \geq 0.2$ m/s.

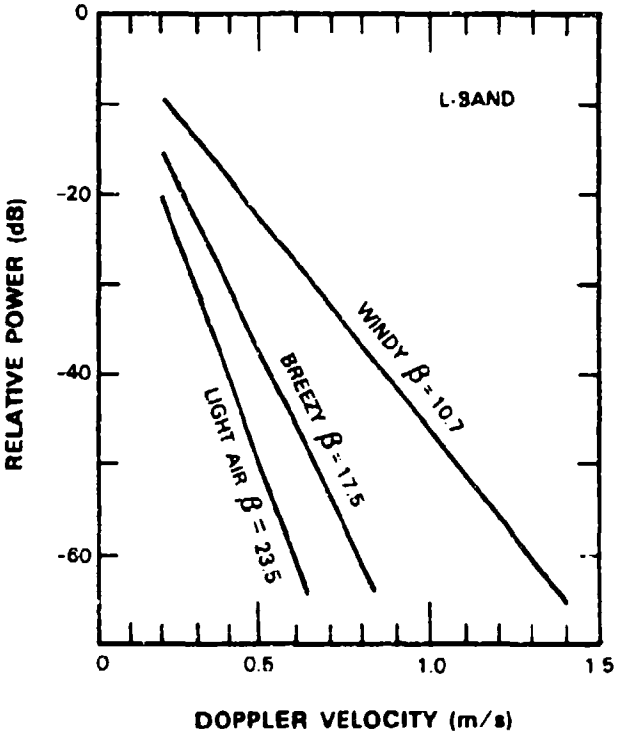

FIG. 10 APPROXIMATE RATES OF EXPONENTIAL DECAY IN THE TAILS OF L-BAND SPECTRA FROM WIND-BLOWN TREES, IN THREE REGIMES OF WINDSPEED.

model for spectral extent from wind-blown trees. We certainly do not propose that such a model apply over the full spectrum including the zero-Doppler region, or that even in the tails of spectra it has statistical validity in the sense of passing rigorous hypothesis testing. In the face of any particular concern with fidelity of spectral detail, we prefer to quickly come away from the approximating information of Table 3 and Figure 10, and let the actual data such as are shown in Figure 8 stand on their own, to be modeled as any investigator so wishes. But for those, like us, who wish simple approximating information on rates of spectral decay from wind-blown trees as a function of windspeed, we believe the information of Table 3 and Figure 10 usefully represents what we have often generally observed in our measurements.

4. TEMPORAL CORRELATION

In theoretical terms, knowledge of the spectral characteristics of some random process in the frequency domain is equivalent to knowledge of the correlation characteristics of the process in the time domain. That is, the power spectrum is simply the Fourier transform of the autocorrelation function. Even in practical terms, it is always broadly observable that the wider the spectrum, the faster the process decorrelates. However, in analyzing our measured clutter data, neither the power spectrum nor the autocorrelation function are exactly and completely describable in simple analytic form easily amenable to Fourier transformation. As a result, if we are interested in both spectral and correlative properties, we need to numerically generate both the power spectrum and the autocorrelation function. In Section 4.1 we provide some examples from our Phase One Katahdin Hill measurements of radar returns from wind-blown trees showing how correlation time varies with RF frequency and with windspeed. In Section 4.2 we relate spectral width to correlation time in one of these measurements. In all of the measured results in Section 4, the dc component has been removed from the received time-varying RCS record.

4.1 Dependence on RF Frequency and Windspeed

Let us concern ourselves with the question of how long it takes for radar returns from wind-blown trees to decorrelate, which is complementary to the question of spectral extent in such returns. To provide information on this subject, we investigated the temporal correlation properties in some of the long time dwell Phase One Katahdin Hill experiments described in Section 2. Thus Figure 11 shows the normalized autocorrelation function[1] at all five Phase One frequencies for the returns from the forested cell on Jupiter Ridge at range = 2.5 km and

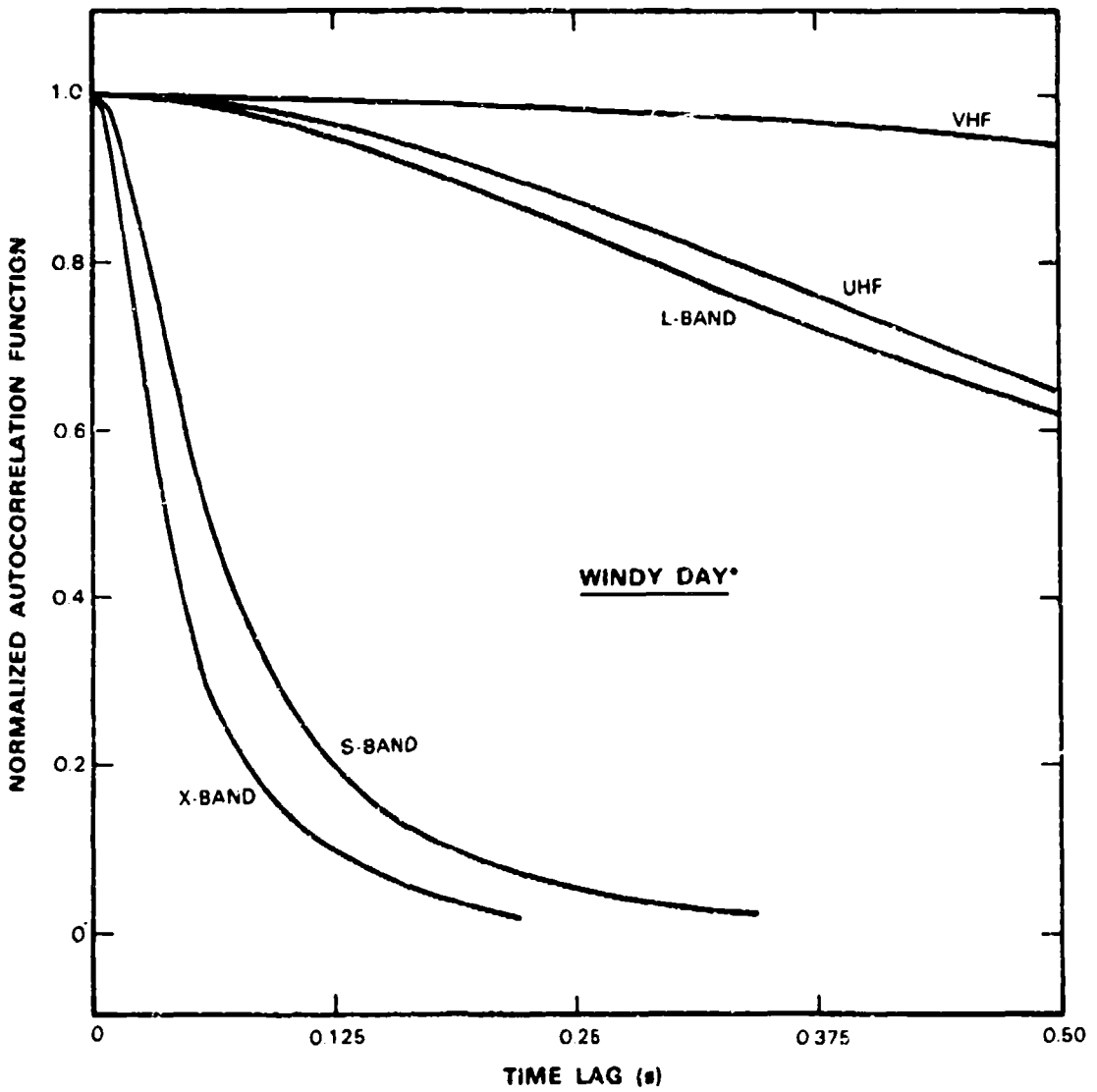

* Not simultaneous measurements by frequency band

FIG. 11 AUTOCORRELATION FUNCTIONS OF RADAR RETURNS FROM WIND-BLOWN TREES, MEASURED FROM KATAHDIN HILL ON A WINDY DAY AT FIVE RADAR FREQUENCIES. Measurement day, 17 April 1985. Windspeed = 15 kn gusting to 25 kn. Range = 2.5 km, azimuth = 235°. Range res. = 150 m, pol. = horizontal. Pri = 2, 10, 10, 6, 2 ms and record duration = 1.02, 5.12, 5.12, 3.07, 1.02 min at VHF, UHF, L-, S-, X-bands, respectively. In all cases, no. of pulses = 30,720.

azimuth = 235°, as measured on the windy day of 17 April 1985 (see Table 2). The time-of-day (hr:min) at which data collection commenced for each of these five experiments was as follows: X-band, 10:24; S-band, 11:30; L-band, 14:12, VHF, 15:00; UHF, 15:27. Each of these five experiments consisted of 30,720 pulses at pri's of 2 ms, 10 ms, 10 ms, 6 ms, and 2 ms for VHF, UHF, L-, S-, and X-bands, respectively. For all five experiments, the polarization was horizontal and the range resolution was 150 m. At each of the five Phase One frequencies, the autocorrelation of the return from the water tower reference target remains essentially at unity over the 0.5 s time lag shown in Figure 11. Let us define correlation times $\tau_{1/e}$ and $\tau_{1/2}$ as the times required for the normalized correlation function to decrease to 1/e (=0.368) or 1/2 (=0.5), respectively. Then Table 4 gives these measures of time required for decorrelation of the radar returns from wind-blown trees, as determined from the data shown in Figure 11. If the scattering centers and their motion were

TABLE 4
CORRELATION TIMES FOR RADAR RETURNS FROM WIND-BLOWN TREES AT KATAHDIN HILL ON A WINDY DAY.
(See Fig. 11)

FREQUENCY BAND	CORRELATION TIME (s) $\tau_{1/2}$	$\tau_{1/e}$
VHF	4.01*	5.04*
UHF	0.69	0.94
L-Band	0.67	0.95
S-Band	0.062	0.081
X-Band	0.033	0.049

Note: * = extrapolated estimate

the same at all five frequencies, simple Doppler considerations would lead us to expect that correlation times would decrease inversely with RF frequency, all else being equal. We certainly observe an approximate trend indicative of an effect in this direction in the data of Figure 11 and Table 4, although the results do not scale exactly linearly with frequency. This reflects the facts that: a) the experiments were conducted at different times and thus under different specific wind conditions on 17 April; b) the cell sizes and hence scattering center ensembles were different (e.g., due to azimuth beamwidth varying with frequency band, see Table 1); and c) the scattering centers and their velocities would be expected to vary with RF wavelength (i.e., twigs at X-band, branches at L-band, limbs at VHF).

The correlative properties of radar returns from wind-blown trees shown in Figure 11 and Table 4 apply for the particularly windy day of 17 April. Correlation times from wind-blown trees would be expected to increase with decreasing windspeed. Figure 12 shows the normalized autocorrelation function[1] for the L-band returns from the Jupiter Ridge forested cell, measured on three different days under three quite different wind conditions. The autocorrelation function is here shown only over the correlation interval from 1.0 to 0.9 to emphasize the region where the data just begins to decorrelate. In Figure 12, the windy day was 17 April (i.e., the same data as is shown in Figure 11), the breezy day was 10 April, and the light air day was 5 June (see Table 2). Time of measurement (hr:min) for these three experiments was 14:12, 11:26, and 14:16, respectively. Each of these three experiments consisted of 30,720 pulses at pri's of 10, 2, and 10 ms for the windy day, breezy day, and light air day, respectively. Polarization was horizontal on the windy and

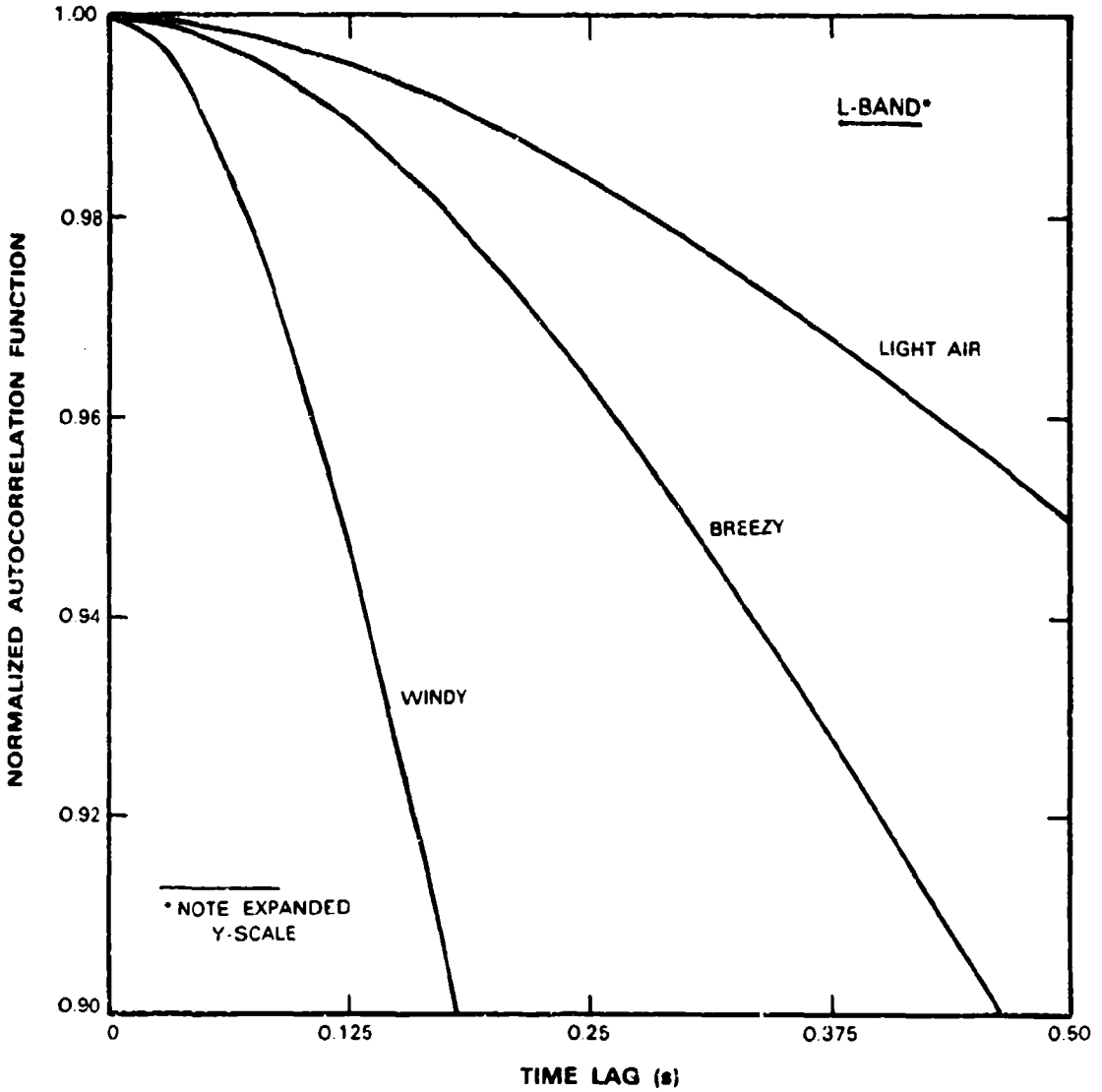

FIG. 12 AUTOCORRELATION FUNCTIONS OF L-BAND RADAR RETURNS FROM WIND-BLOWN TREES, MEASURED FROM KATAHDIN HILL FOR THREE DIFFERENT WIND CONDITIONS. Windy day, 17 April 1985, windspeed = 15 kn gusting to 25 kn, pri = 10 ms, pol. = horizontal, same data as in Fig. 11. Breezy day, 10 April 1985, windspeed = 11 knots, pri = 2 ms, pol. = horizontal. Light air day, 5 June 1985, windspeed = 8 kn, pri = 10 ms, pol. = vertical. In all cases, no. of pulses = 30,720. Range = 2.5 km, azimuth = 235°, range res. = 150 m.

breezy days, vertical on the light air day. In all three cases, range resolution was 150 m, start range to the cell was 2486 m, and azimuth was 235°. The results in Figure 12 clearly indicate how temporal correlation in L-band radar returns from wind-blown trees increases with decreasing windspeed. In these results, the correlation times $\tau_{1/e}$ on the windy, breezy, and light air days were 0.95, 2.11, and 5.56 s, respectively.

4.2 Correlation Time and Spectral Width

The main focus of consideration in this report is on how far out discernible energy occurs in the tails of Doppler spectra of radar returns from wind-blown trees, and the rates of decay of energy in these tails. In Section 4 we have departed from this focus to consider a few examples of temporal correlative properties in radar returns from wind-blown trees. Another useful objective within this whole subject area would be to provide modeling information not only for predicting spectral width, but also for relating spectral width to correlation time. Although we are not at present actively involved in pursuing this objective, we now present an example along these lines to shed additional light on the information about spectral tails that is presented in this report. We select the windy day X-band experiment of Figure 11 because both its spectrum and correlation time are well resolved and well defined in our data, and because the rate of decay of energy in its spectral tail is well-approximated as exponential. On the basis of the spectral results presented in Section 3, we arbitrarily select the 40 dB below peak level in the ac spectrum as the level at which we define spectral width. This level is well above radar noise level, yet is well out on the tail in the region where our exponential rate of decay applies and is well removed from the zero-Doppler region where the exponential model does not apply and where we are apt to lose

resolution on calm days. We define the Doppler frequency at which this level occurs in the spectrum to be f_{-40} Hz. For the windy day X-band experiment of Figure 11, f_{-40} = 58.8 Hz, and $\tau_{1/e}$ = 0.04942 s. We know that, in some broad sense, correlation time is inversely proportional to spectral width. If we assume that $\tau_{1/e} = K/f_{-40}$, for the windy day X-band experiment K = 2.91. We believe it would be useful to investigate more fully and to have modeling information available for these three quantities, f_{-40}, $\tau_{1/e}$, and K, or similar quantities specifying and reflecting the relationship between spectral width and correlation time in radar returns from wind-blown foliage. The information in this report makes a beginning toward specification of spectral width, but is not directly useful for estimating correlation time. For example, for the hypothetical spectral distribution which is exponential over its full extent including the zero-Doppler region, K = 1.92.† This hypothetical value of K underestimates the actual correlation time in the windy day X-band example of Figure 11. That is, the hypothetical exponential spectral distribution underestimates the low-frequency components in the near-zero Doppler region in the spectrum. This example brings out more clearly why we do not advocate an exponential model over the full extent of the spectrum but only in the tail. It also tantalizes us as to what better and more general relationships in these matters might apply, but we leave these issues to future investigations.

---

†Let the power spectrum be represented by $P(f) = \frac{1}{\alpha} e^{-\alpha|f|}$, where f is Doppler frequency. This provides $\int_{-\infty}^{\infty} P(f)d(f)=1$. The corresponding autocorrelation function is: $R(\tau) = \frac{\alpha^2}{\alpha^2 + (2\pi\tau)^2}$, where τ is time lag, and R(0) = 1. Then, for this theoretical relationship, $\tau_{1/e} = 1.92/f_{-40}$.

5. SUMMARY

Long temporal records were measured of radar backscatter from wind-blown trees. These measurements were conducted on an approximately once-a-week basis over a period of about 6 months on a few forested resolution cells. Power spectra showing the Doppler frequency content of these measured records were generated.

In absolute terms, the widths of these spectra are very narrow. The maximum Doppler velocity at which discernible energy appears in the spectra is often less than 1.0 m/s, and almost always less than 2.0 m/s. By discernible, we mean to levels of about 60 dB or so below the peak zero-Doppler level and above our system noise level.

Over and above the fact that wind-blown tree spectra are narrow, we definitely observe a predictable association of spectral width with the nominal windspeed in the neighborhood during our measurements, whereby spectral widths increase with increasing windspeed. Furthermore, we often observe that the energy in the tails of the spectra, at spectral off-sets well removed from zero, decays approximately exponentially with increasing Doppler velocity. Estimates of rates of exponential decay in the spectral tails as a function of windspeed are provided in three regimes of windspeed, as: 1) light air, 5 to 8 kn; 2) breezy, 10 to 11 kn; and 3) windy, 15 to 25 kn.

On the basis of numerous observations, we see little general dependency of spectral shape or extent on other ground truth parameters such as prevailing wind direction or whether leaves are on or off the trees, or on the radar parameters of polarization and resolution. Neither do we observe any strong dependence of spectral shape and extent on the radar frequency

between L-band and X-band, although this is based on a much more limited set of observations to date.

Correlation times in our temporal records of radar returns from wind-blown trees are expected to vary inversely with spectral widths, but except for a few examples, this report does not provide general information for predicting correlation times as a function of windspeed or establishing the constants of proportionality.

APPENDIX A

TIME AND SPECTRAL HISTORIES FOR A LONG PULSE SEQUENCE OF RADAR RETURNS FROM WIND-BLOWN TREES ON A WINDY DAY

A.1 INTRODUCTION

In the body of this report, we present many power spectra from wind-blown trees usually obtained from 30,720 pulse sequences at a pulse repetition interval (pri) of 10 ms. These power spectra are computed as the average of 30 sequential 1024 point Fast Fourier Transforms (FFT's) in which the pulses are taken 1024 at a time until 30,720 pulses are used up. The individual FFT's are computed as complex FFT's of sequential intervals of the in-phase and quadrature coherent measured data record. The averaged power spectrum is computed simply as the arithmetic mean of the 30 contributing amplitudes in each Doppler resolution cell. The averaged spectra shown in the body of the report are not decomposed to show the 30 individual power spectra which go into each one. Each of these individual spectra is obtained from a 10.24 s sequence of 1024 pulses. This 10.24 s interval or dwell of time is long enough to encompass a number of correlation periods and hence to incorporate a substantial amount of temporal variation in the received signals (see Table 4). However wind is a dynamic random process with complex short-term and long-term variation. The wind conditions within a treed resolution cell are expected to vary with local gustiness from one 10.24 s interval to the next. Among themselves, how variable are the 30 individual power spectra formed from 30 sequential 10.24 s dwells covering a total period of 5.12 min? In this appendix, we provide an answer to this question by showing the 30 individual power spectra for one particular, windy day, averaged spectrum shown in the body of this report.

The particular averaged spectrum selected is that shown in Figure 7(b), which was generated from data measured on the windy day of 3 May 1985 (see Table 2). This is one of the widest L-band spectra from wind-blown trees that we have so far found in our measurement data base. In Sect. A.2, we first list the

measurement parameters of this experiment. Then in Sect. A.3 we plot time histories of amplitude (RCS per unit area, or σ^o, in dB) and phase (in deg) over their complete record lengths of 30,720 pulses. These time histories explicitly show the detailed pulse-by-pulse temporal variation for which we are determining the spectral content.

In Section A.4, we go on and show the overall spectrum resulting from averaging the 30 individual component spectra. Finally, in Section A.5, we sequentially show each of the individual spectra. The dc level in the received RCS signal has not been removed in any of the results shown in this Appendix.

A.2 EXPERIMENT PARAMETERS

Site: Katahdin Hill
Date: 3 May 1985
Cell: 2411 m, 235°
Wind: 17 kn, 80° (rain)

Radar Parameters
- Range res. = 15 m
- Polarization = vertical
- L-Band

Processing Parameters
- Number of samples = 30,720
- Pri = 10 ms
- Record duration = 5.12 min
- 1024 point FFT's, dc in.
- Blackman-Harris window.

A.3 RCS AMPLITUDE AND PHASE TIME HISTORIES

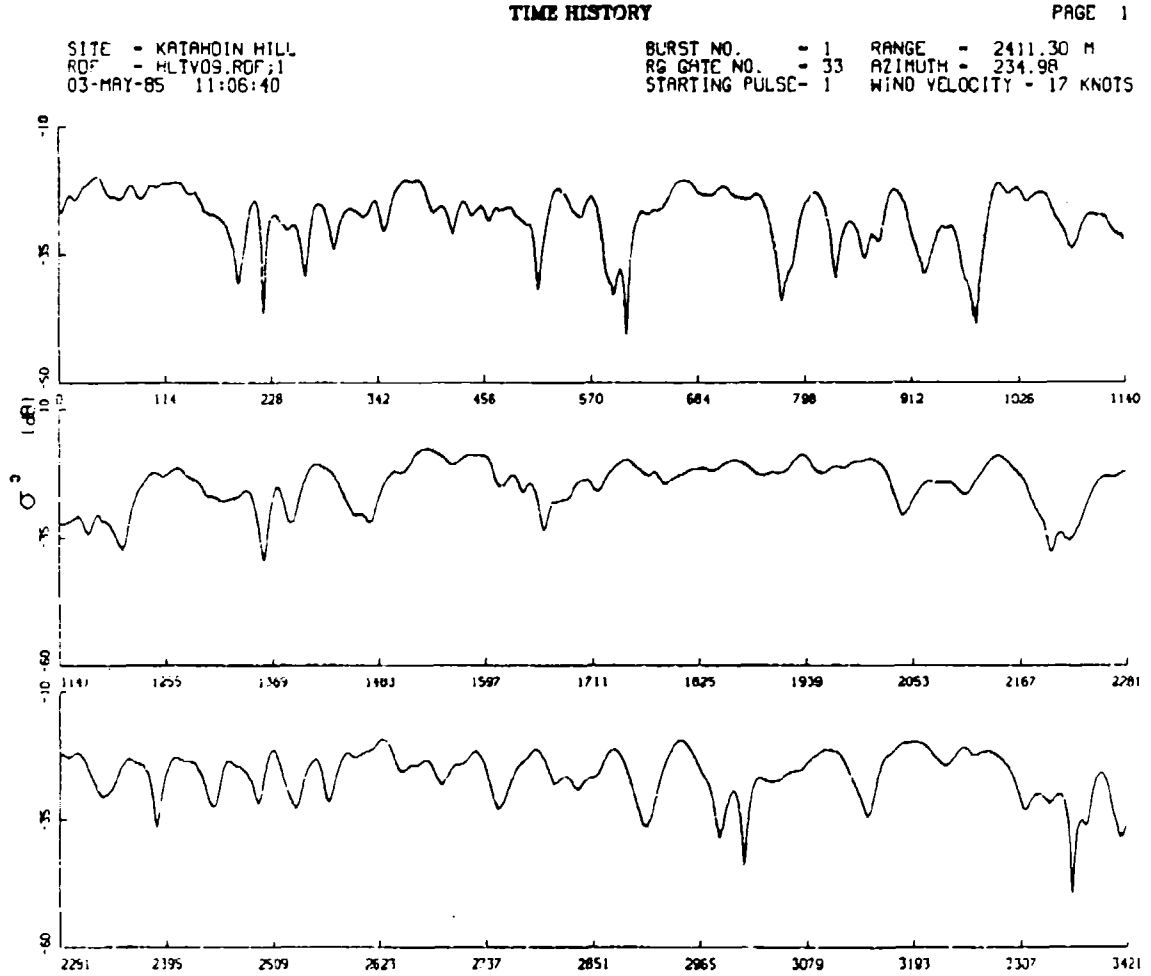

FIG. A.1 L-BAND RCS AMPLITUDE TIME HISTORY FROM WIND-BLOWN FOLIAGE ON A WINDY DAY, PULSE-BY-PULSE OVER 30,720 PULSES.

Continued...

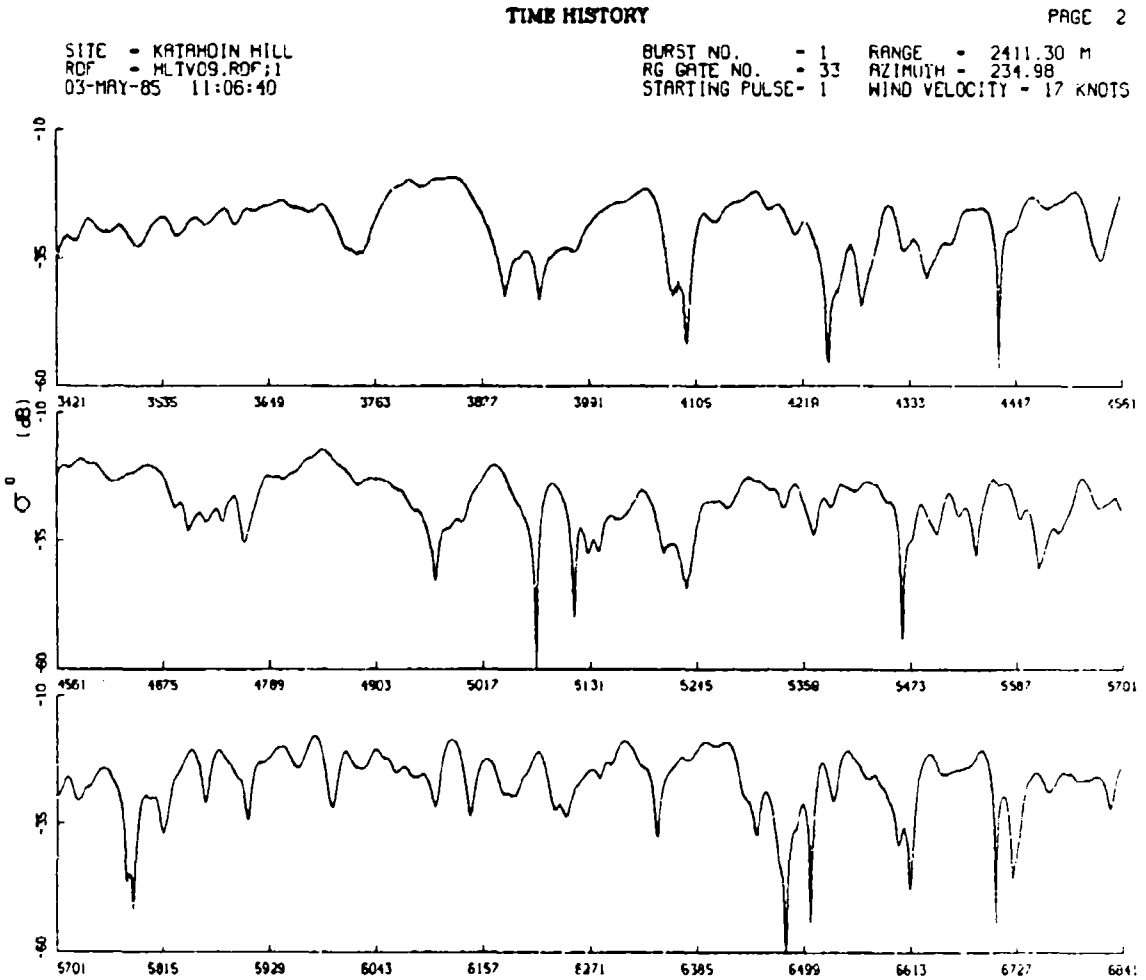

FIG. A.1 L-BAND RCS AMPLITUDE TIME HISTORY FROM WIND-BLOWN FOLIAGE ON A WINDY DAY, PULSE-BY-PULSE OVER 30,720 PULSES.

Continued...

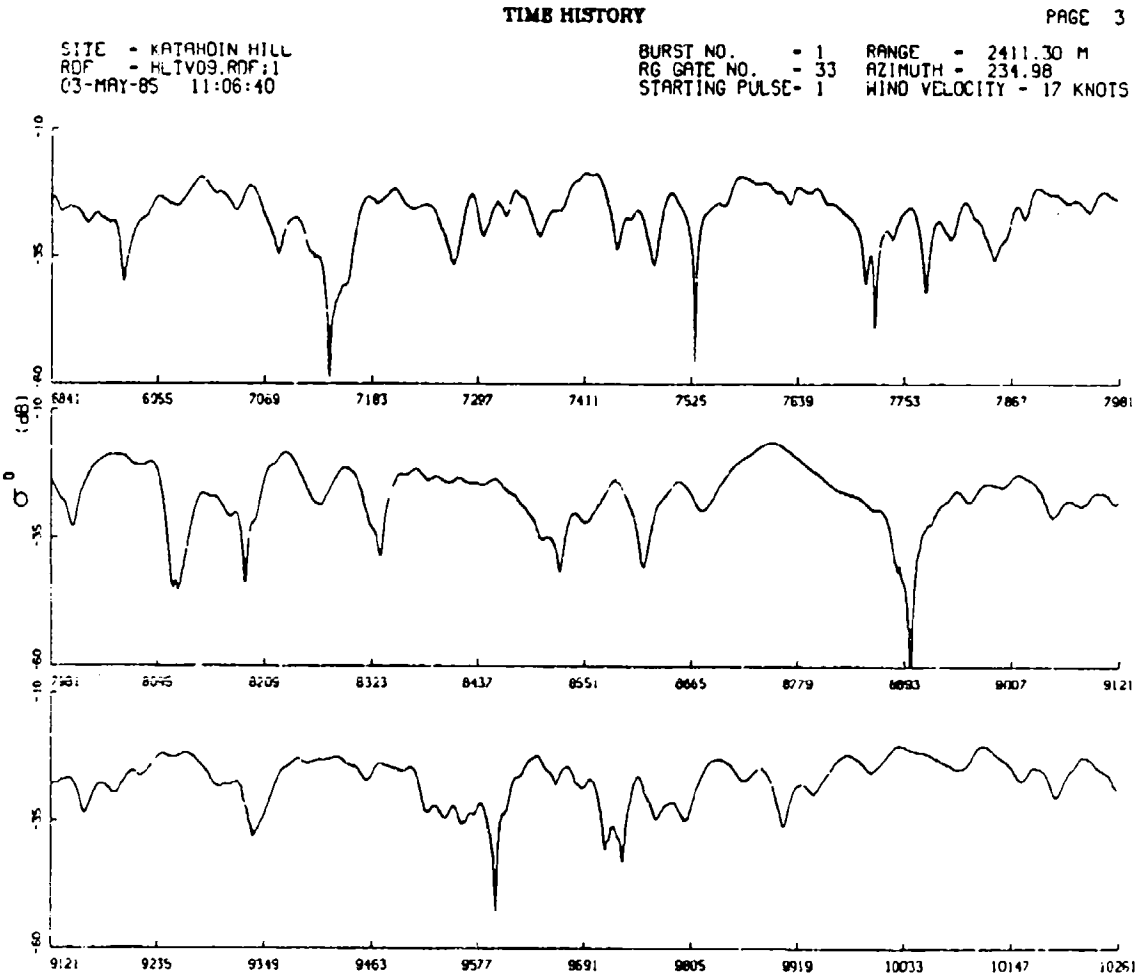

FIG. A.1 L-BAND RCS AMPLITUDE TIME HISTORY FROM WIND-BLOWN FOLIAGE ON A WINDY DAY, PULSE-BY-PULSE OVER 30,720 PULSES.

Continued...

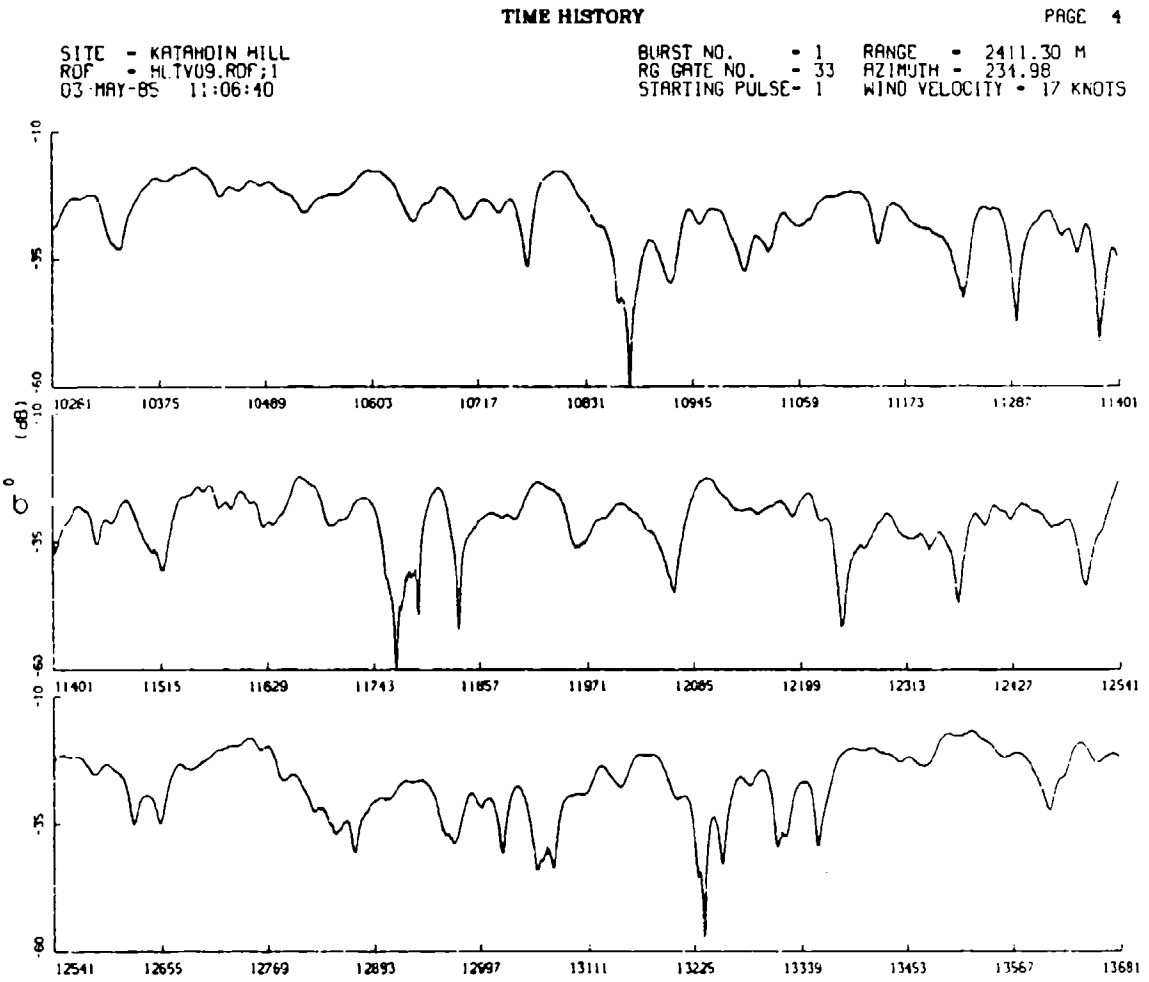

FIG. A.1 L-BAND RCS AMPLITUDE TIME HISTORY FROM WIND-BLOWN FOLIAGE ON A WINDY DAY, PULSE-BY-PULSE OVER 30,720 PULSES.

Continued...

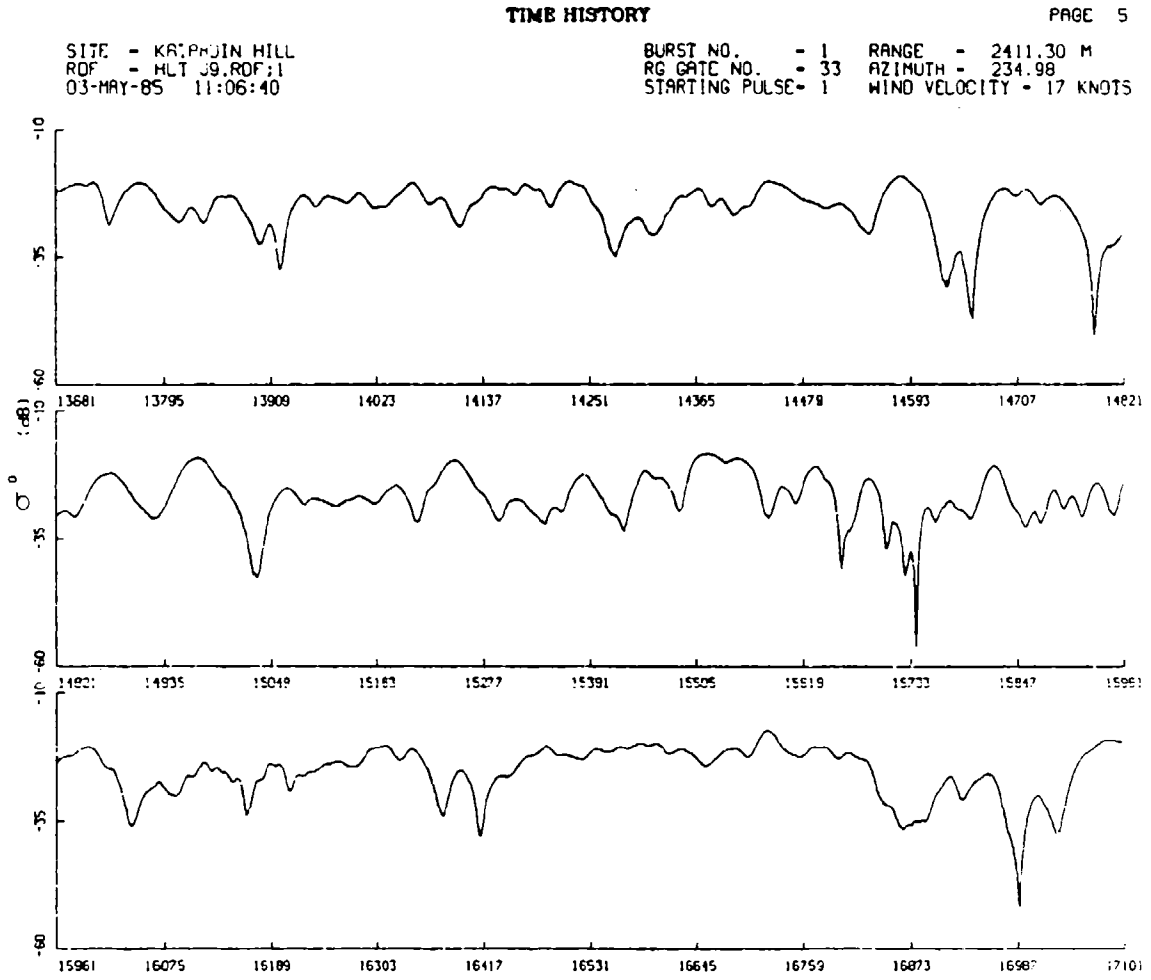

FIG. A.1 L-BAND RCS AMPLITUDE TIME HISTORY FROM WIND-BLOWN FOLIAGE ON A WINDY DAY, PULSE-BY-PULSE OVER 30,720 PULSES.

Continued...

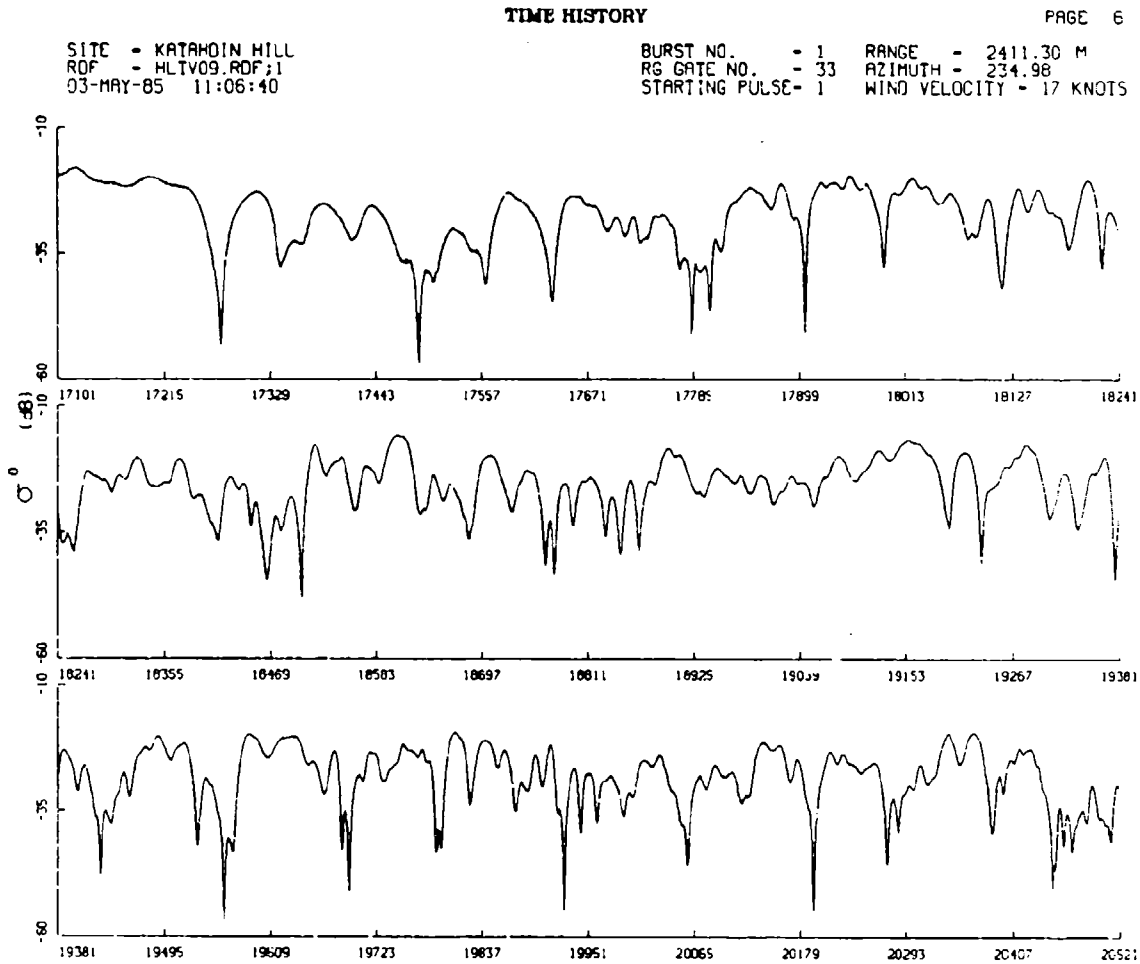

FIG. A.1 L-BAND RCS AMPLITUDE TIME HISTORY FROM WIND-BLOWN FOLIAGE ON A WINDY DAY, PULSE-BY-PULSE OVER 30,720 PULSES.

Continued...

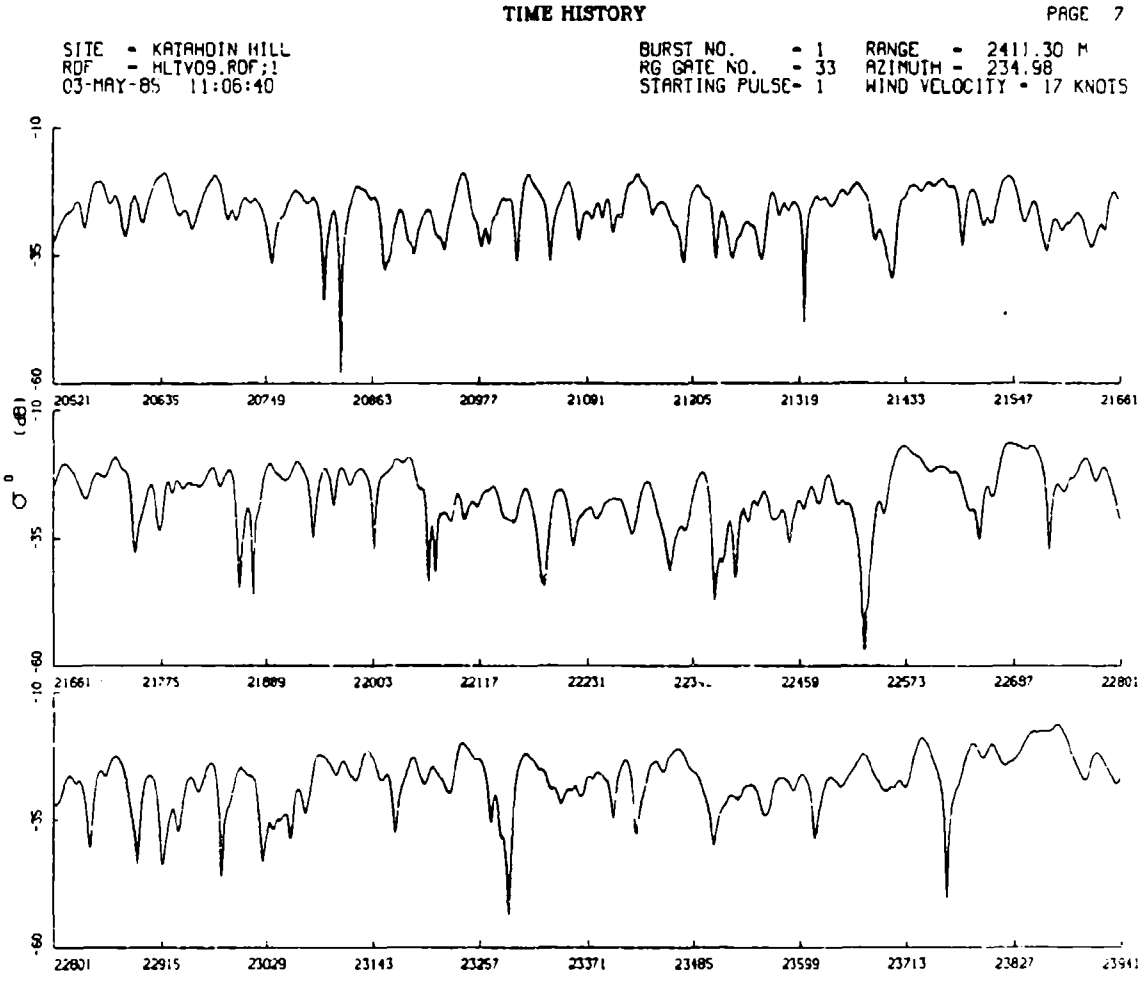

FIG. A.1 L-BAND RCS AMPLITUDE TIME HISTORY FROM WIND-BLOWN FOLIAGE ON A WINDY DAY, PULSE-BY-PULSE OVER 30,720 PULSES.

Continued...

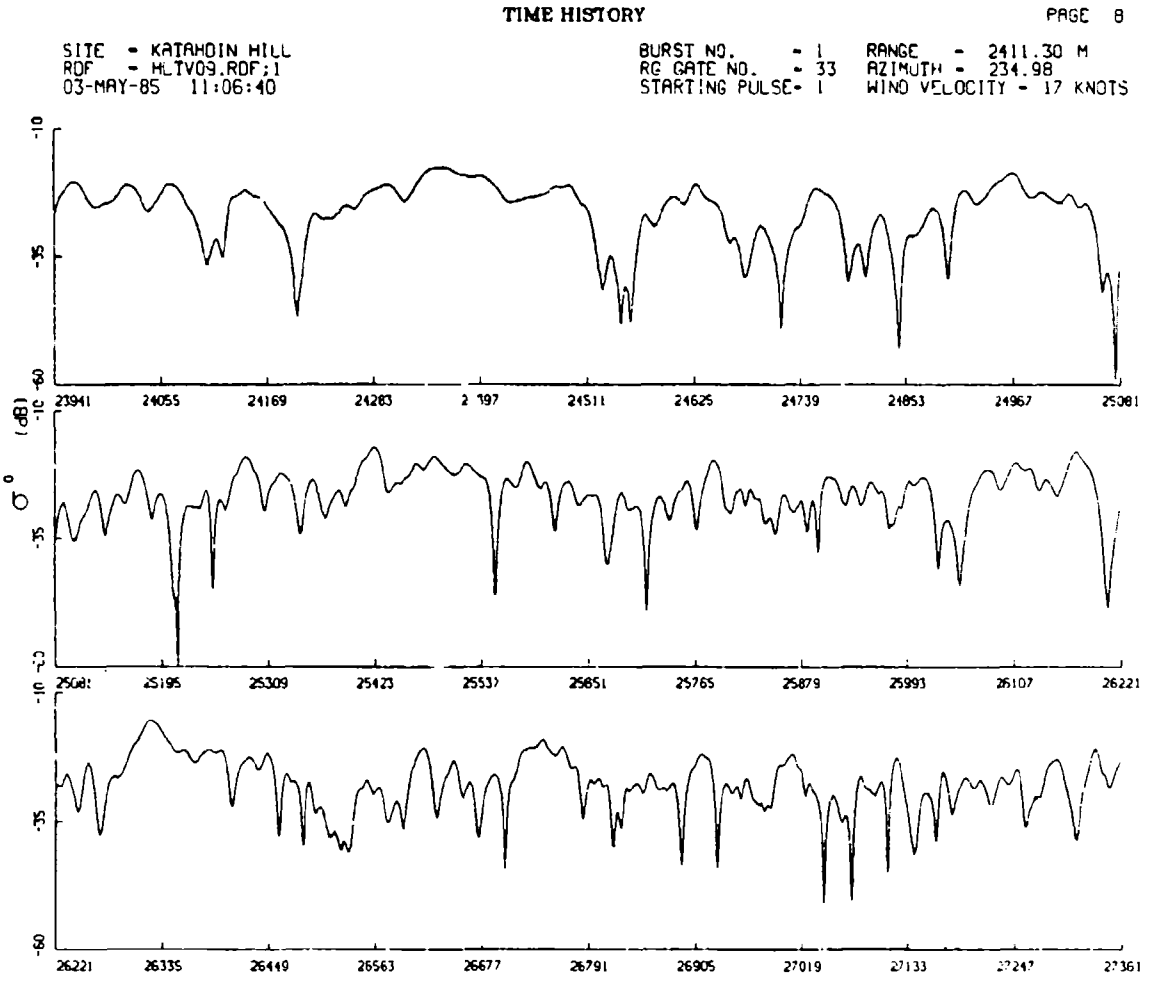

FIG. A.1 L-BAND RCS AMPLITUDE TIME HISTORY FROM WIND-BLOWN FOLIAGE ON A WINDY DAY, PULSE-BY-PULSE OVER 30,720 PULSES.

Continued...

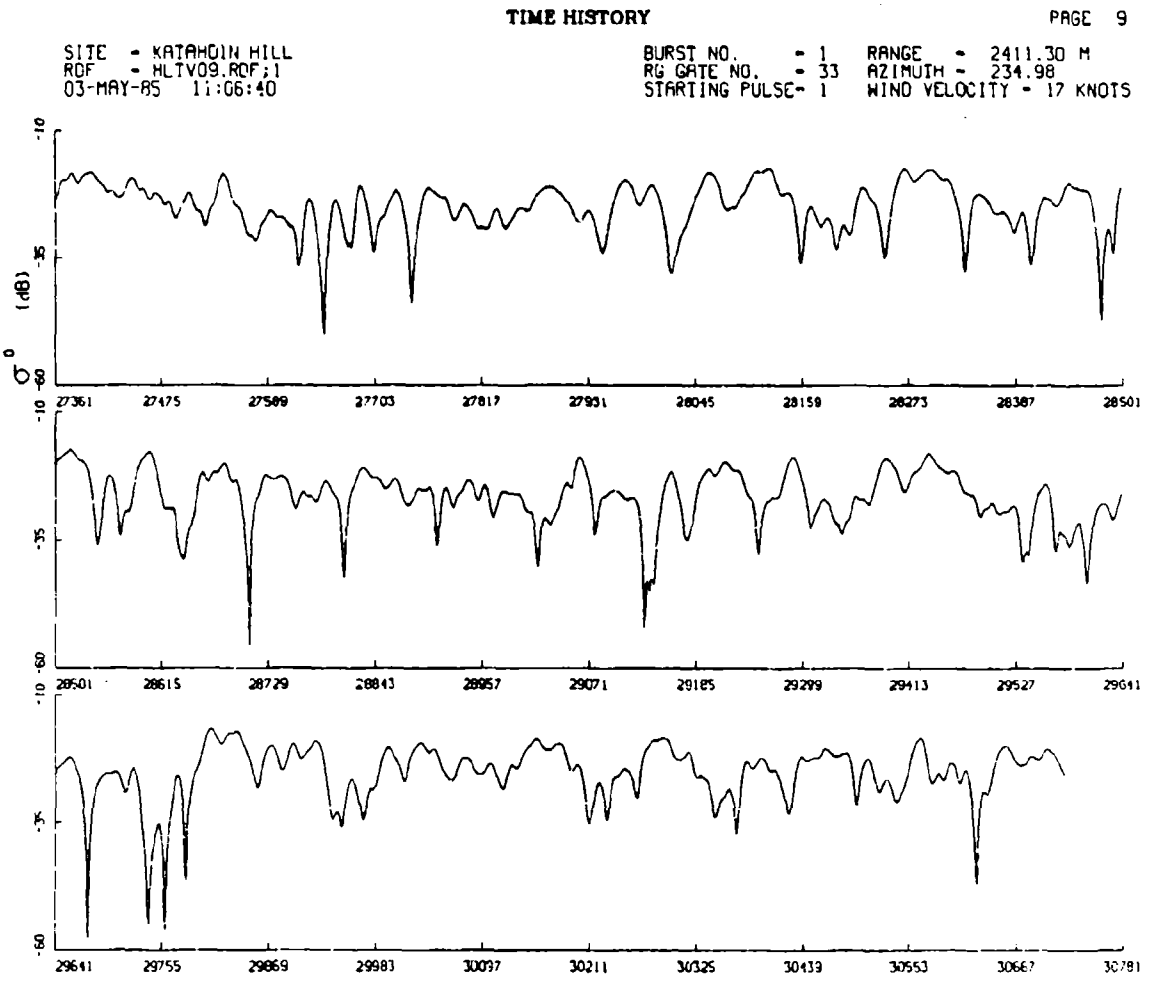

FIG. A.1 L-BAND RCS AMPLITUDE TIME HISTORY FROM WIND-BLOWN FOLIAGE ON A WINDY DAY, PULSE-BY-PULSE OVER 30,720 PULSES.

Concluded.

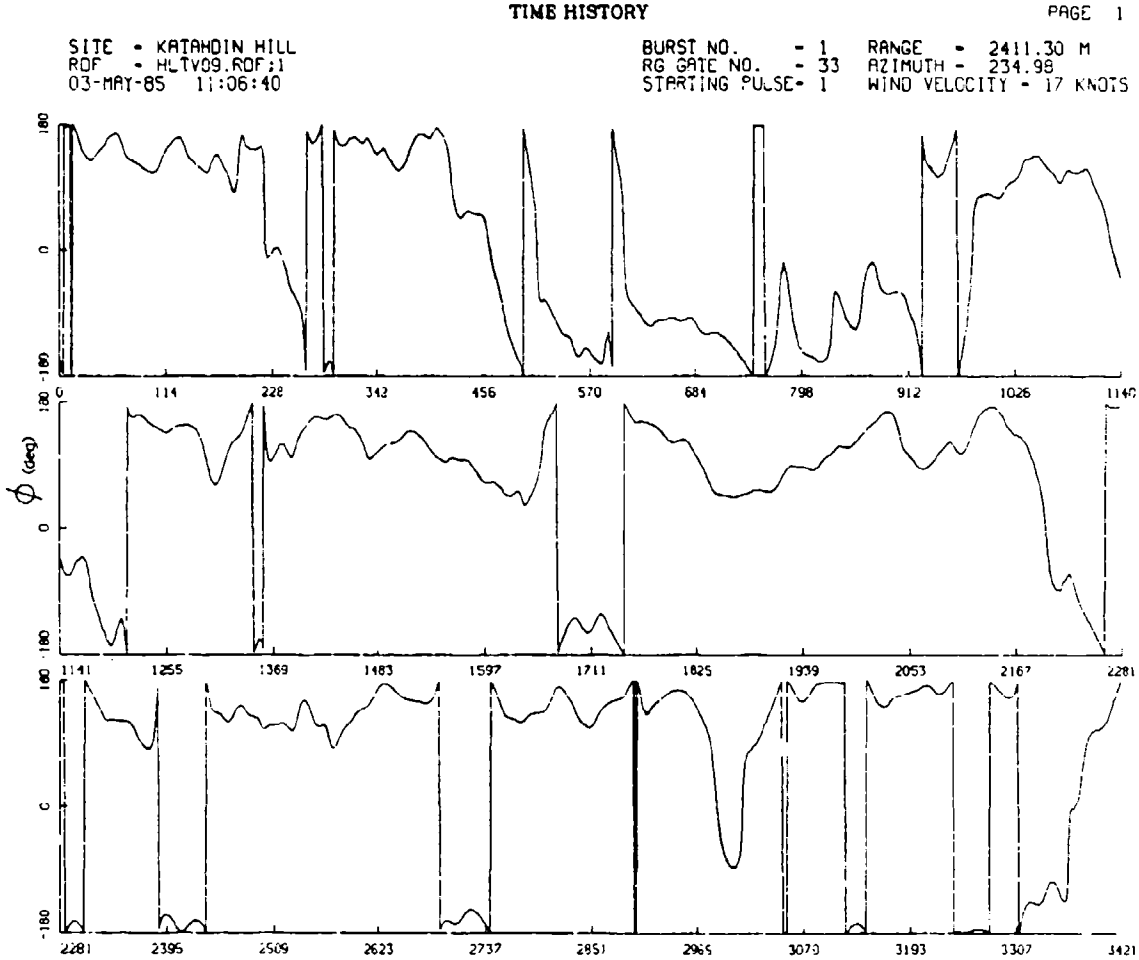

FIG. A.2 L-BAND RCS PHASE TIME HISTORY FROM WIND-BLOWN FOLIAGE ON A WINDY DAY, PULSE-BY-PULSE OVER 30,720 PULSES.

Continued...

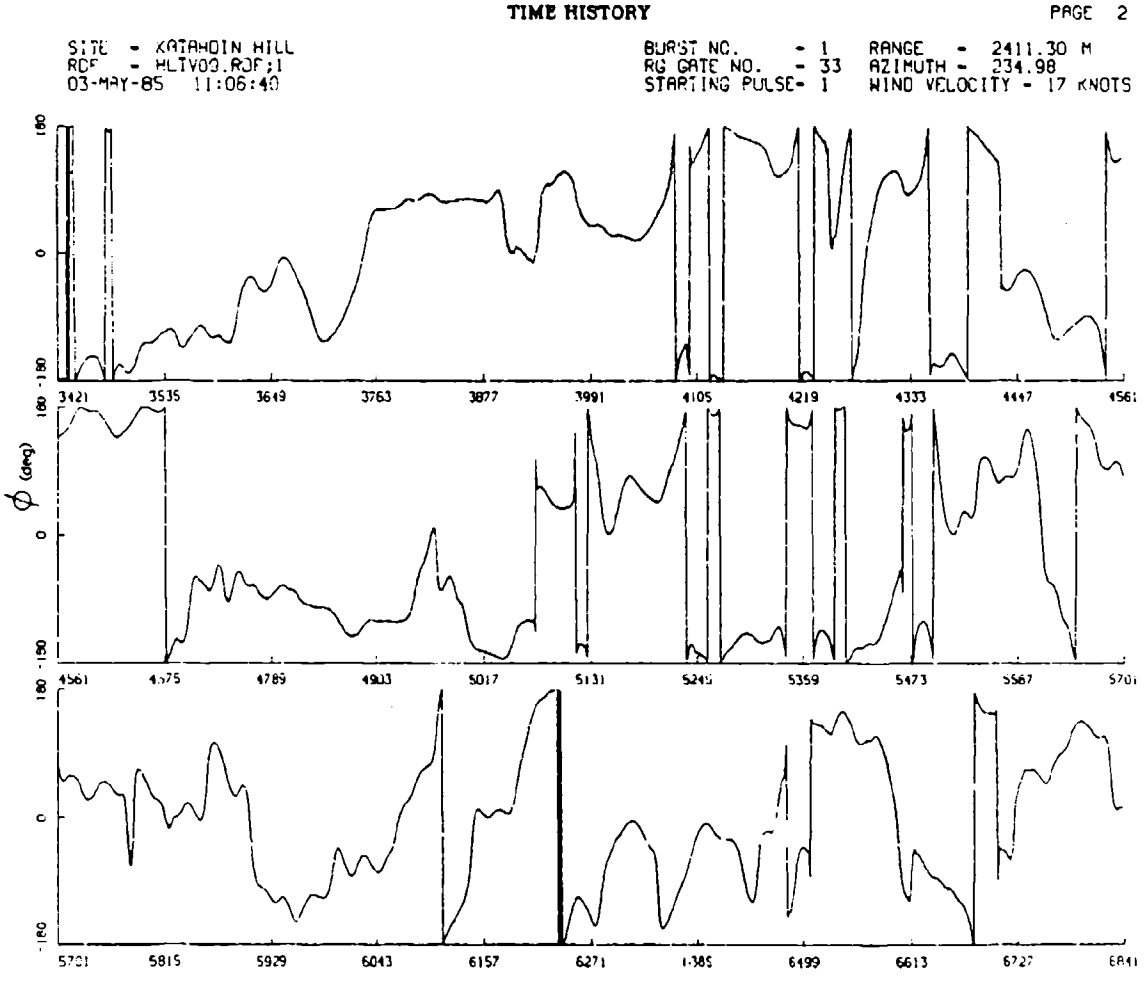

FIG. A.2 L-BAND RCS PHASE TIME HISTORY FROM WIND-BLOWN FOLIAGE ON A WINDY DAY, PULSE-BY-PULSE OVER 30,720 PULSES.

Continued...

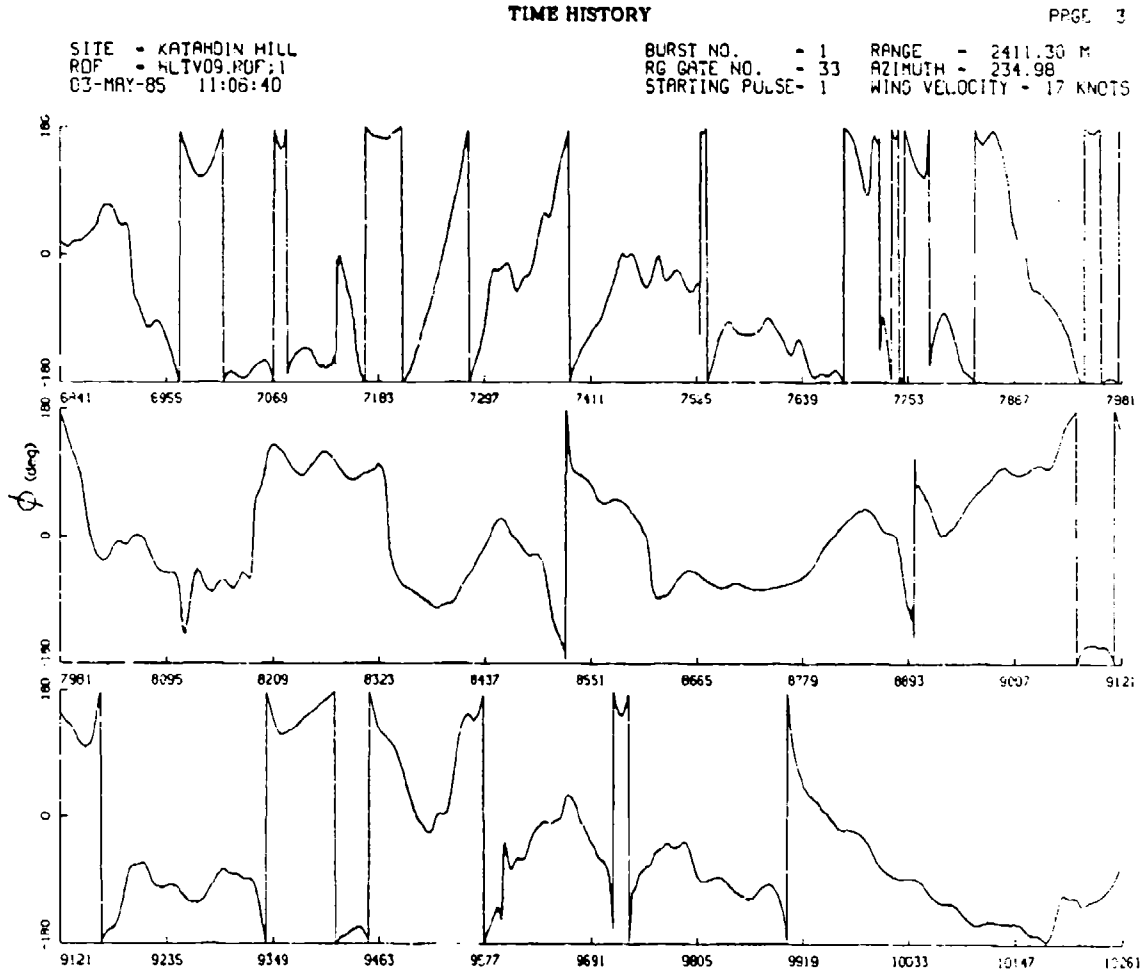

FIG. A.2 L-BAND RCS PHASE TIME HISTORY FROM WIND-BLOWN FOLIAGE ON A WINDY DAY, PULSE-BY-PULSE OVER 30,720 PULSES.

Continued...

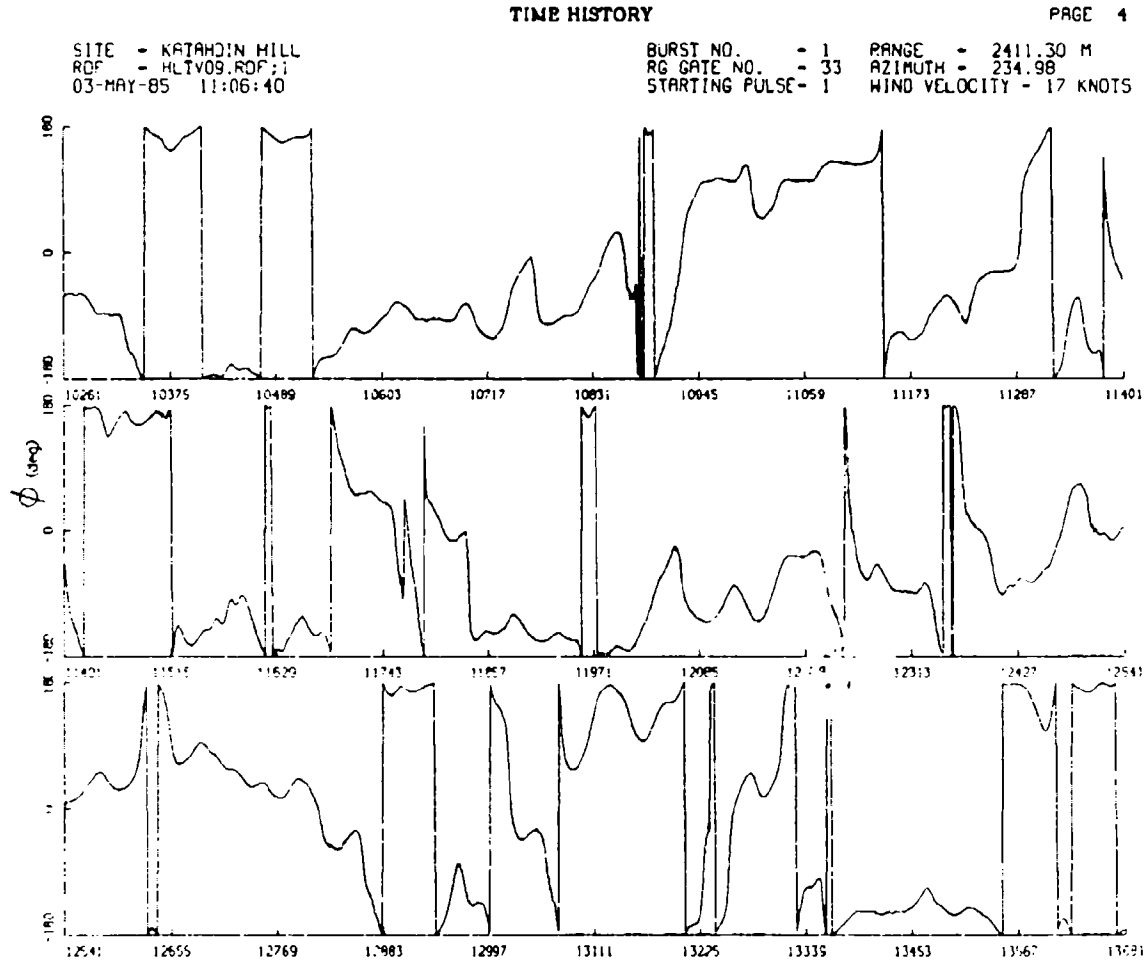

FIG. A.2 L-BAND RCS PHASE TIME HISTORY FROM WIND-BLOWN FOLIAGE ON A WINDY DAY, PULSE-BY-PULSE OVER 30,720 PULSES.

Continued...

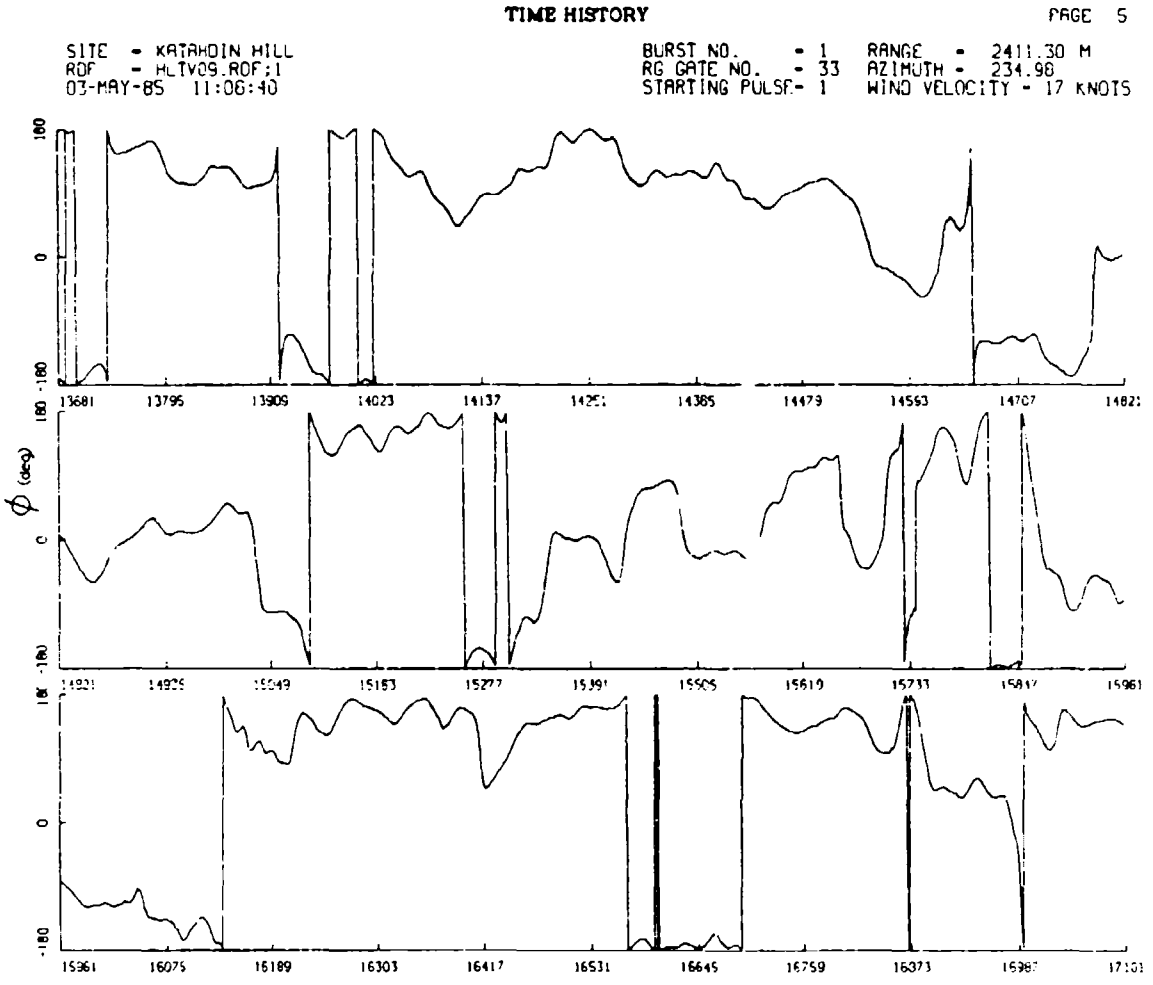

FIG. A.2 L-BAND RCS PHASE TIME HISTORY FROM WIND-BLOWN FOLIAGE ON A WINDY DAY, PULSE-BY-PULSE OVER 30,720 PULSES.

Continued...

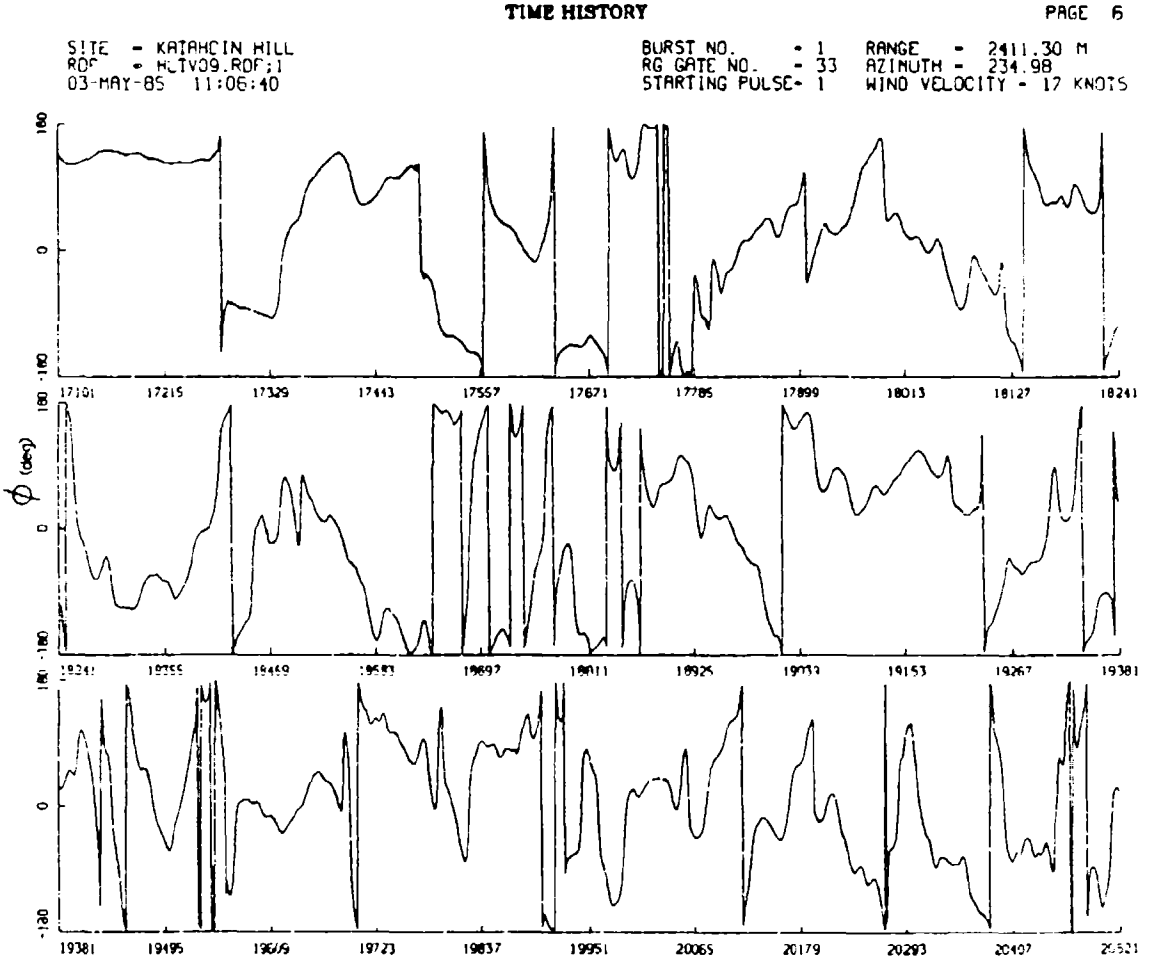

FIG. A.2 L-BAND RCS PHASE TIME HISTORY FROM WIND-BLOWN FOLIAGE ON A WINDY DAY, PULSE-BY-PULSE OVER 30,720 PULSES.

Continued...

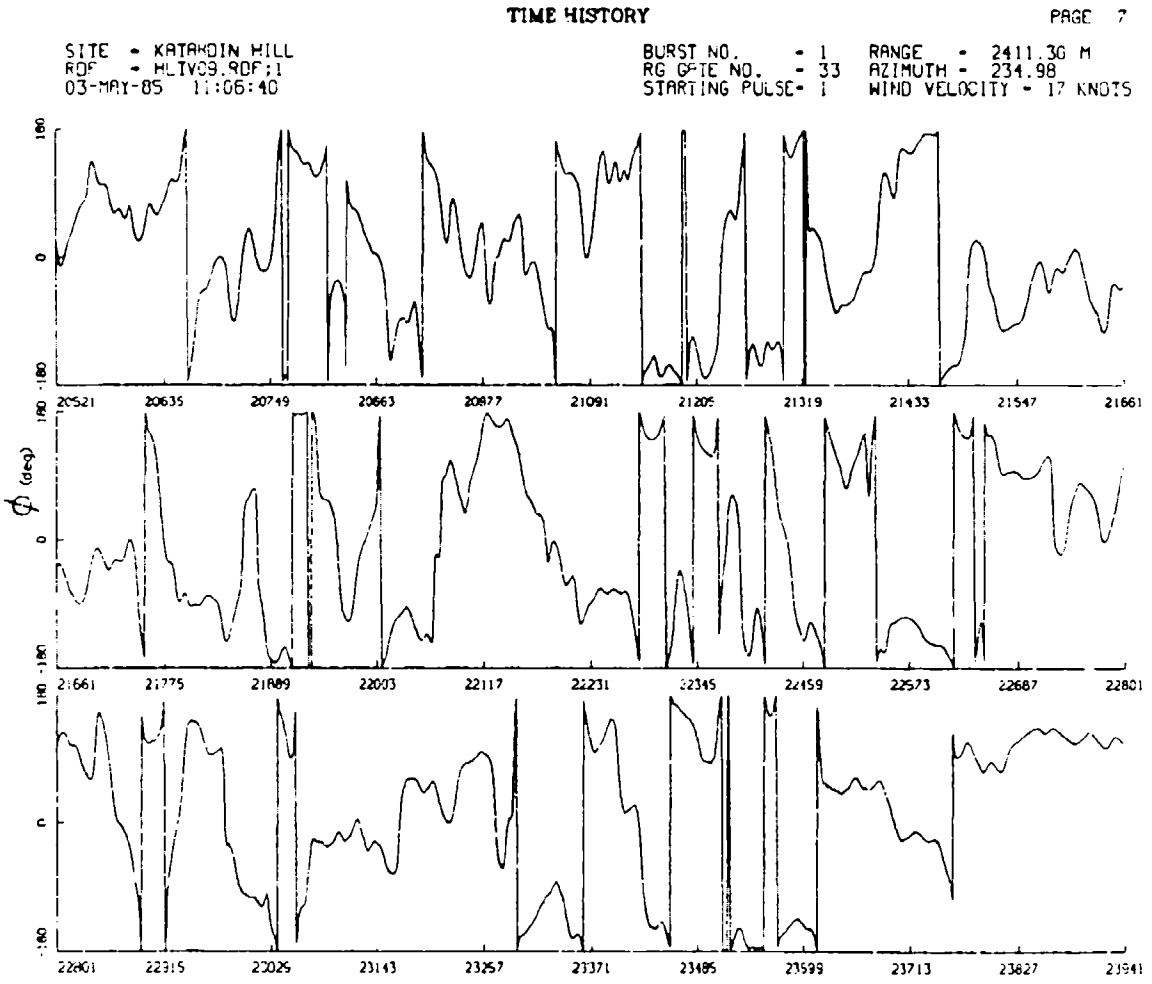

FIG. A.2 L-BAND RCS PHASE TIME HISTORY FROM WIND-BLOWN FOLIAGE ON A WINDY DAY, PULSE-BY-PULSE OVER 30,720 PULSES.

Continued...

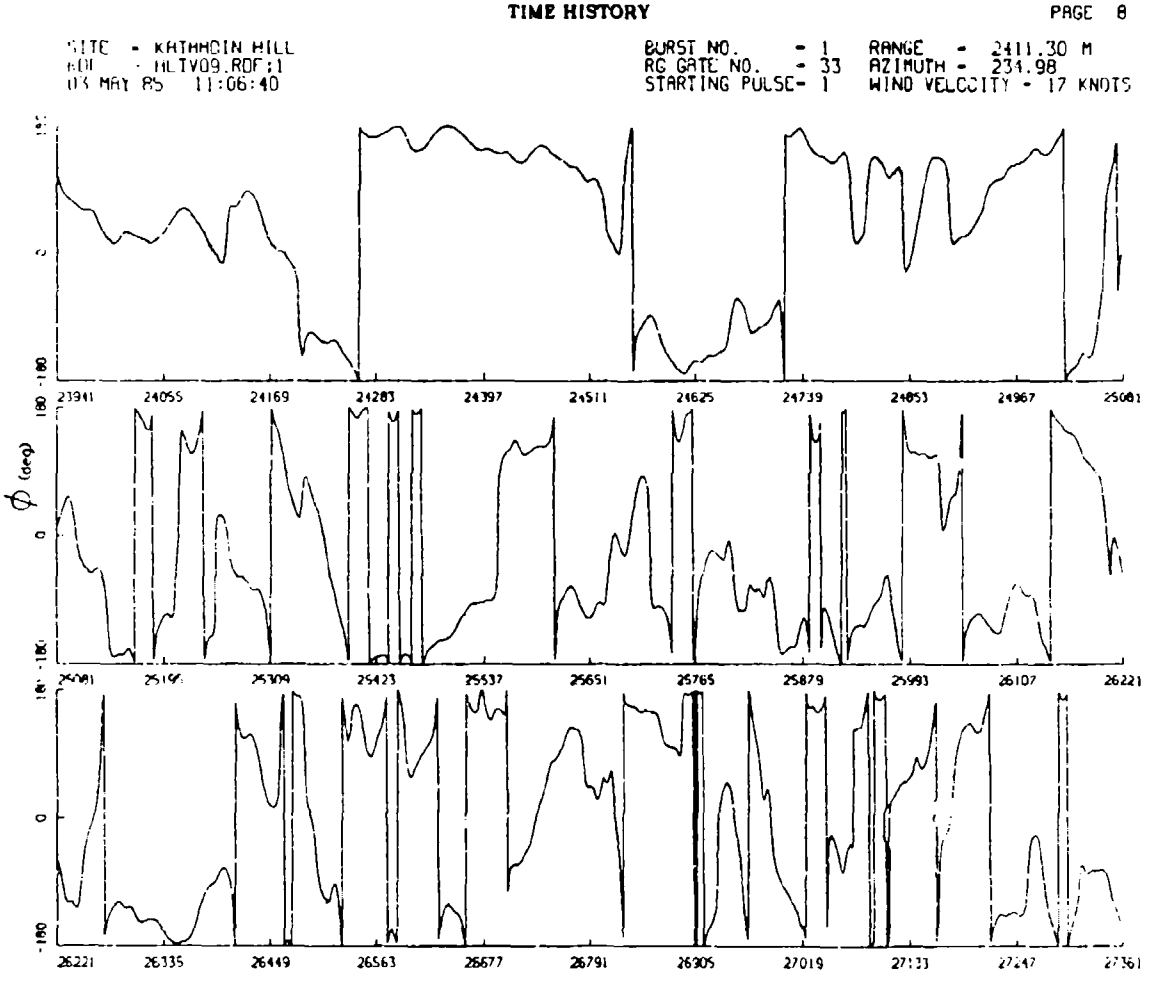

FIG. A.2 L-BAND RCS PHASE TIME HISTORY FROM WIND-BLOWN FOLIAGE ON A WINDY DAY, PULSE-BY-PULSE OVER 30,720 PULSES.

Continued...

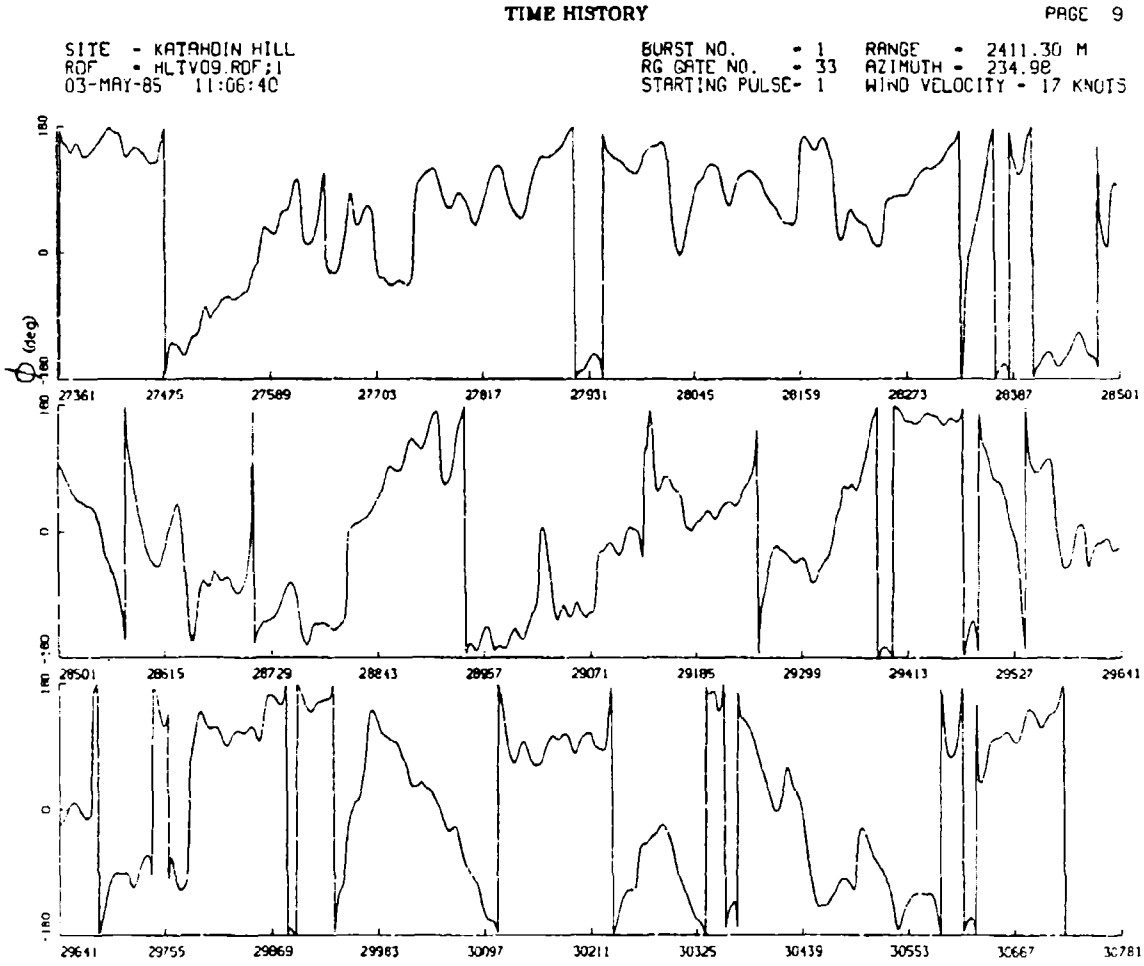

FIG. A.2 L-BAND RCS PHASE TIME HISTORY FROM WIND-BLOWN FOLIAGE ON A WINDY DAY, PULSE-BY-PULSE OVER 30,720 PULSES.

Concluded.

A.4 OVERALL SPECTRUM

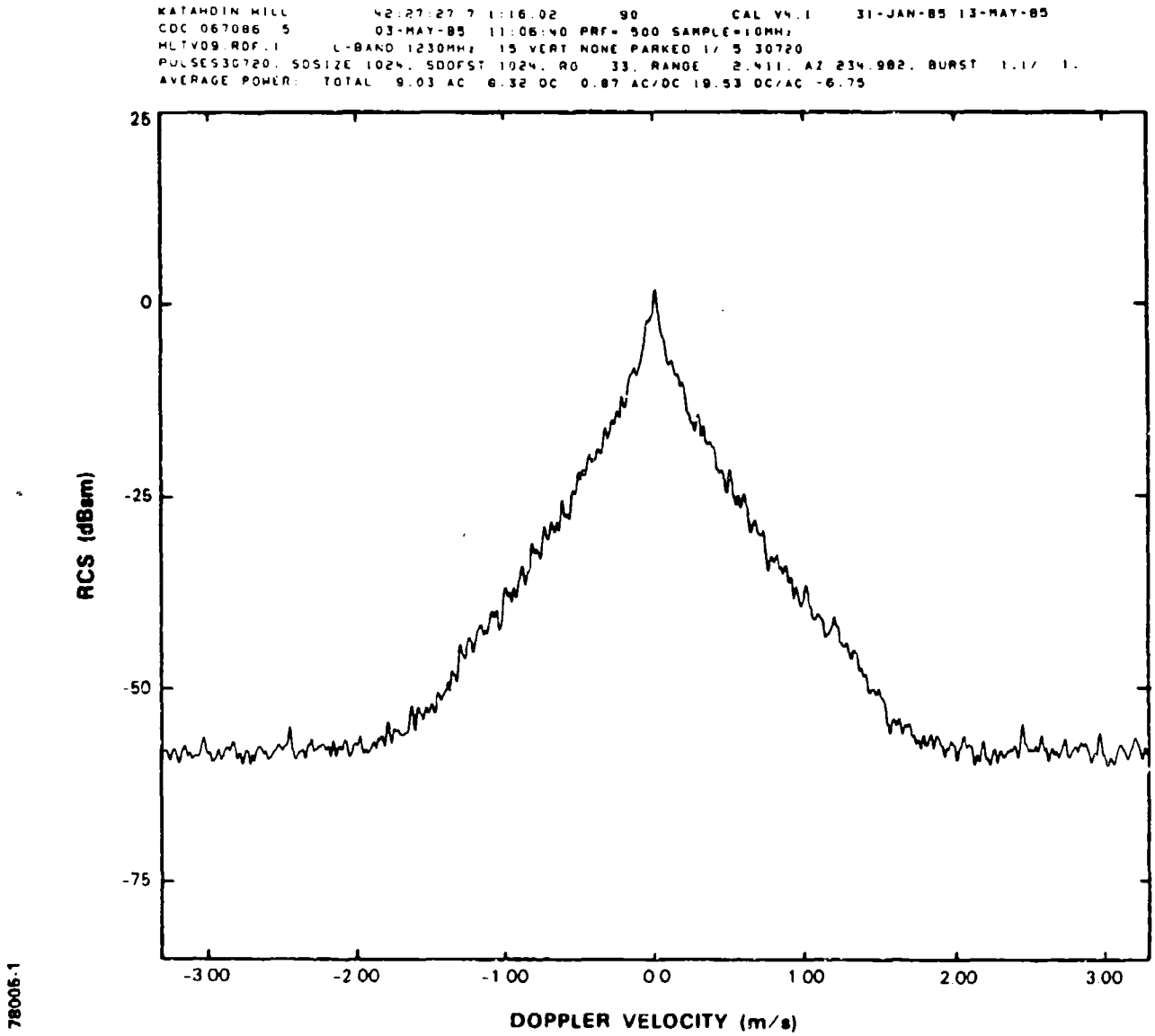

FIG. A.3 RESULTANT OVERALL SPECTRUM INVOLVING 30,720 PULSES. This result is the average of the 30 individual spectra shown in Sect. A.5.

A.5 THIRTY INDIVIDUAL SPECTRA

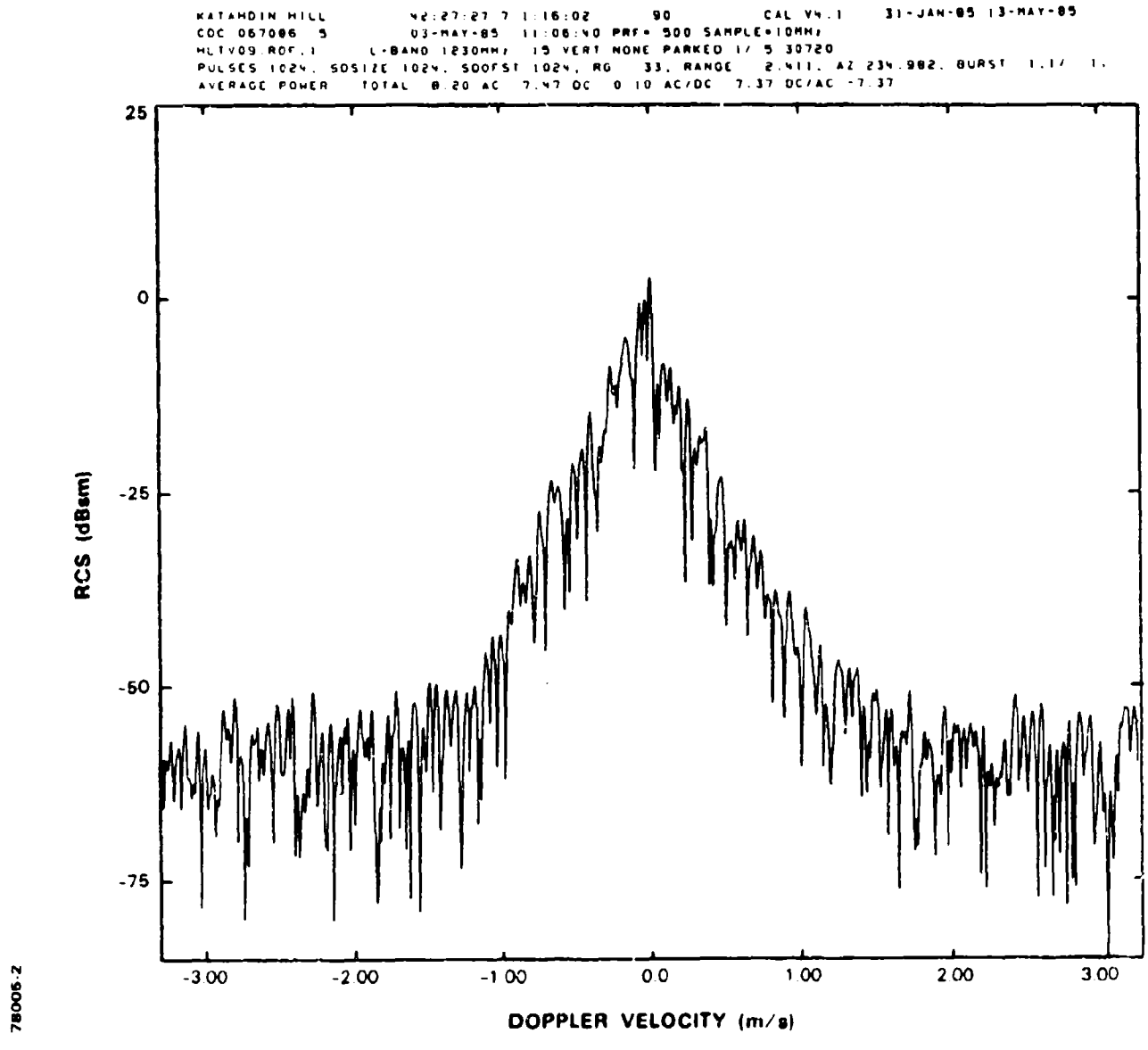

FIG. A.4 INDIVIDUAL SPECTRUM FOR 1ST GROUP OF 1024 PULSES.

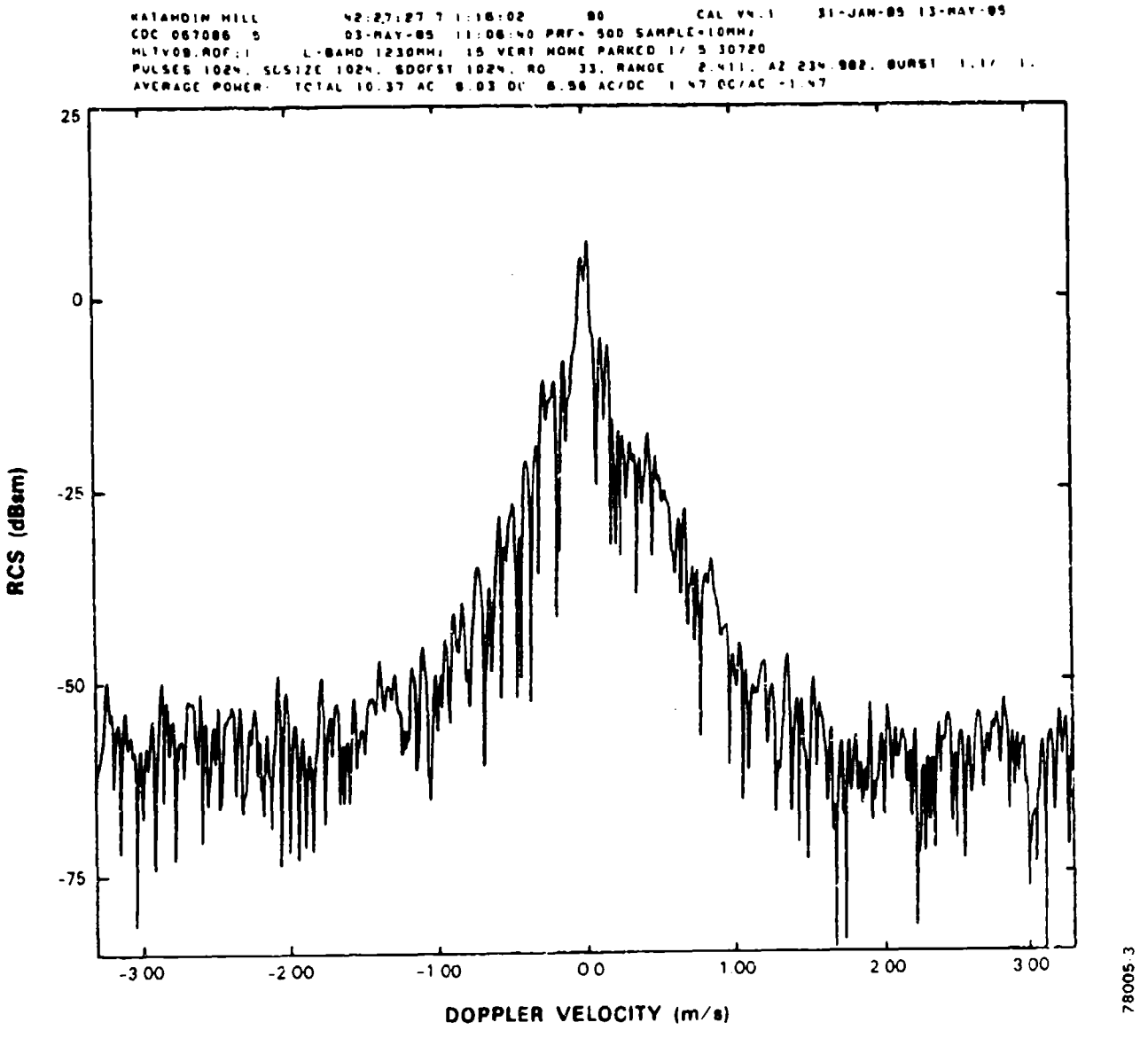

FIG. 4.5 INDIVIDUAL SPECTRUM FOR 2ND GROUP OF 1024 PULSES.

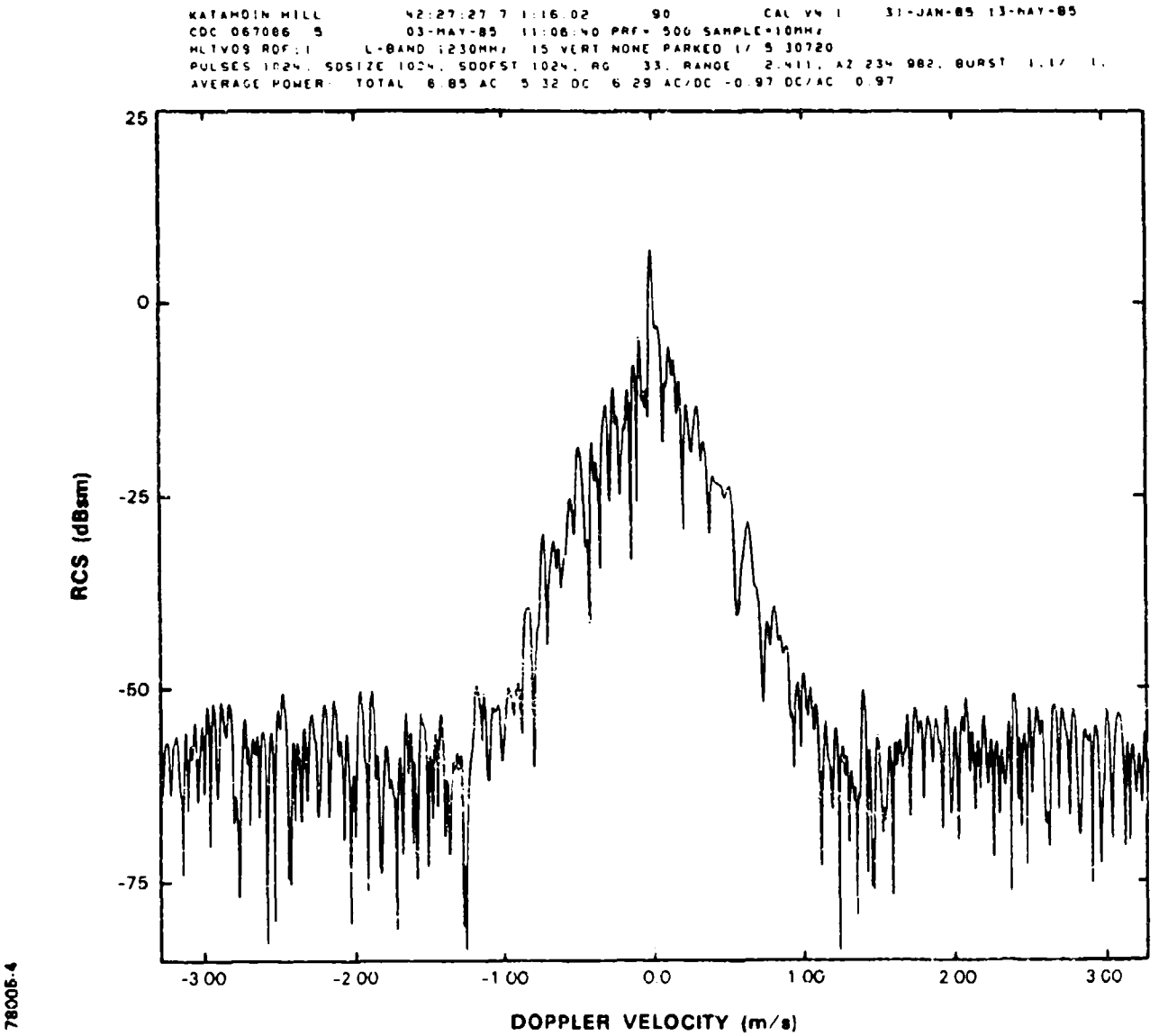

FIG. A.6 INDIVIDUAL SPECTRUM FOR 3RD GROUP OF 1024 PULSES.

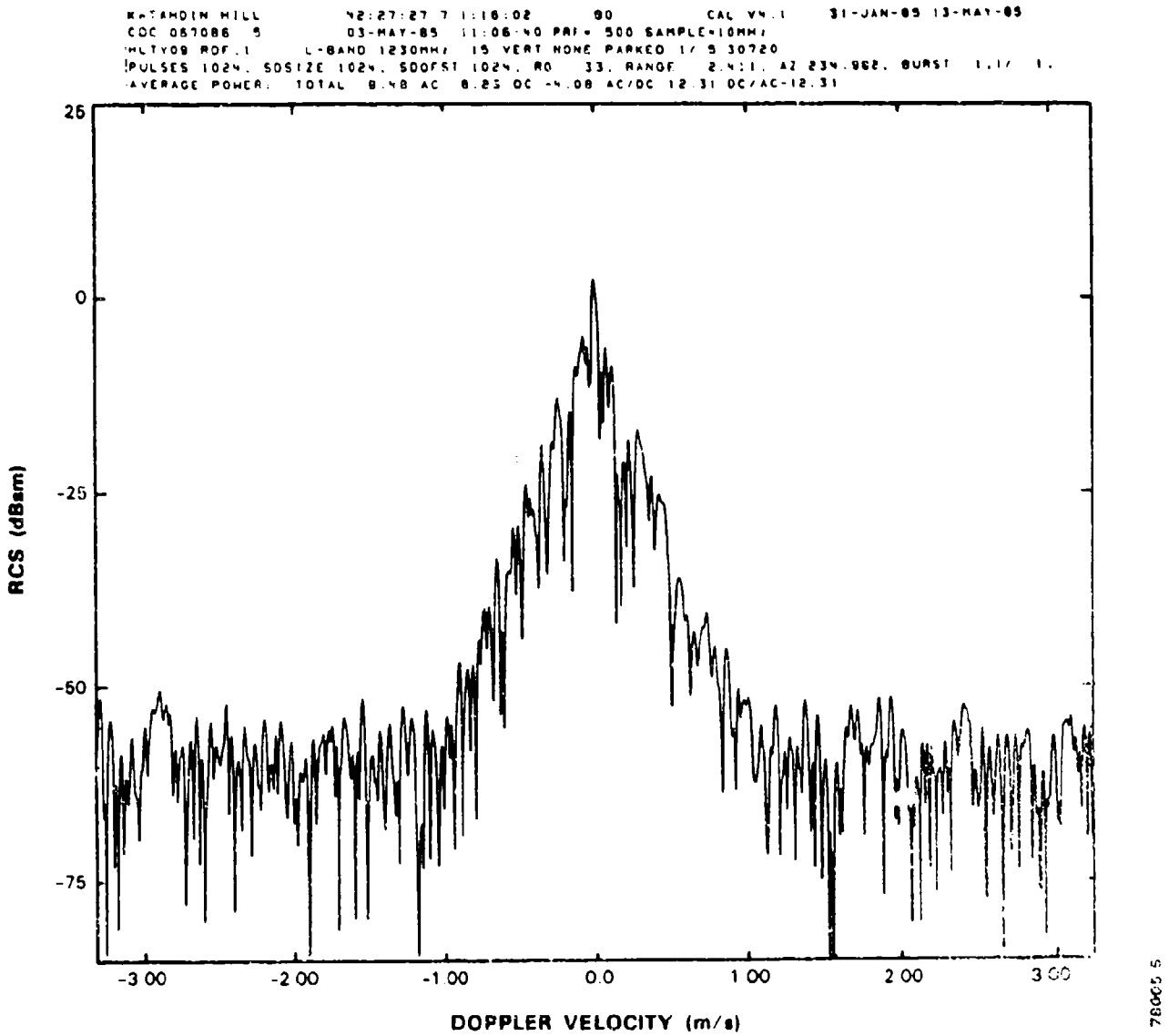

FIG. A.7 INDIVIDUAL SPECTRUM FOR 4TH GROUP OF 1024 PULSES.

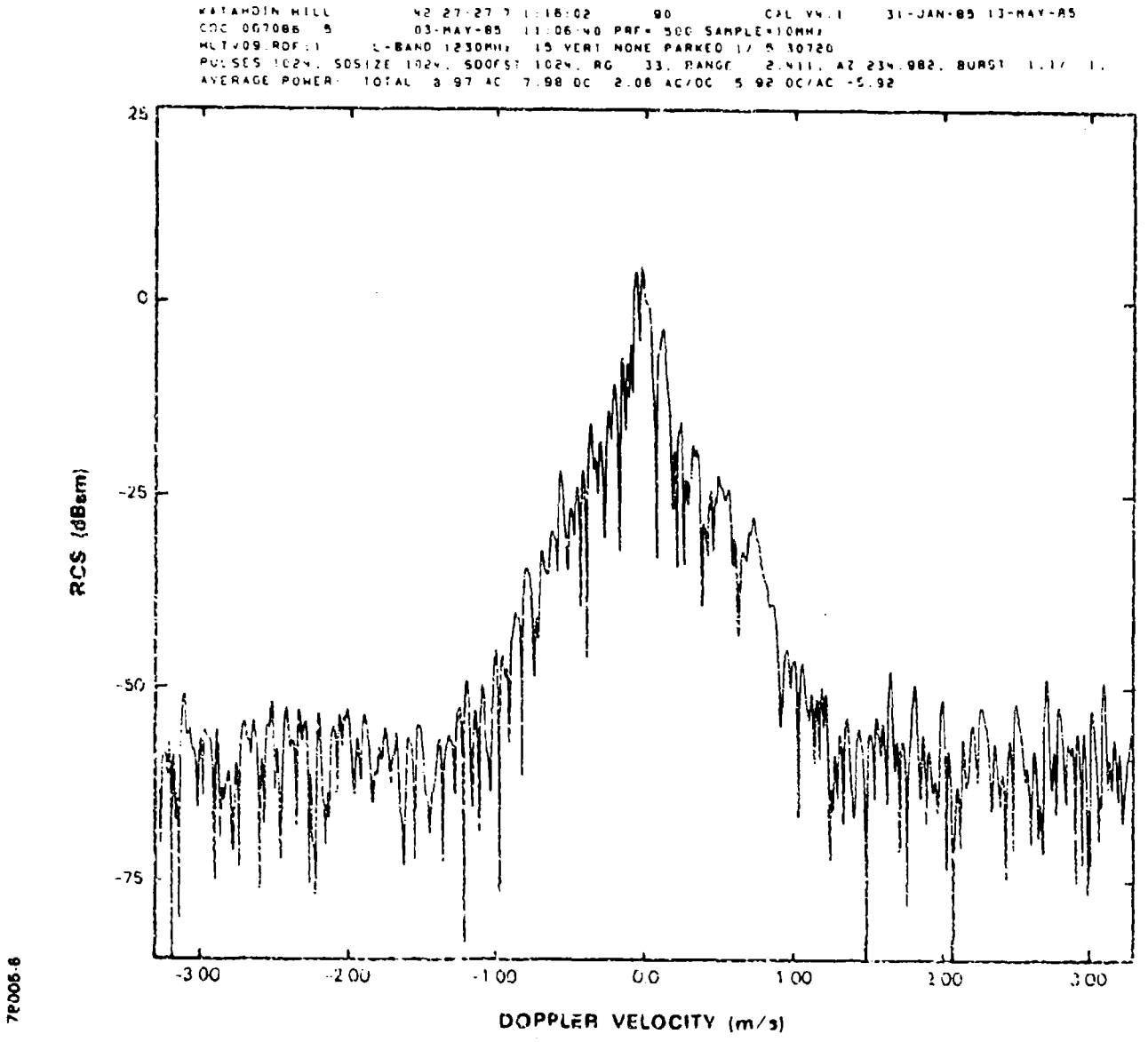

FIG. A.8 INDIVIDUAL SPECTRUM FOR 5TH GROUP OF 1024 PULSES.

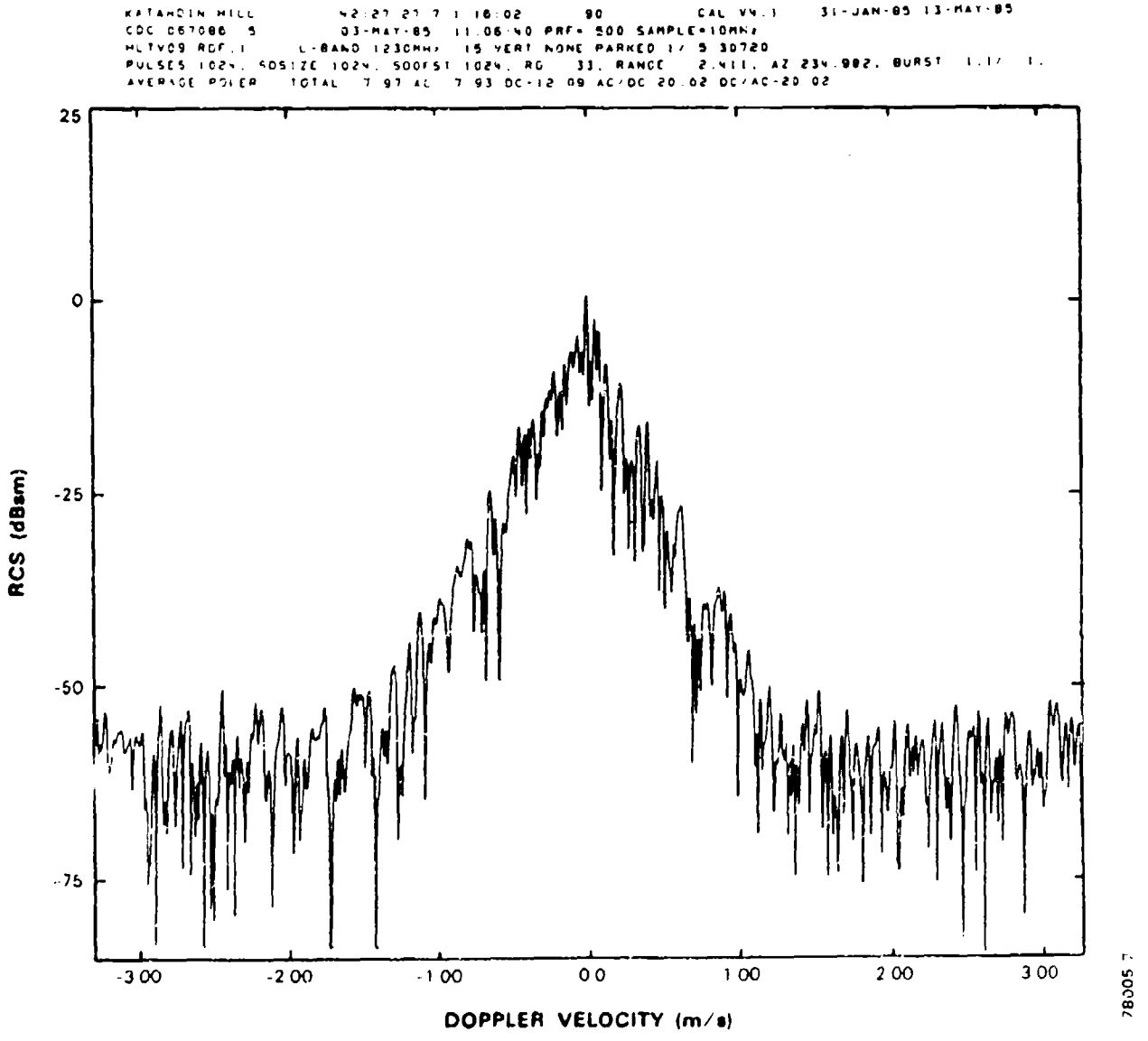

FIC. A.9 INDIVIDUAL SPECTRUM FOR 6TH GROUP OF 1024 PULSES.

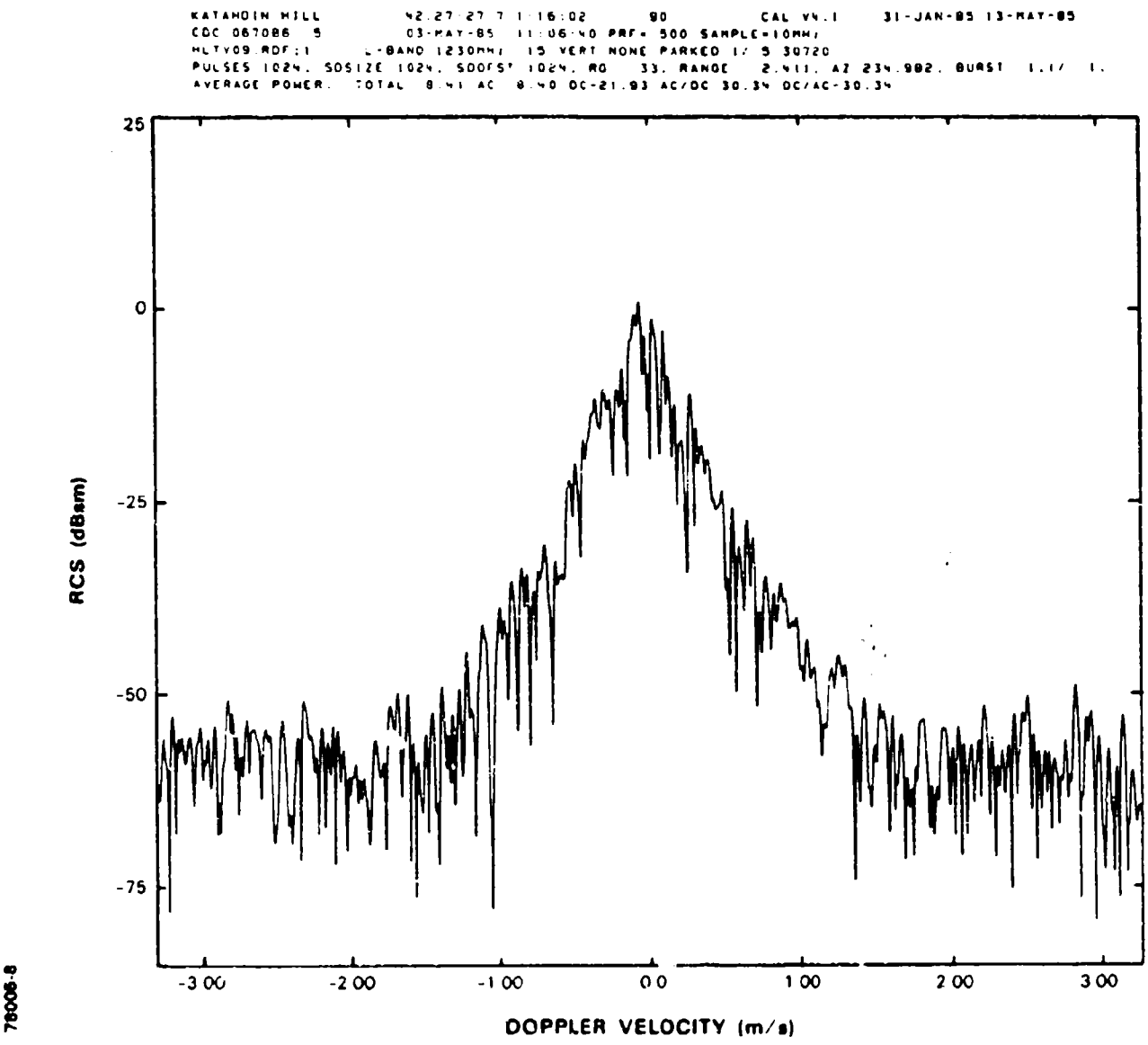

FIG. A.10 INDIVIDUAL SPECTRUM FOR 7TH GROUP OF 1024 PULSES.

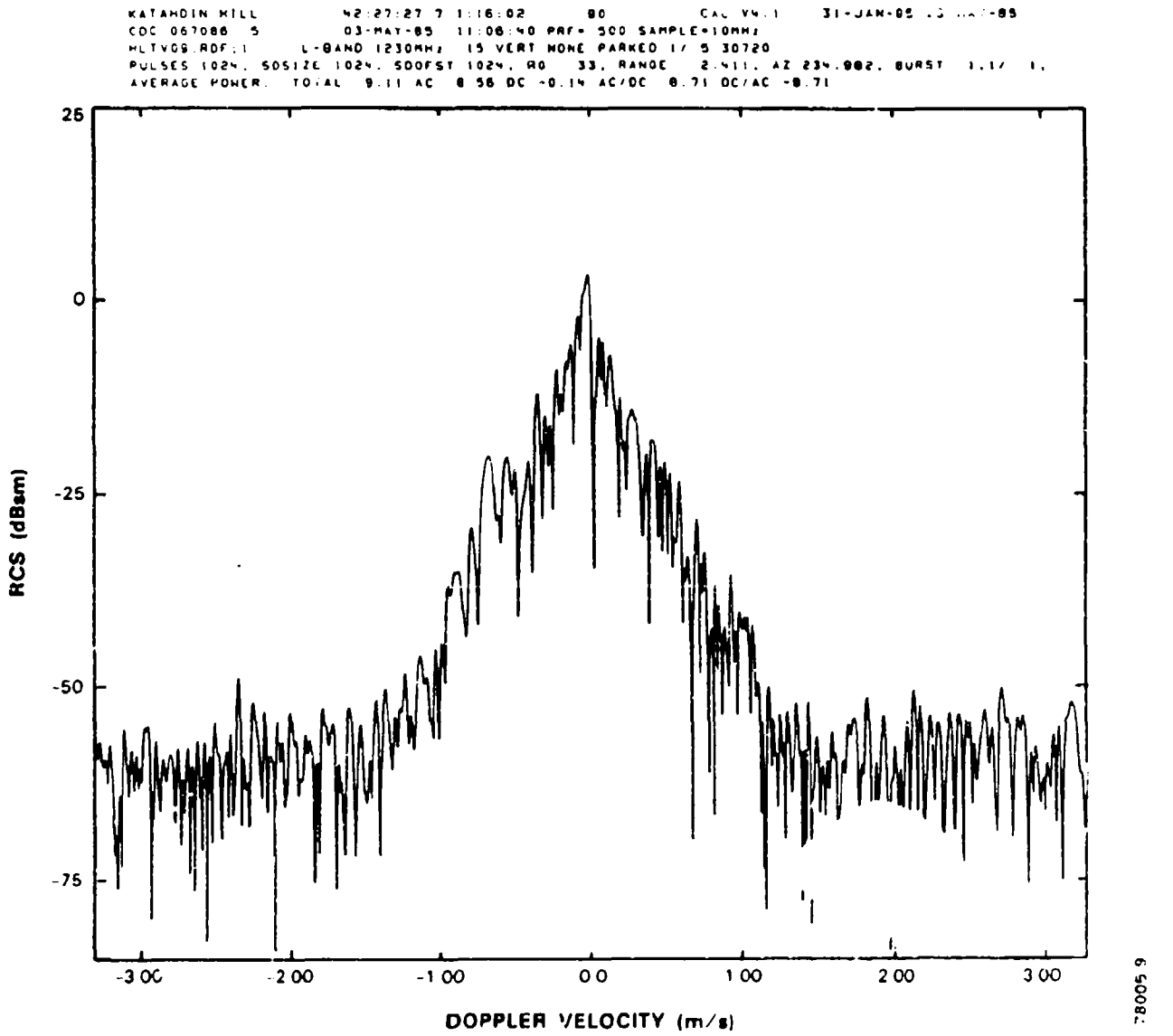

FIG. A.11 INDIVIDUAL SPECTRUM FOR 8TH GROUP OF 1024 PULSES.

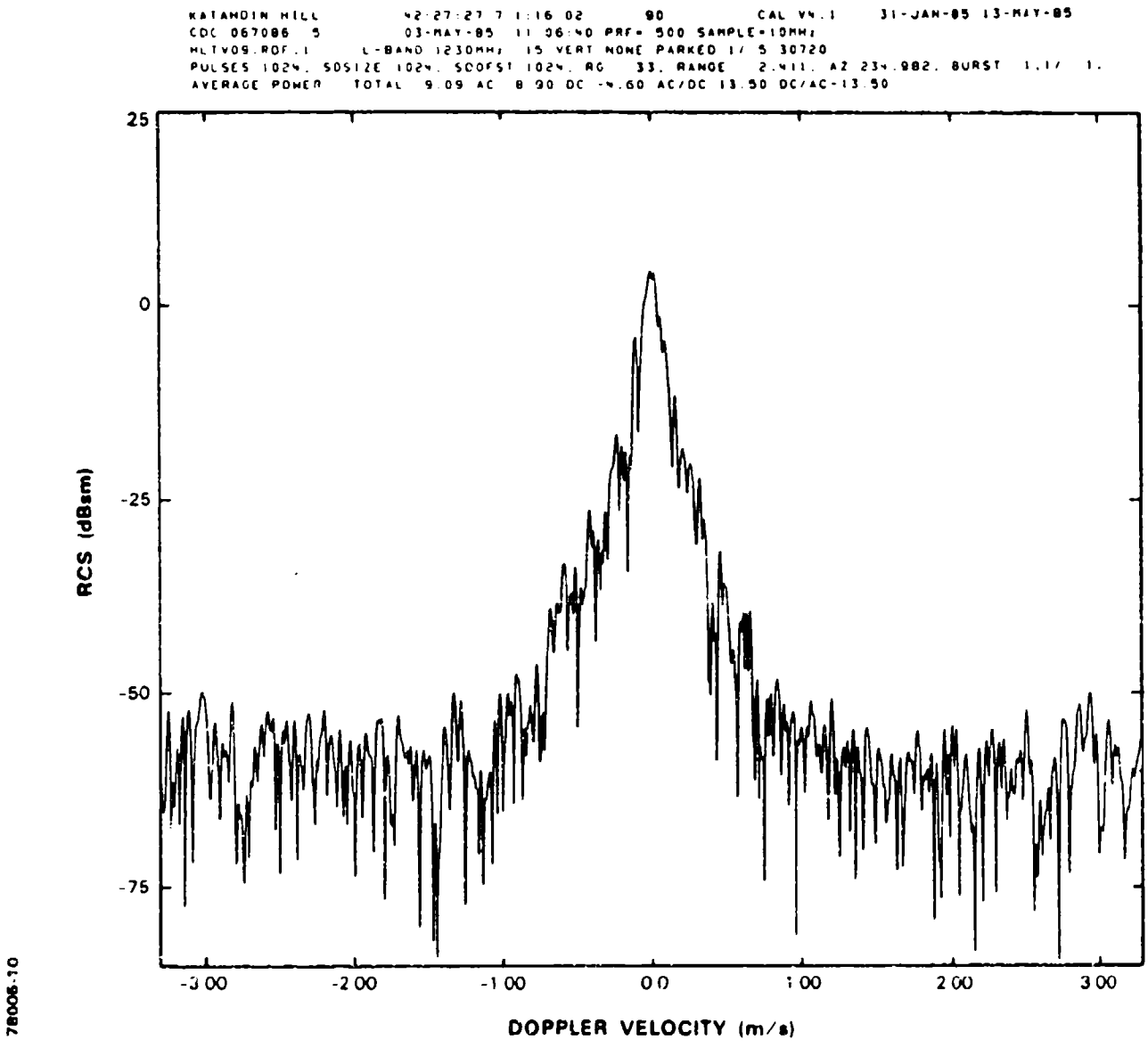

FIG. A.12 INDIVIDUAL SPECTRUM FOR 9TH GROUP OF 1024 PULSES.

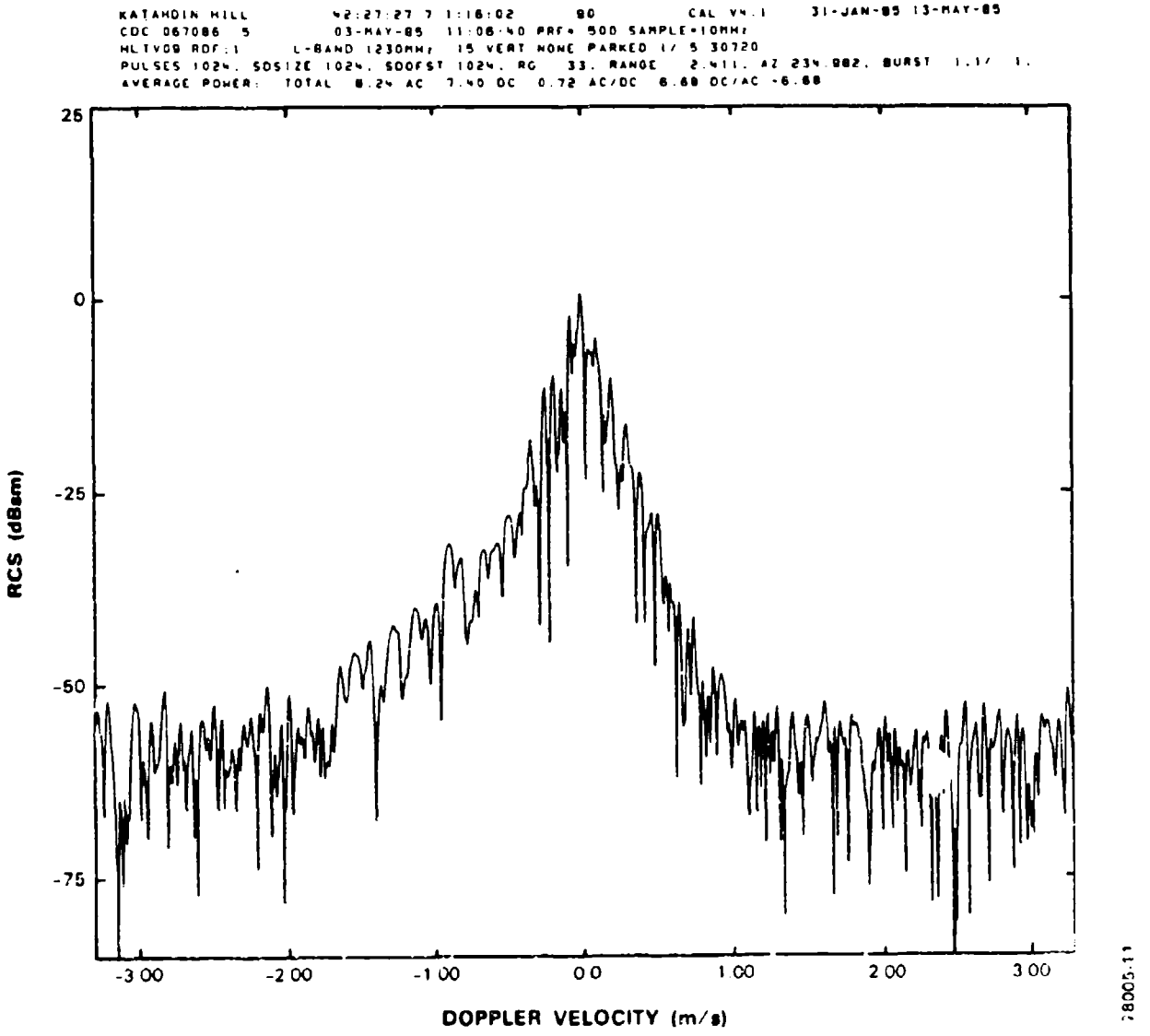

FIG. A.13 INDIVIDUAL SPECTRUM FOR 10TH GROUP OF 1024 PULSES.

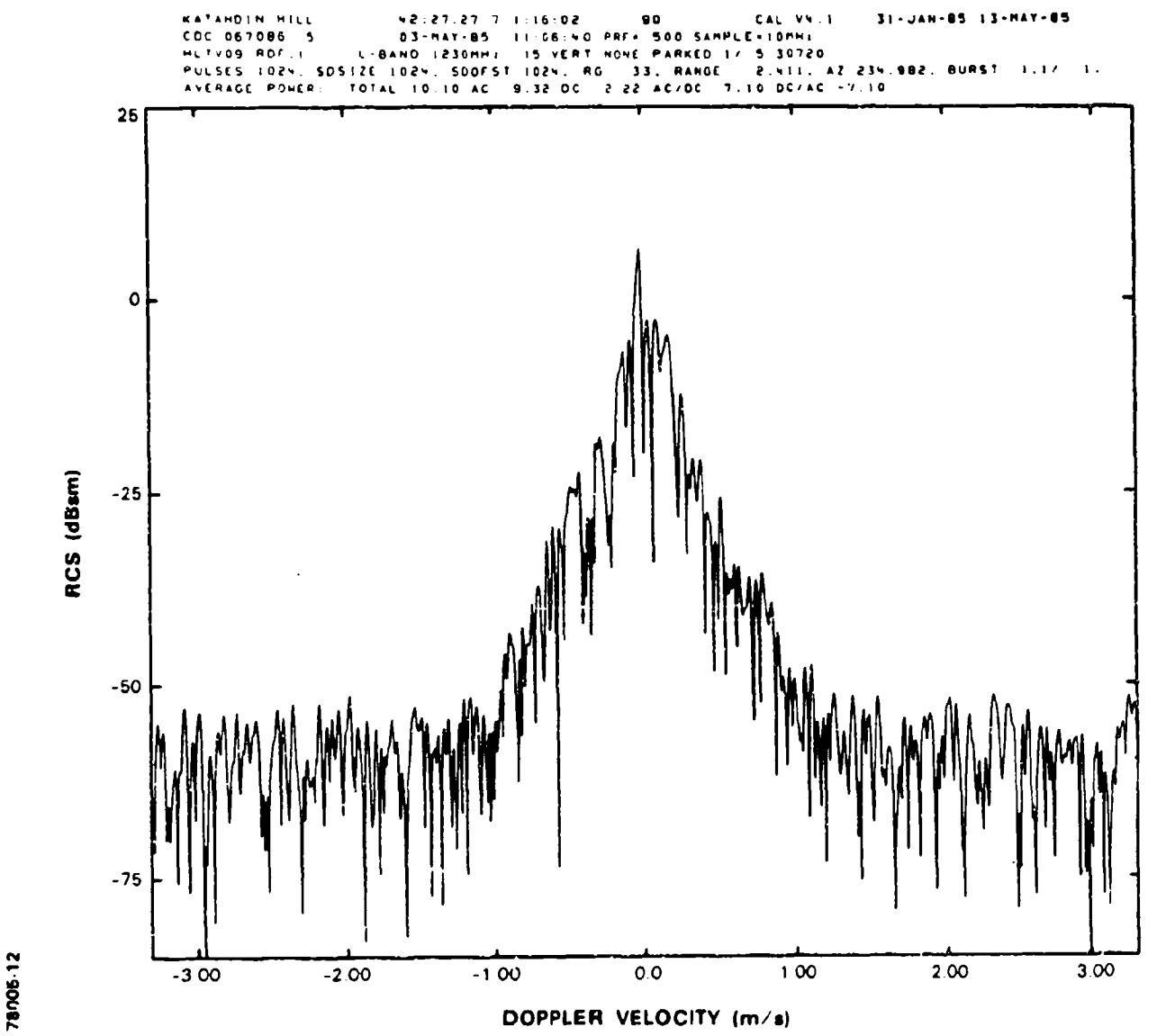

FIG. A.14 INDIVIDUAL SPECTRUM FOR 11TH GROUP OF 1024 PULSES.

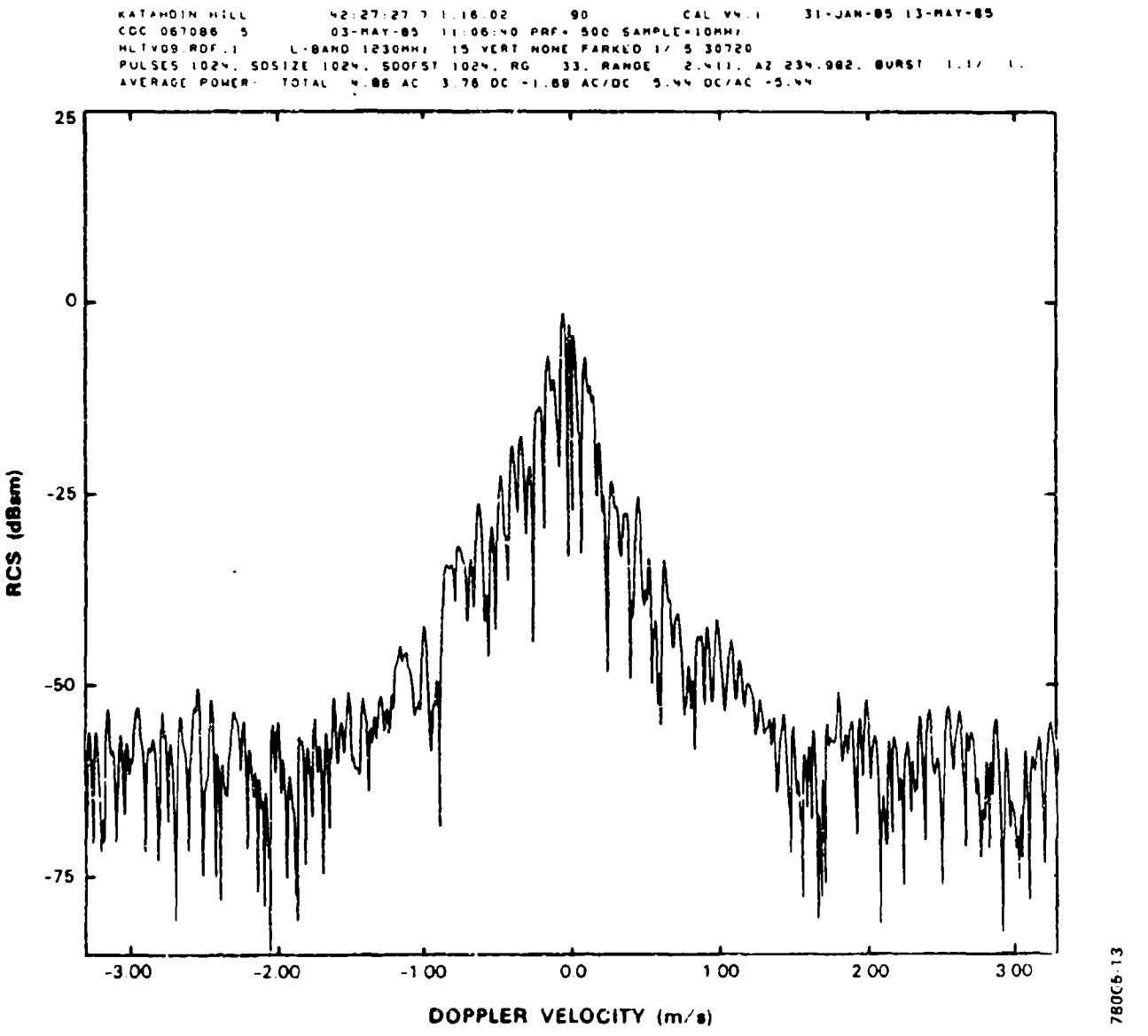

FIG. A.15 INDIVIDUAL SPECTRUM FOR 12TH GROUP OF 1024 PULSES.

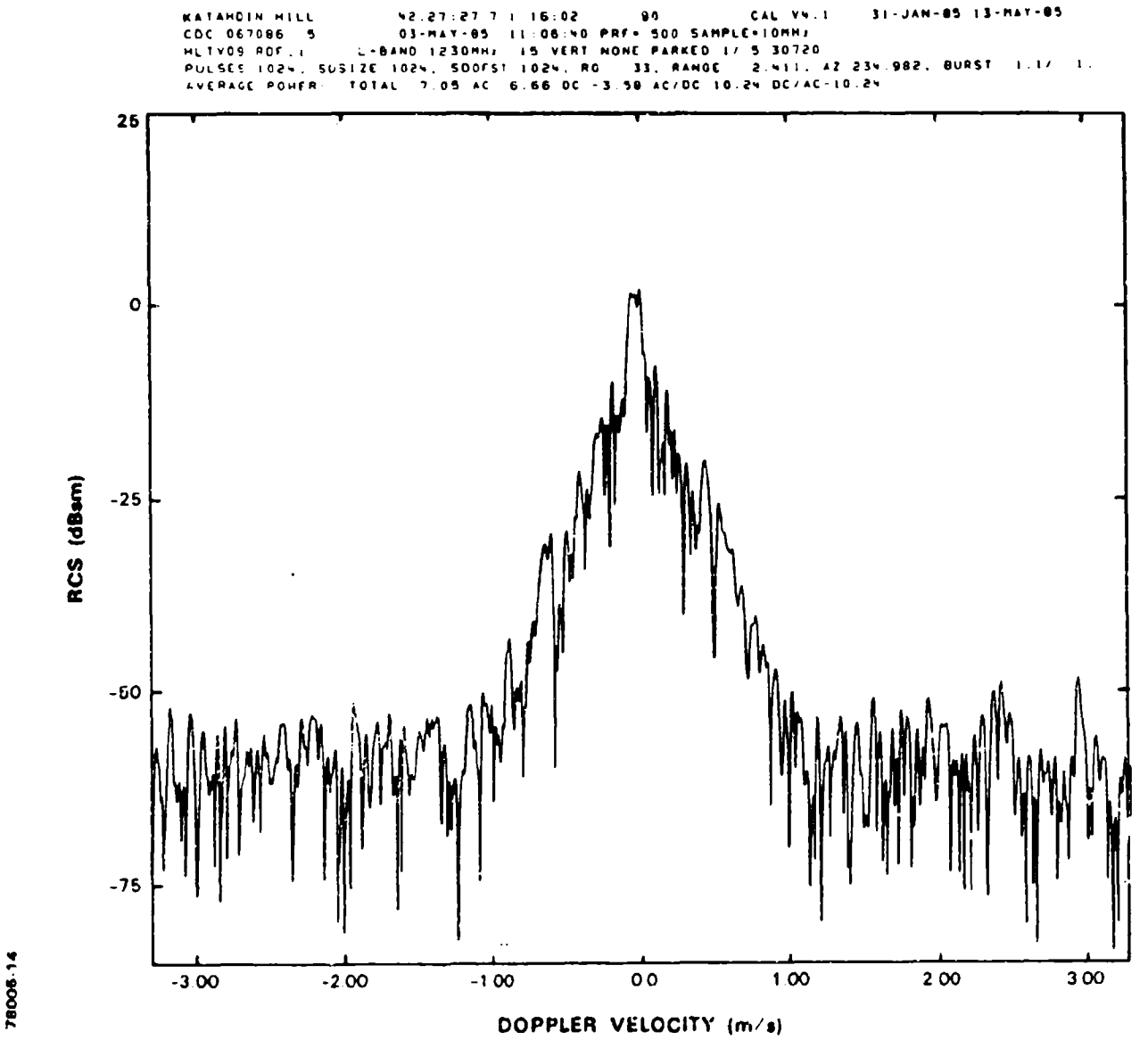

FIG. A.16 INDIVIDUAL SPECTRUM FOR 13TH GROUP OF 1024 PULSES.

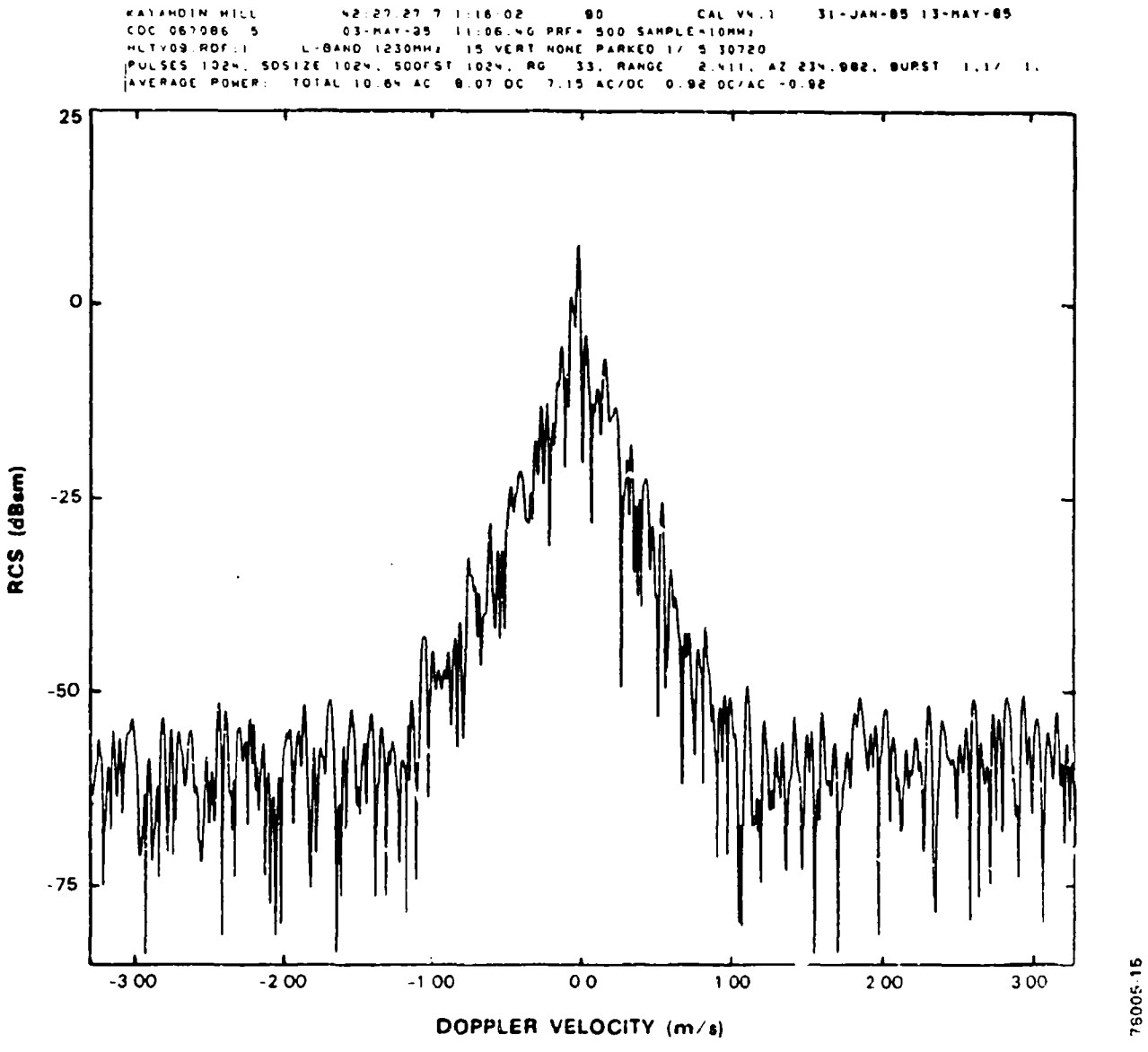

FIG. A.17 INDIVIDUAL SPECTRUM FOR 14TH GROUP OF 1024 PULSES.

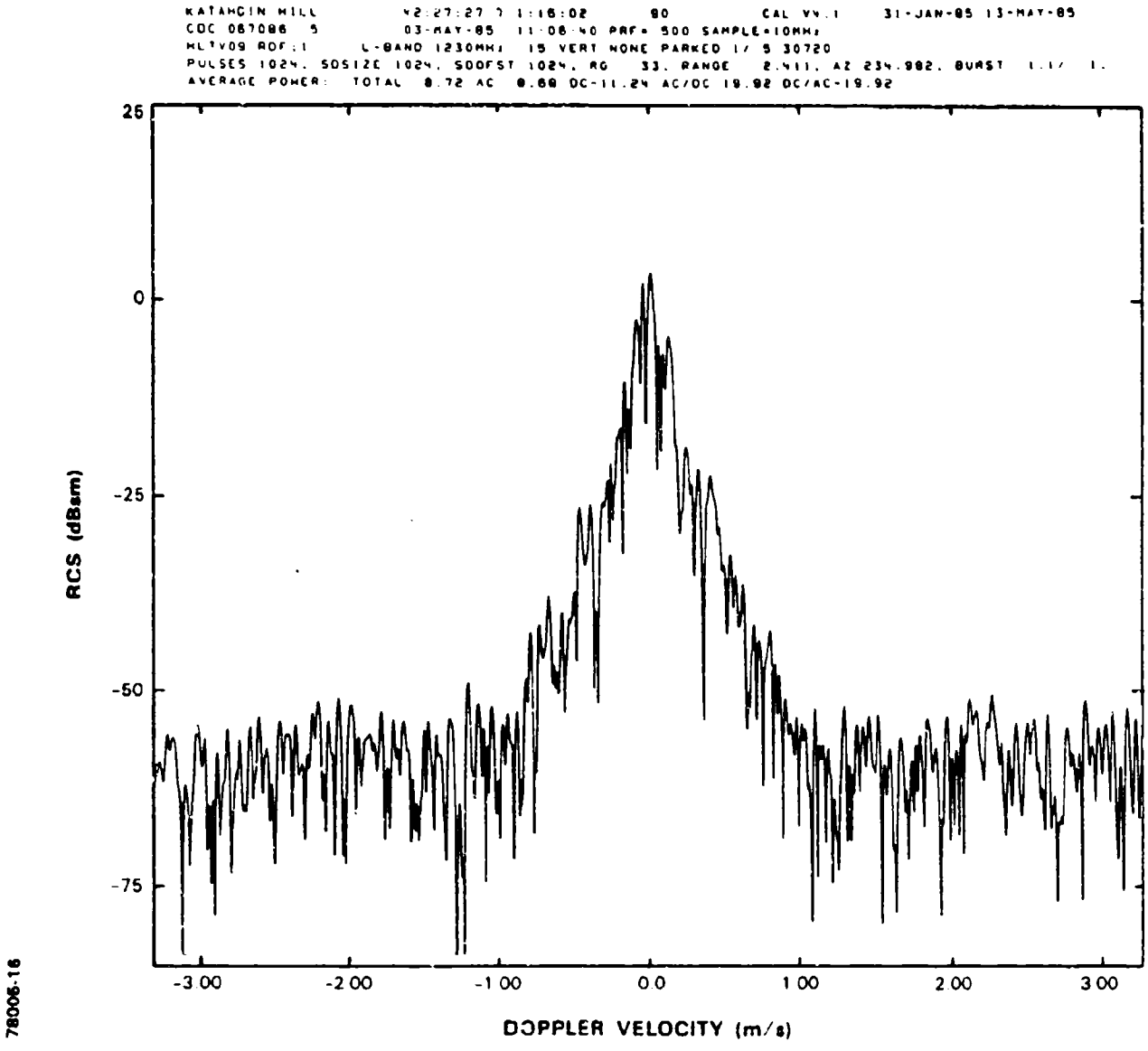

FIG. A.18 INDIVIDUAL SPECTRUM FOR 15TH GROUP OF 1024 PULSES.

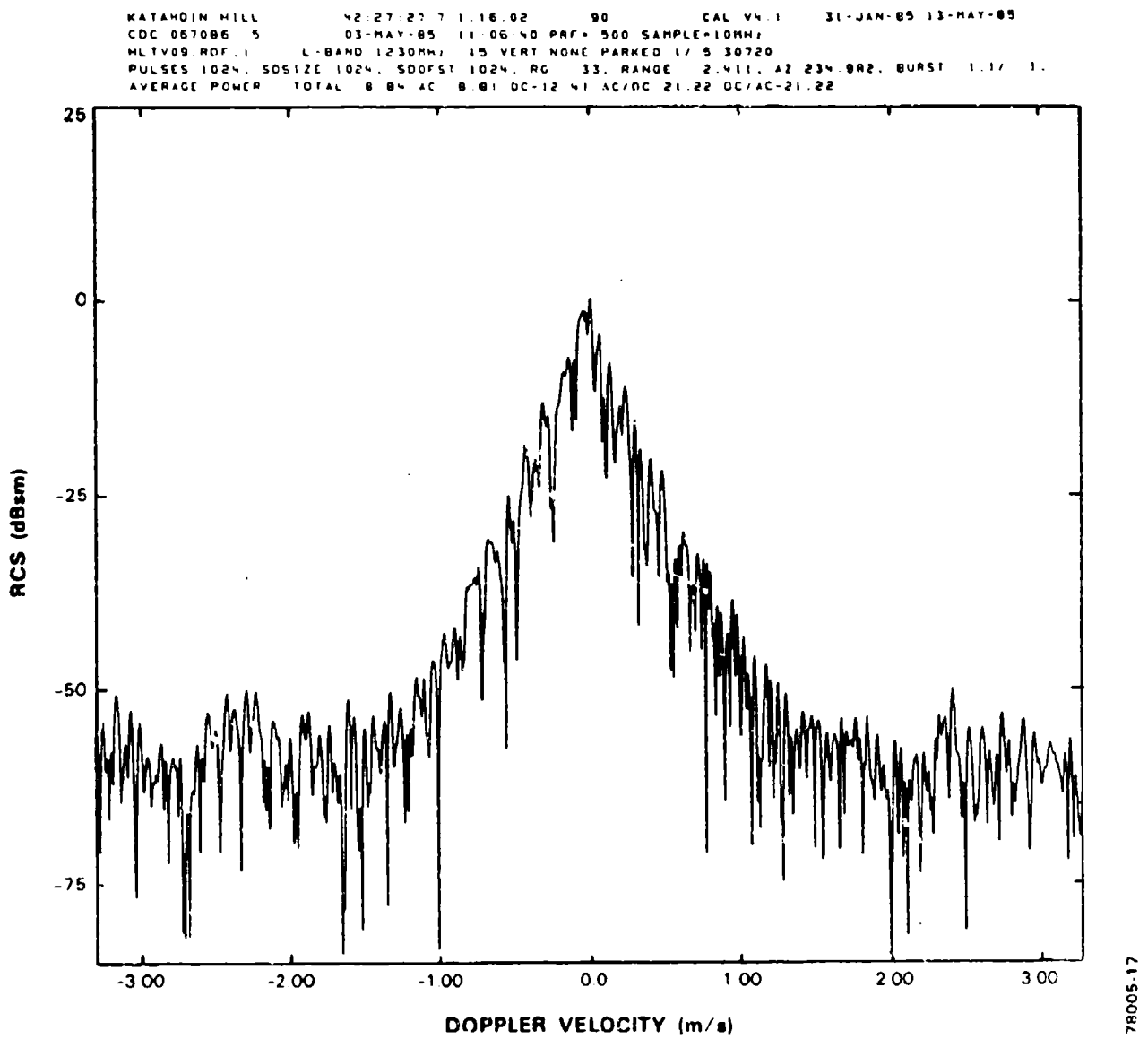

FIG. A.19 INDIVIDUAL SPECTRUM FOR 16TH GROUP OF 1024 PULSES.

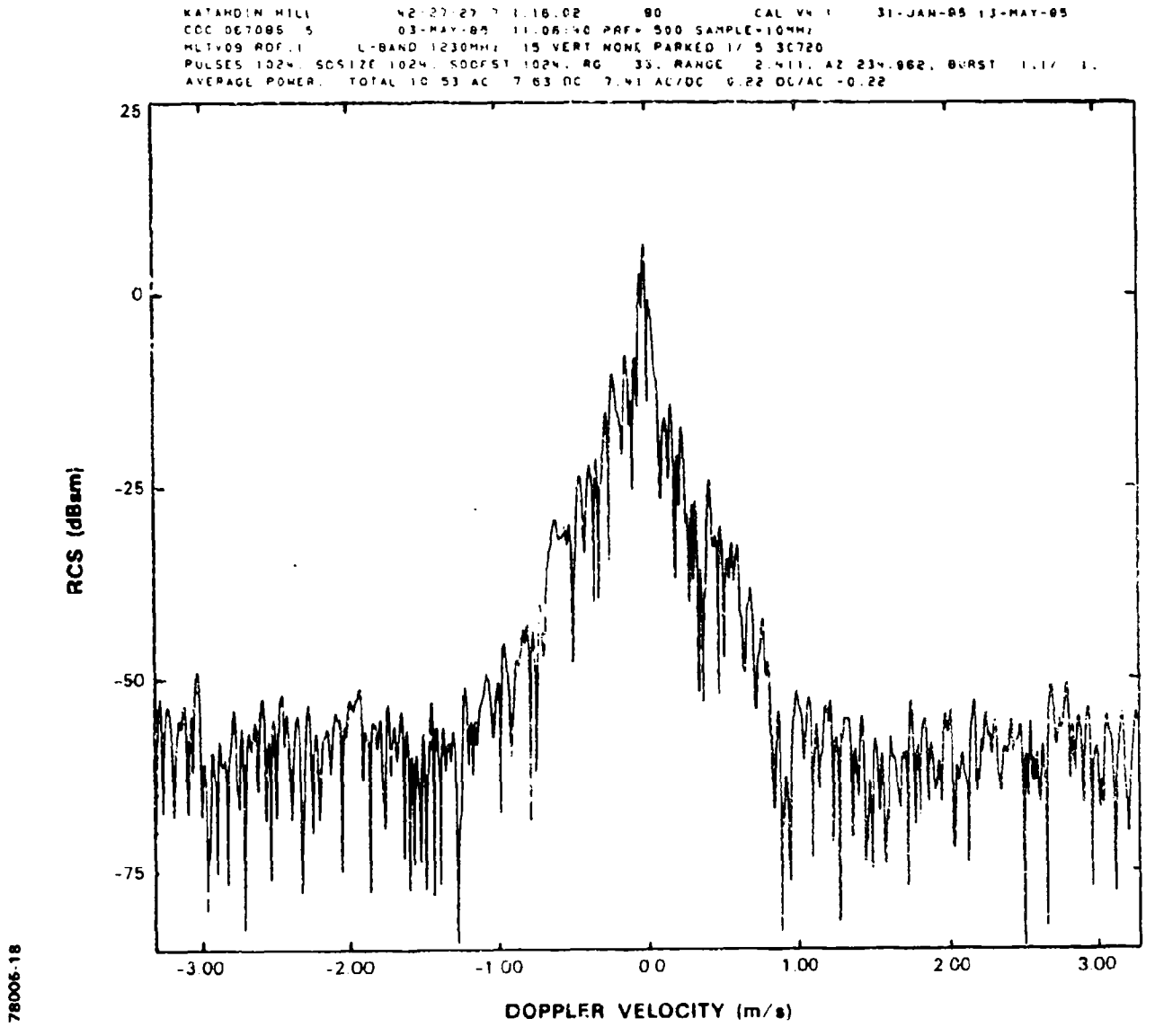

FIG. A.20 INDIVIDUAL SPECTRUM FOR 17TH GROUP OF 1024 PULSES.

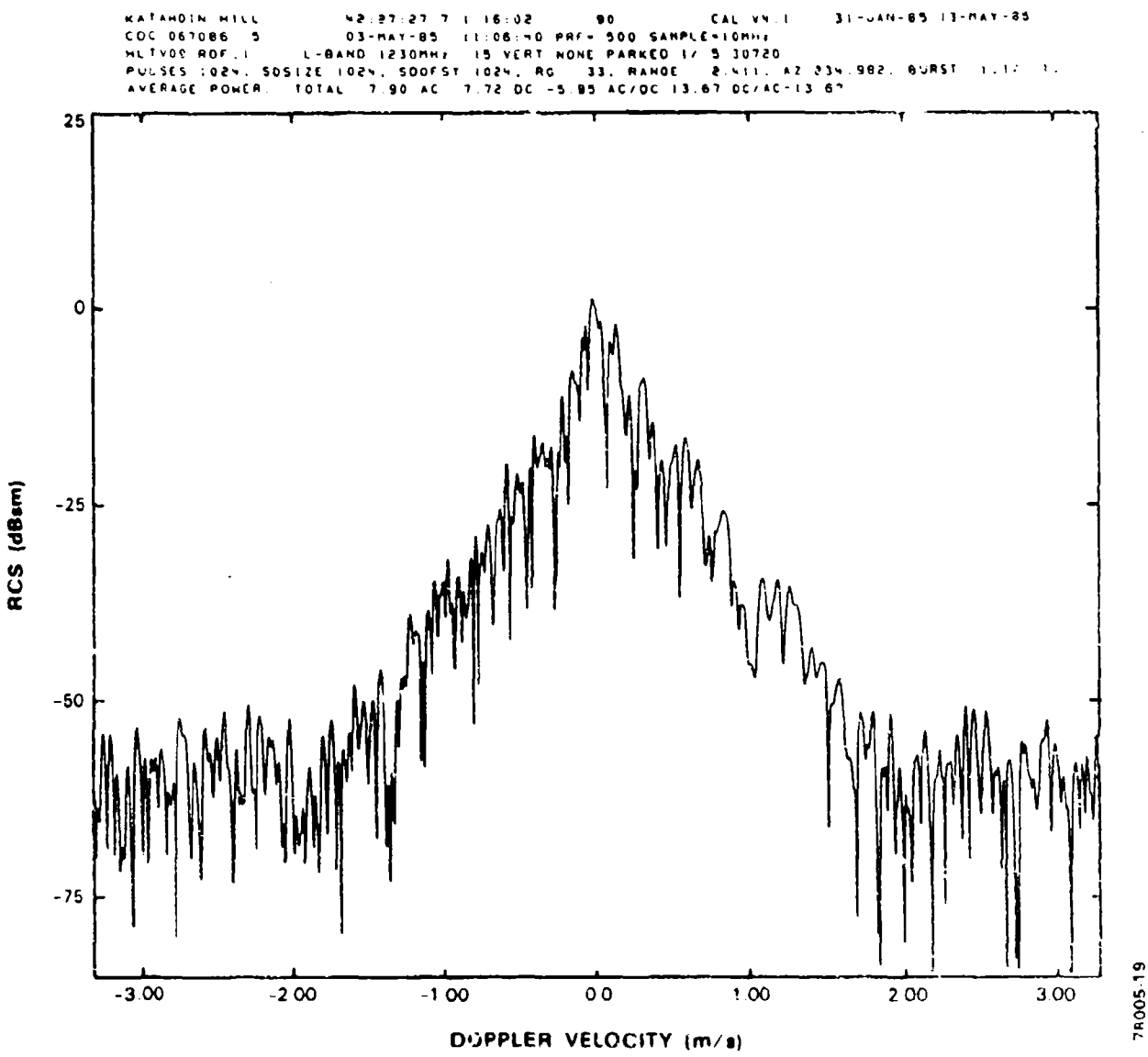

FIG. A.21 INDIVIDUAL SPECTRUM FOR 18TH GROUP OF 1024 PULSES.

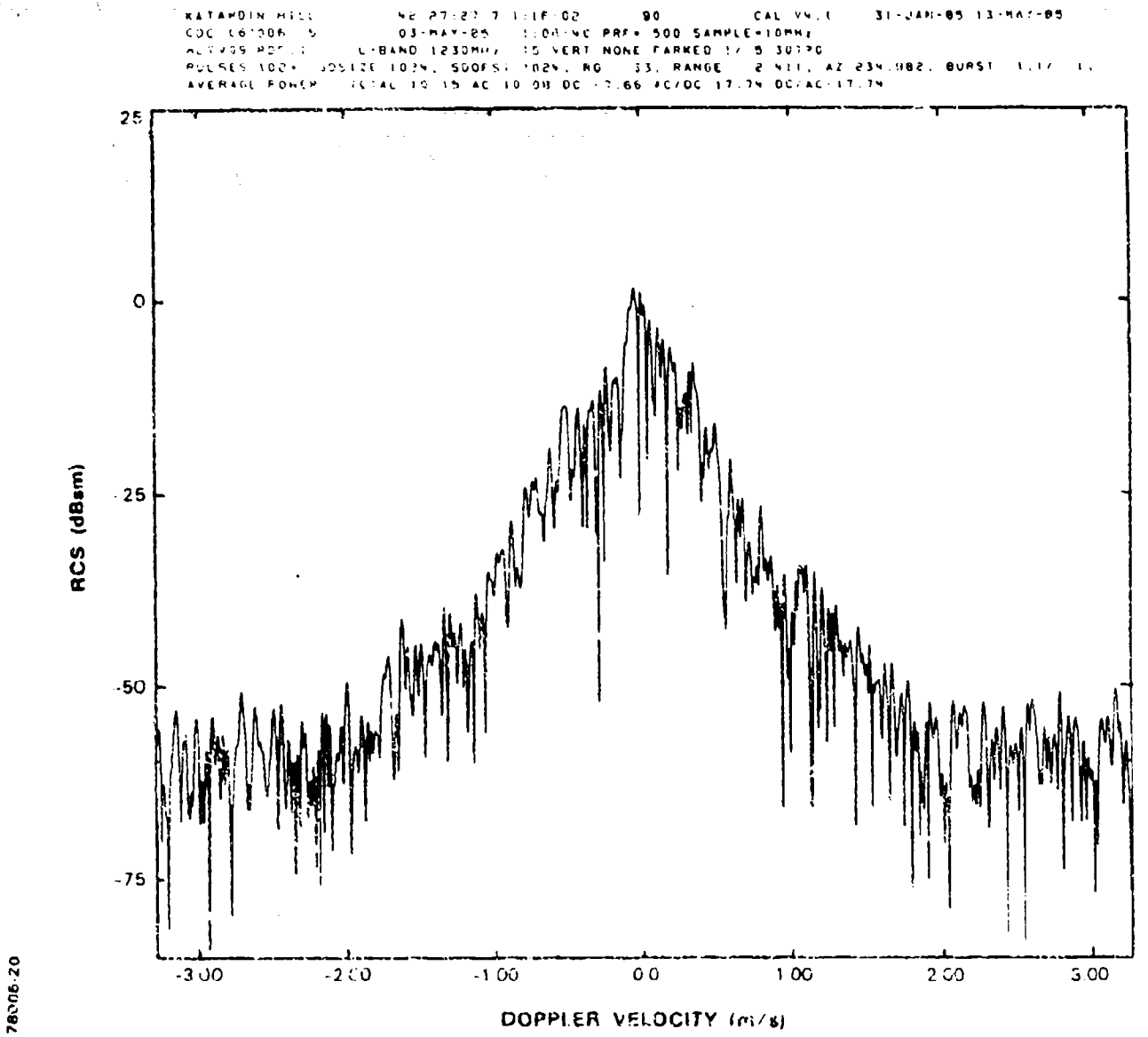

FIG. A.22 INDIVIDUAL SPECTRUM FOR 19TH GROUP OF 1024 PULSES.

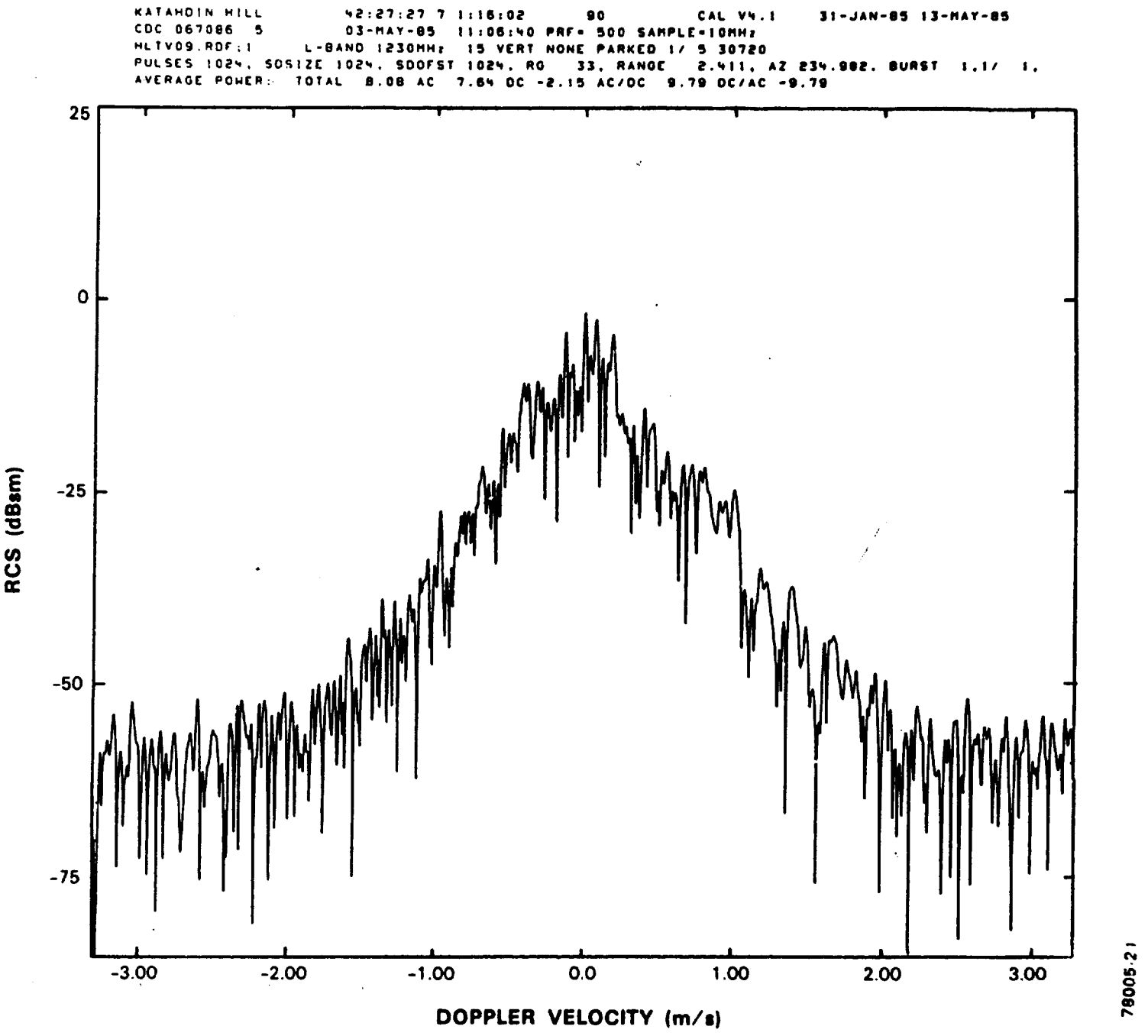

FIG. A.23 INDIVIDUAL SPECTRUM FOR 20TH GROUP OF 1024 PULSES.

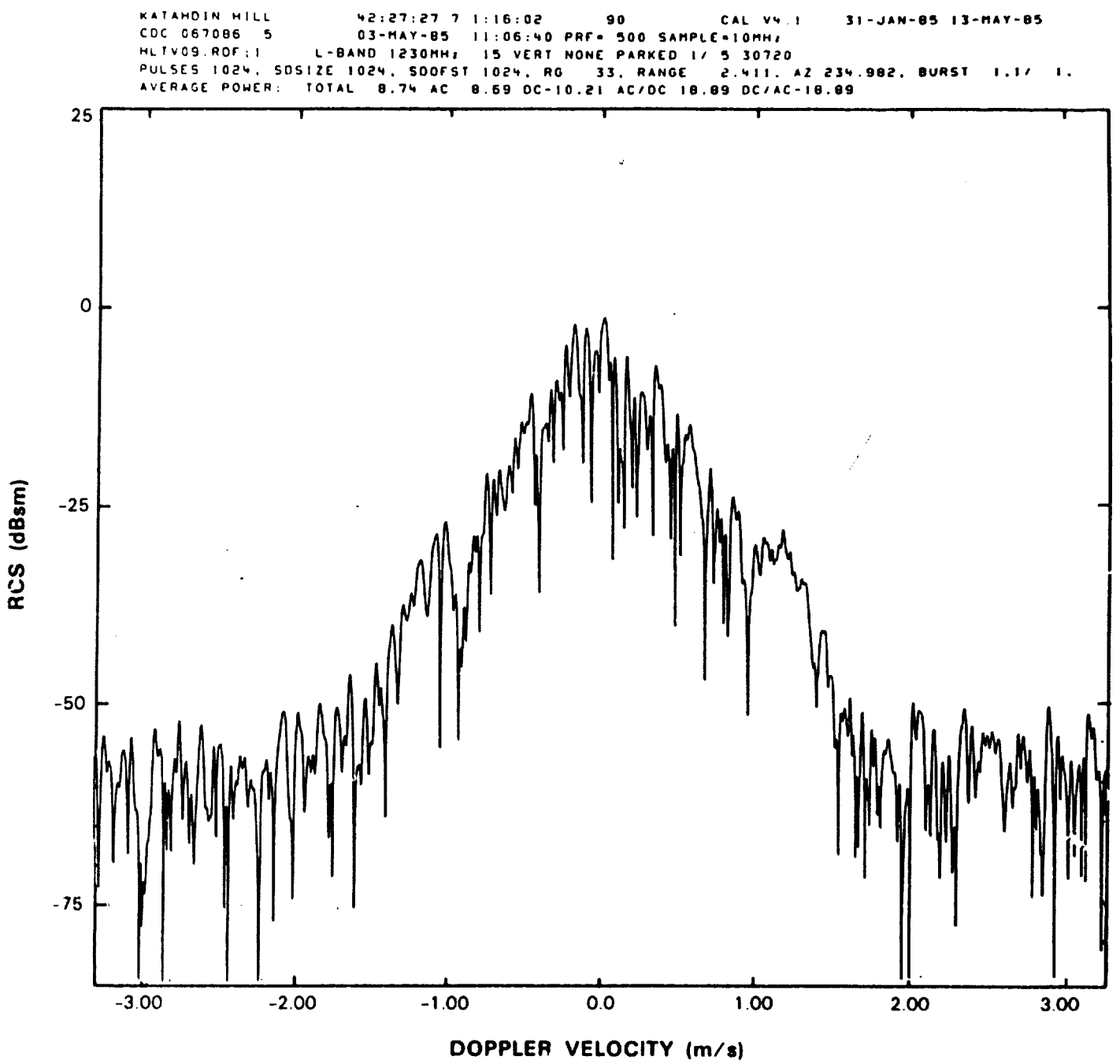

78005-22

FIG. A.24 INDIVIDUAL SPECTRUM FOR 21ST GROUP OF 1024 PULSES.

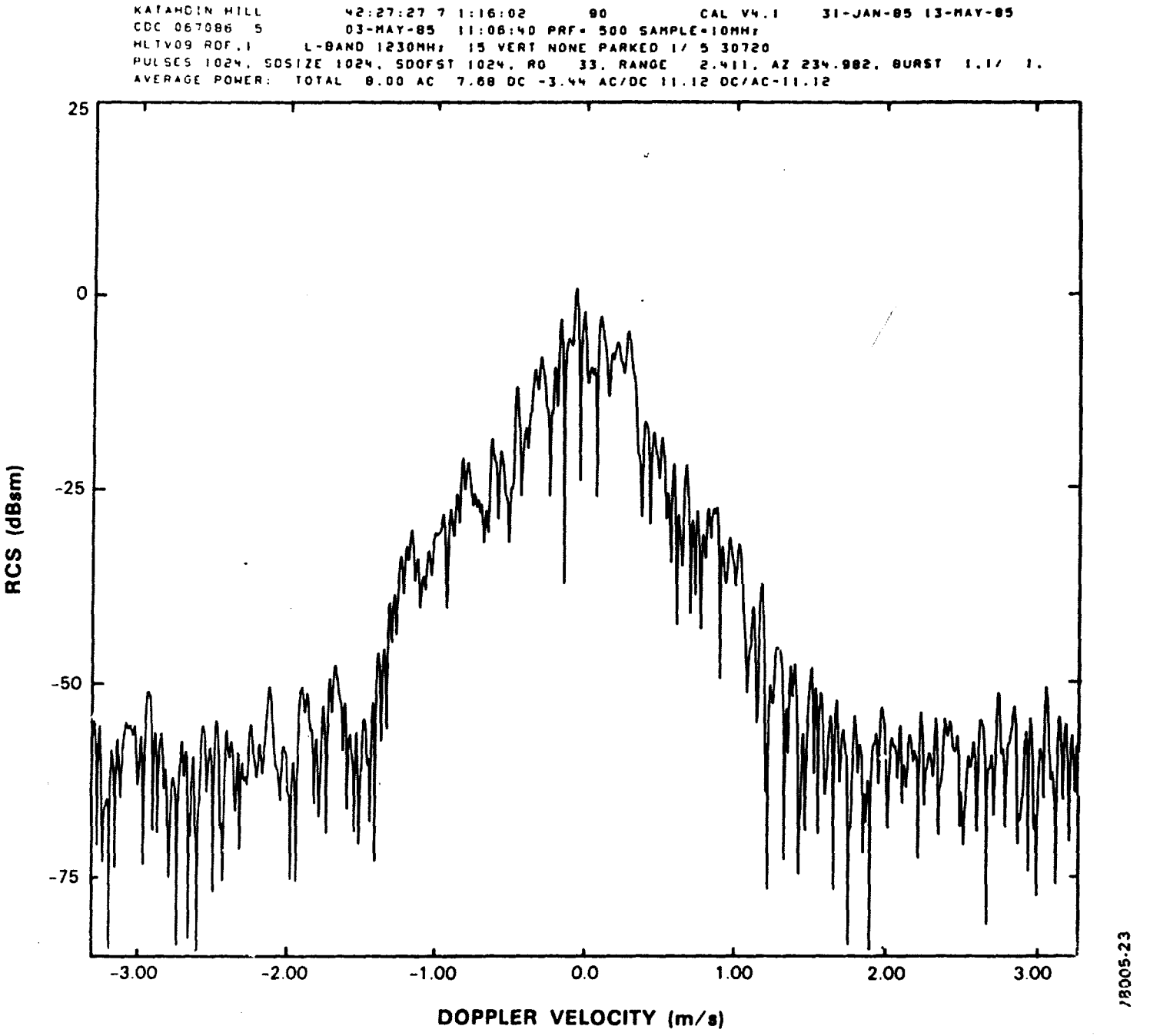

FIG. A.25 INDIVIDUAL SPECTRUM FOR 22ND GROUP OF 1024 PULSES.

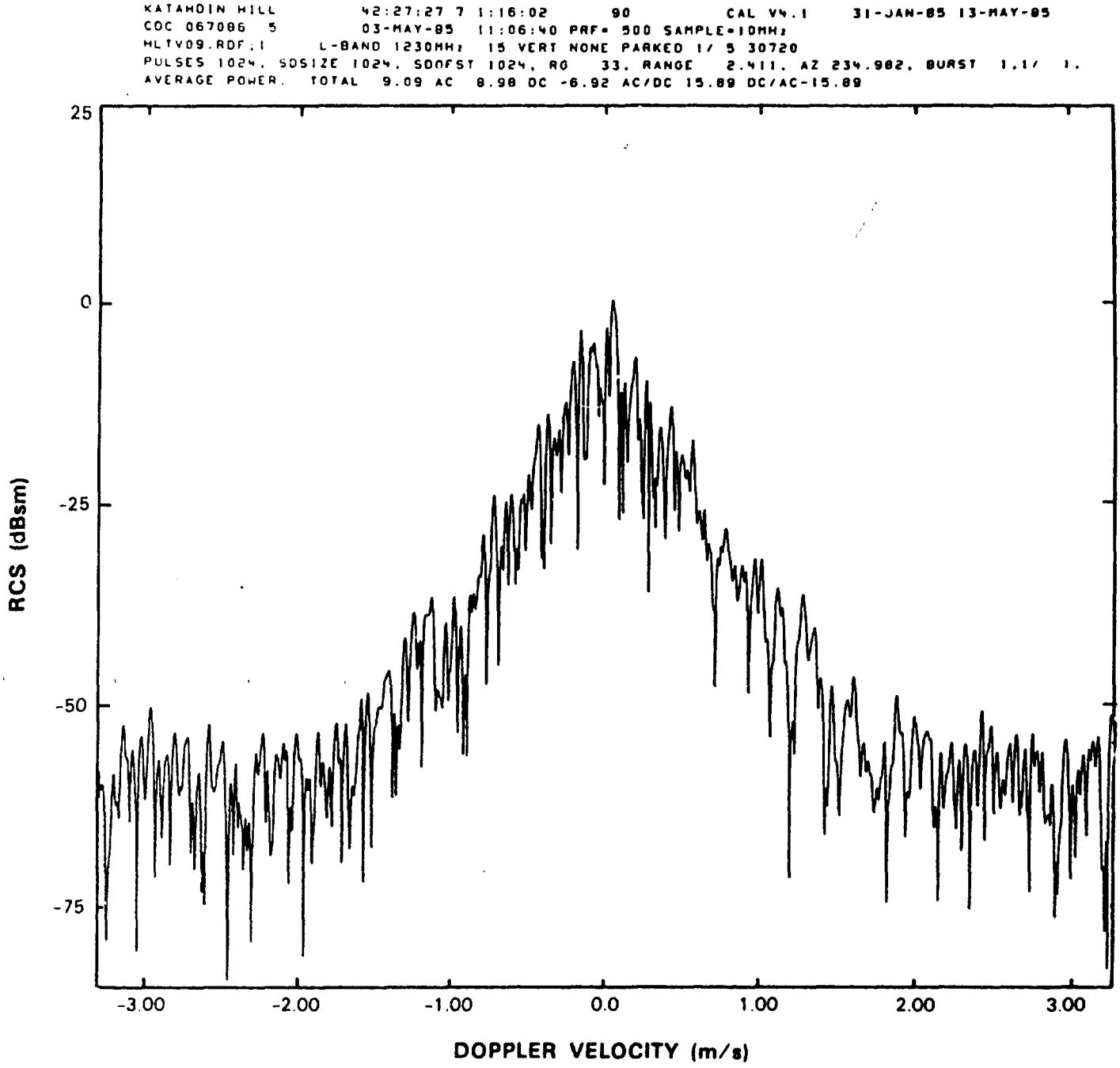

78005-24

FIG. A.26 INDIVIDUAL SPECTRUM FOR 23RD GROUP OF 1024 PULSES.

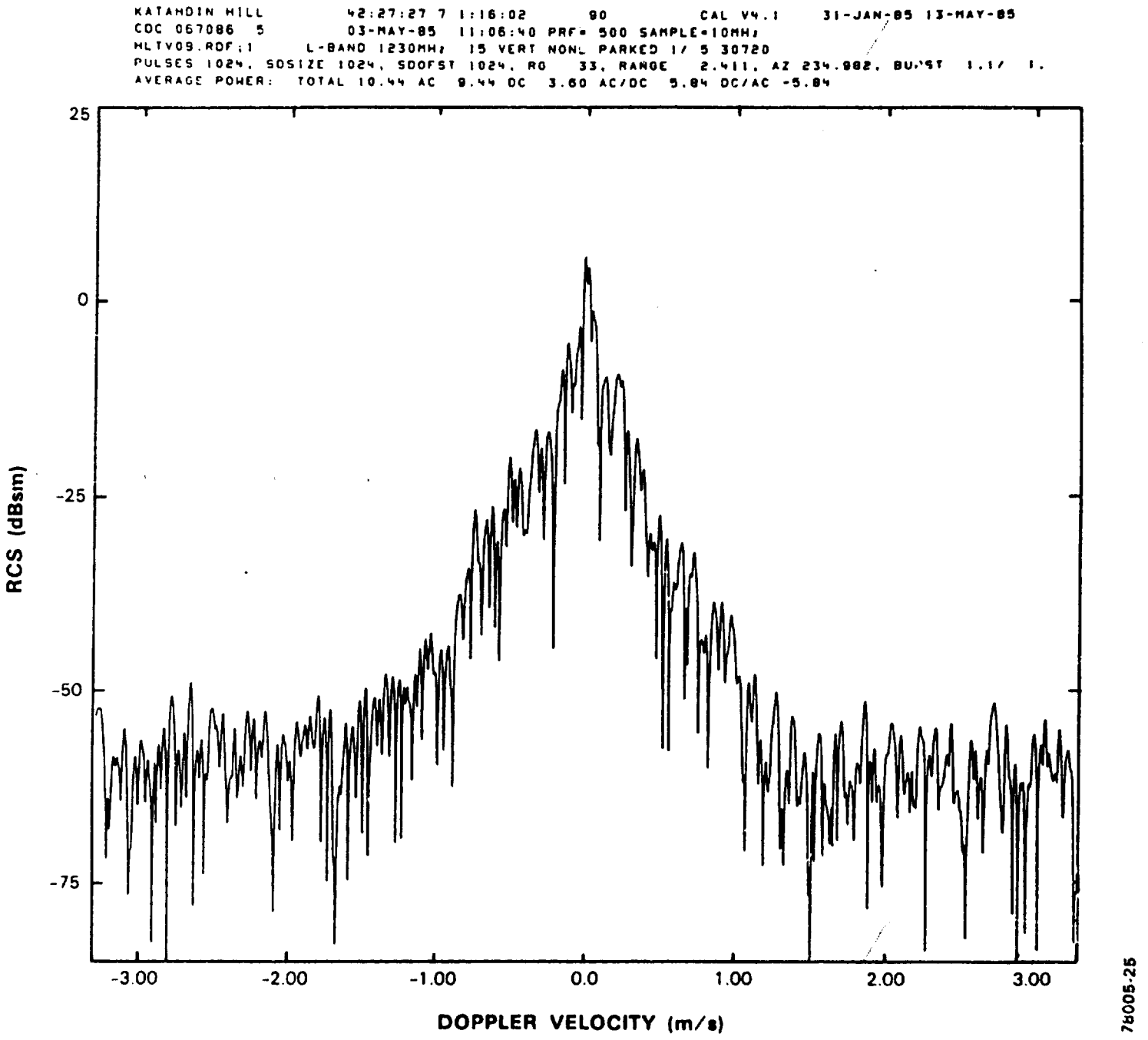

FIG. A.27 INDIVIDUAL SPECTRUM FOR 24TH GROUP OF 1024 PULSES.

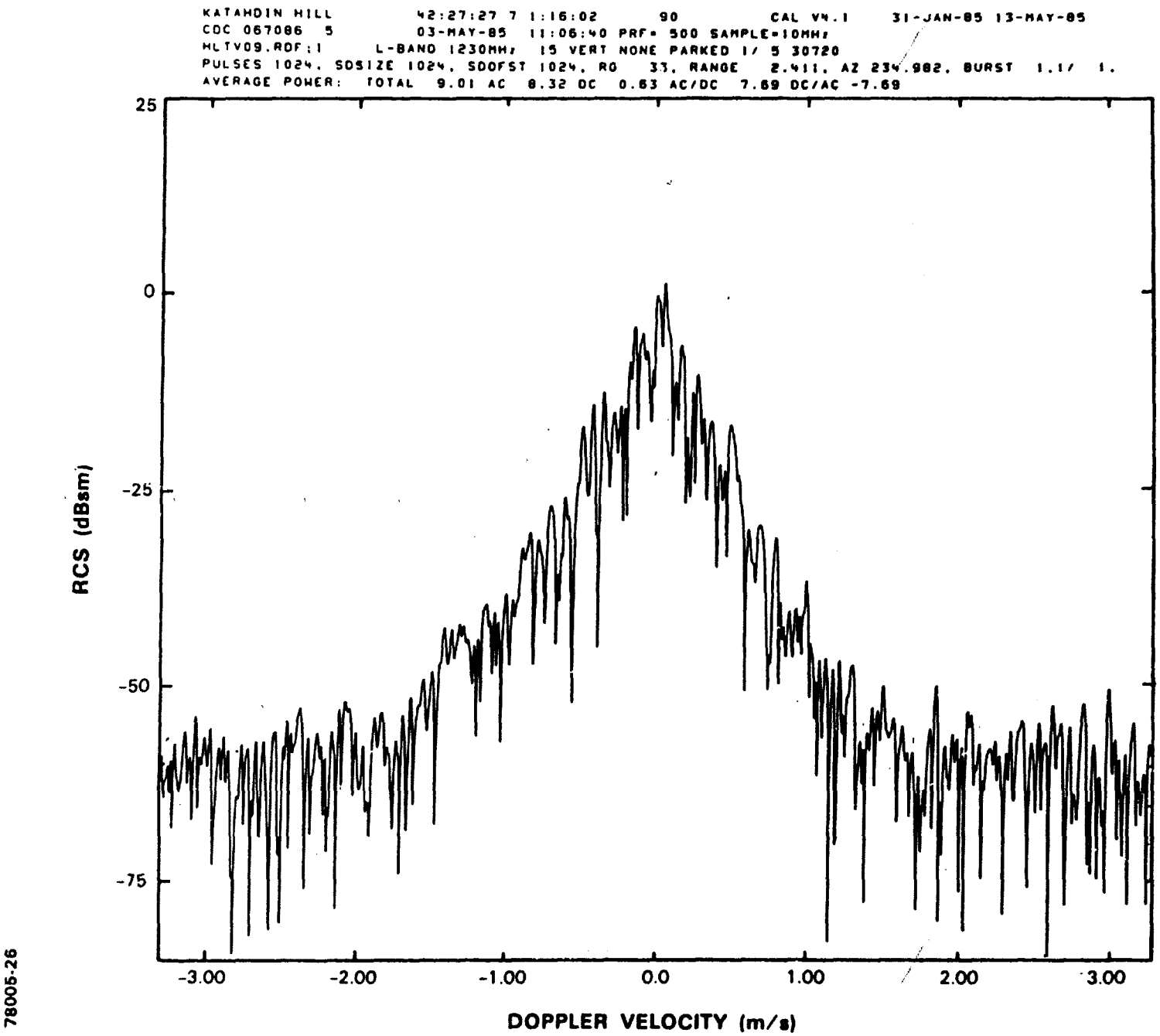

FIG. A.28 INDIVIDUAL SPECTRUM FOR 25TH GROUP OF 1024 PULSES.

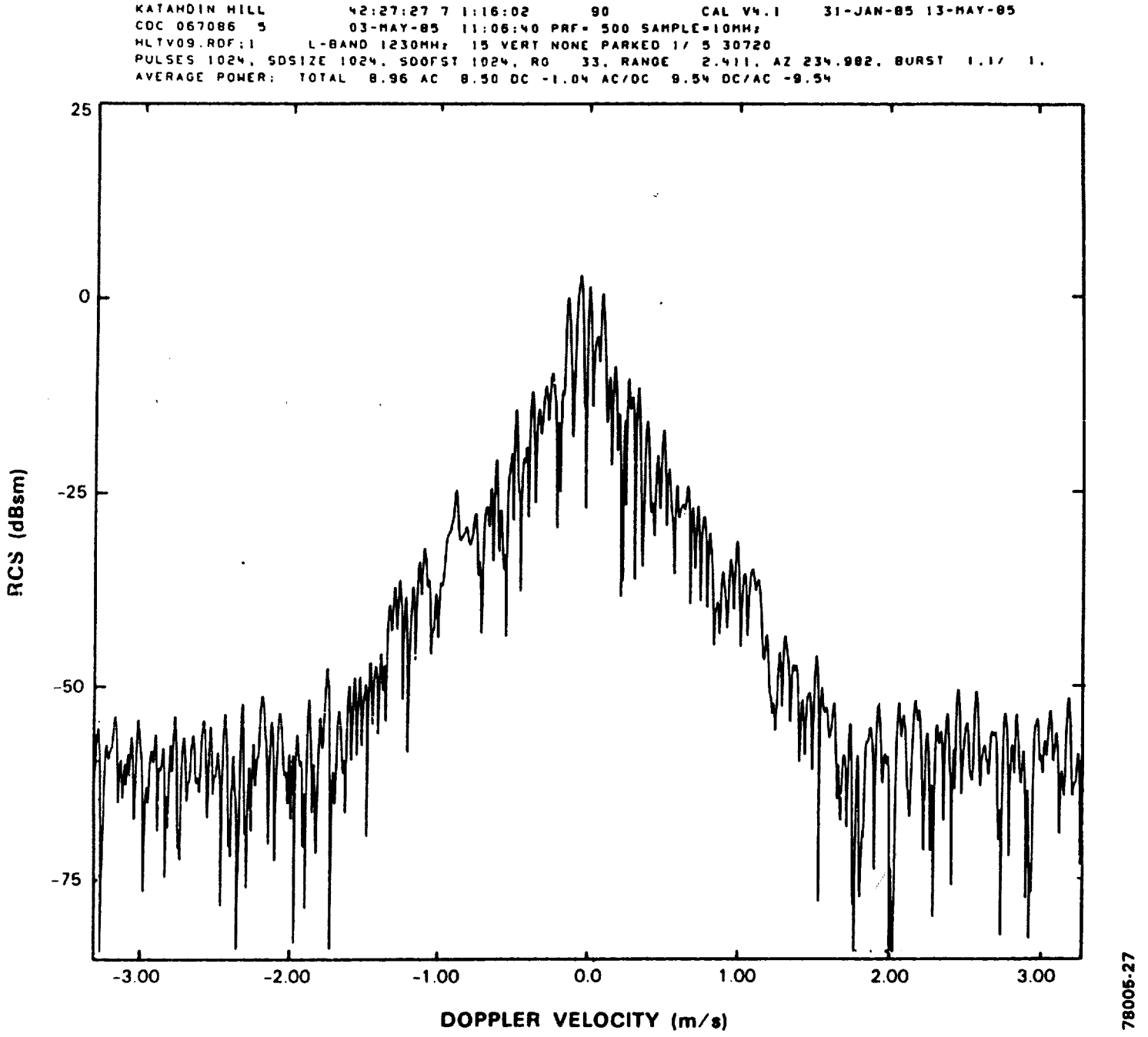

FIG. A.29 INDIVIDUAL SPECTRUM FOR 26TH GROUP OF 1024 PULSES.

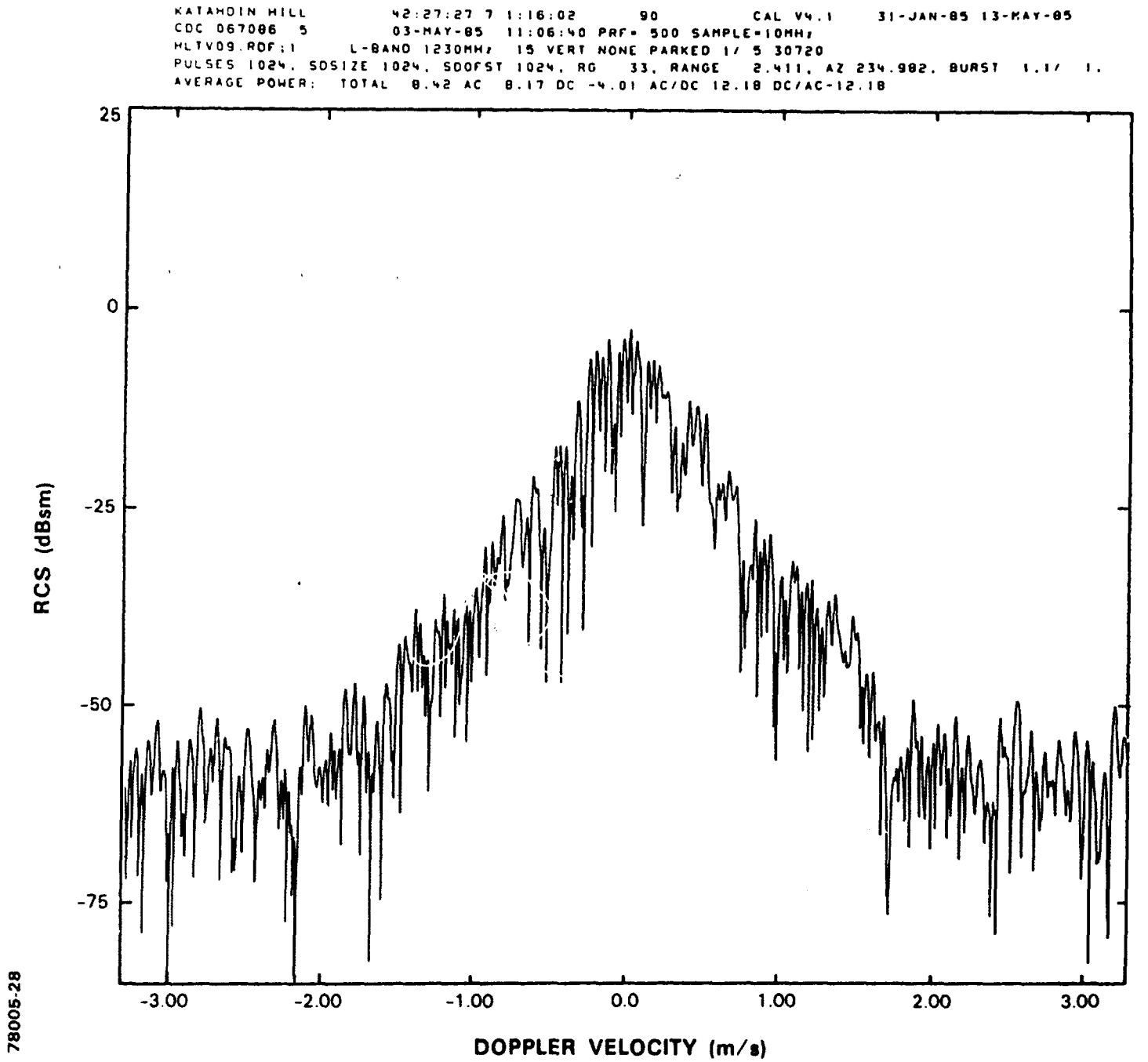

FIG. A.30 INDIVIDUAL SPECTRUM FOR 27TH GROUP OF 1024 PULSES.

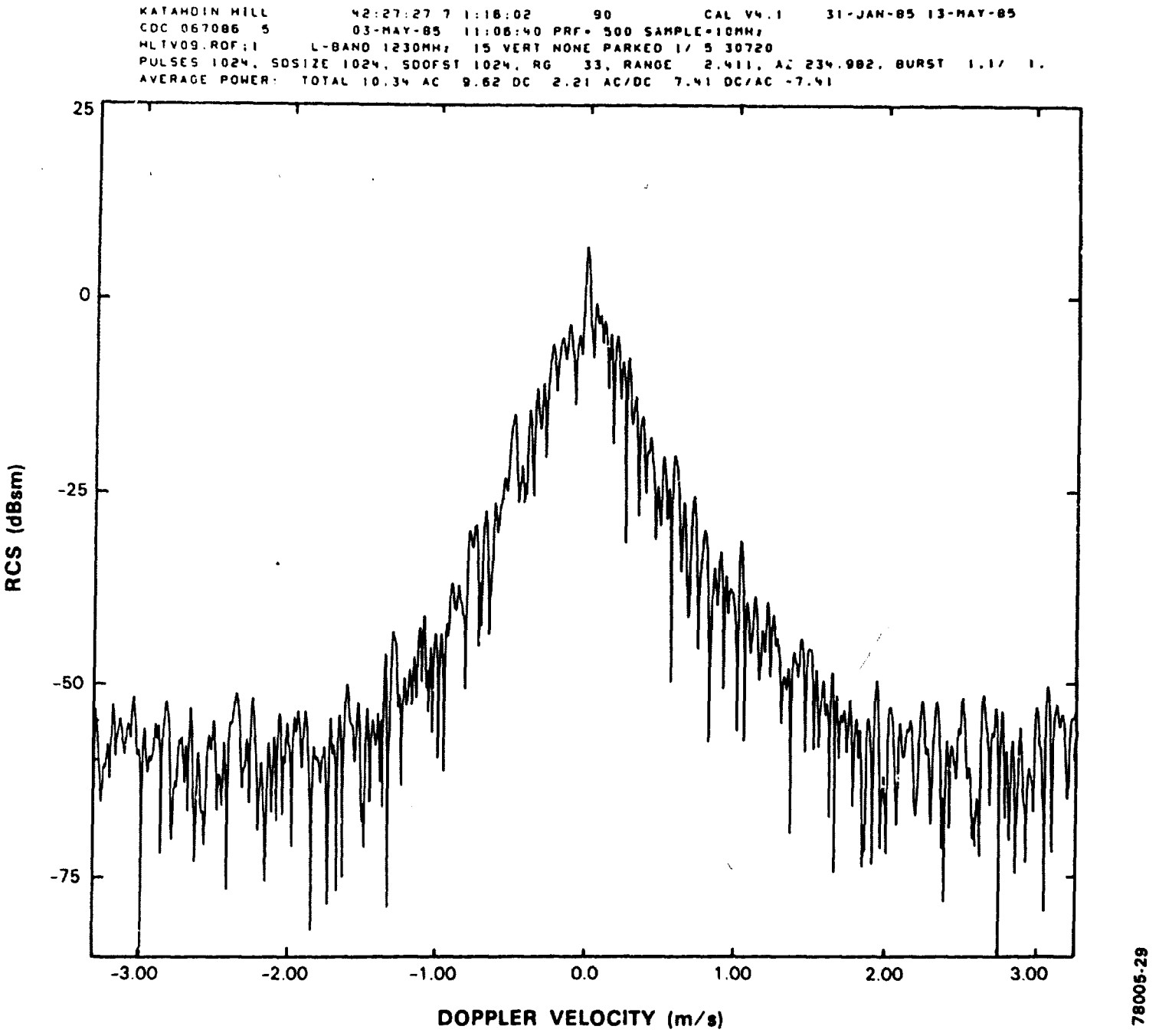

FIG. A.31 INDIVIDUAL SPECTRUM FOR 28TH GROUP OF 1024 PULSES.

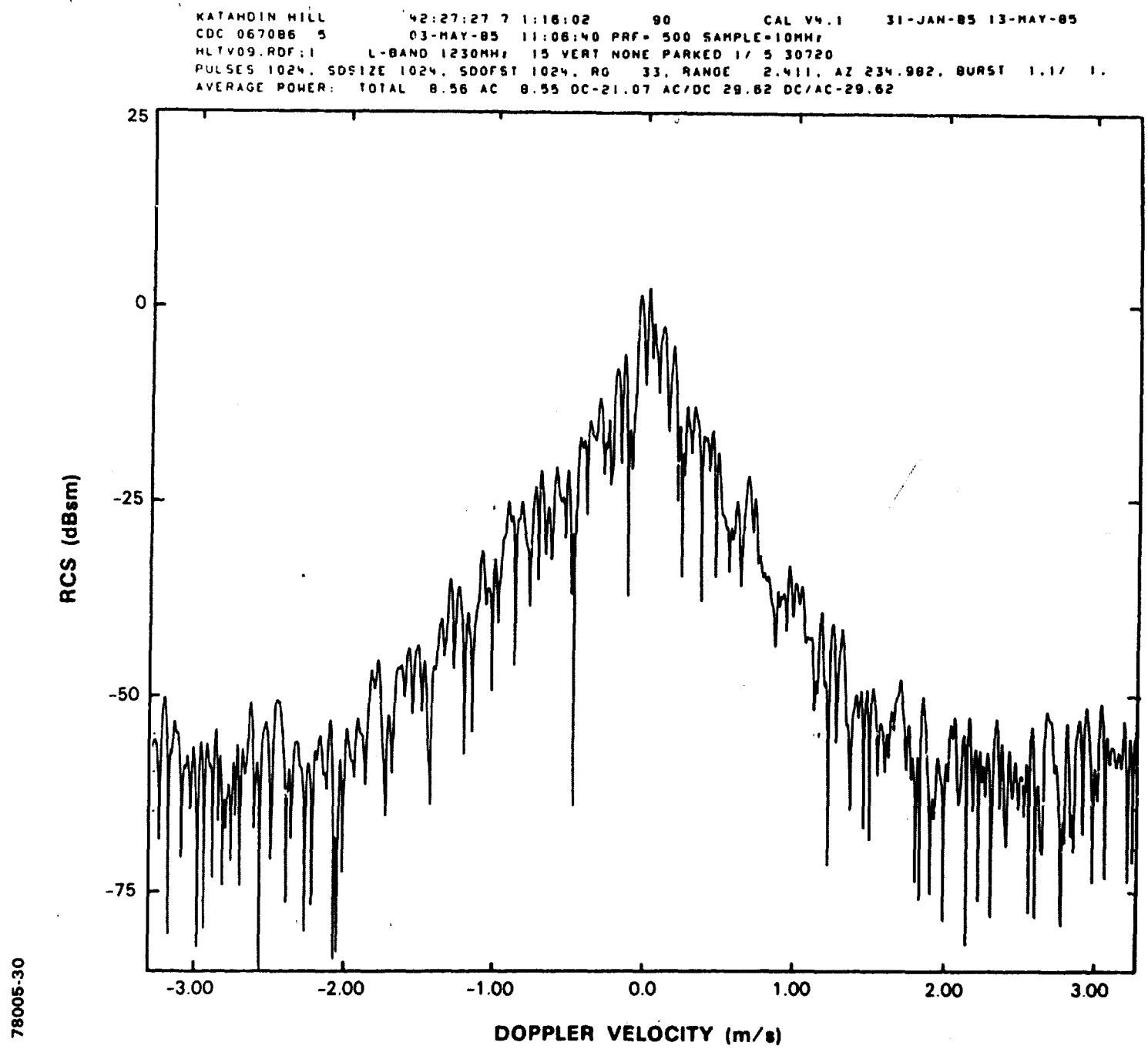

FIG. A.32 INDIVIDUAL SPECTRUM FOR 29TH GROUP OF 1024 PULSES.

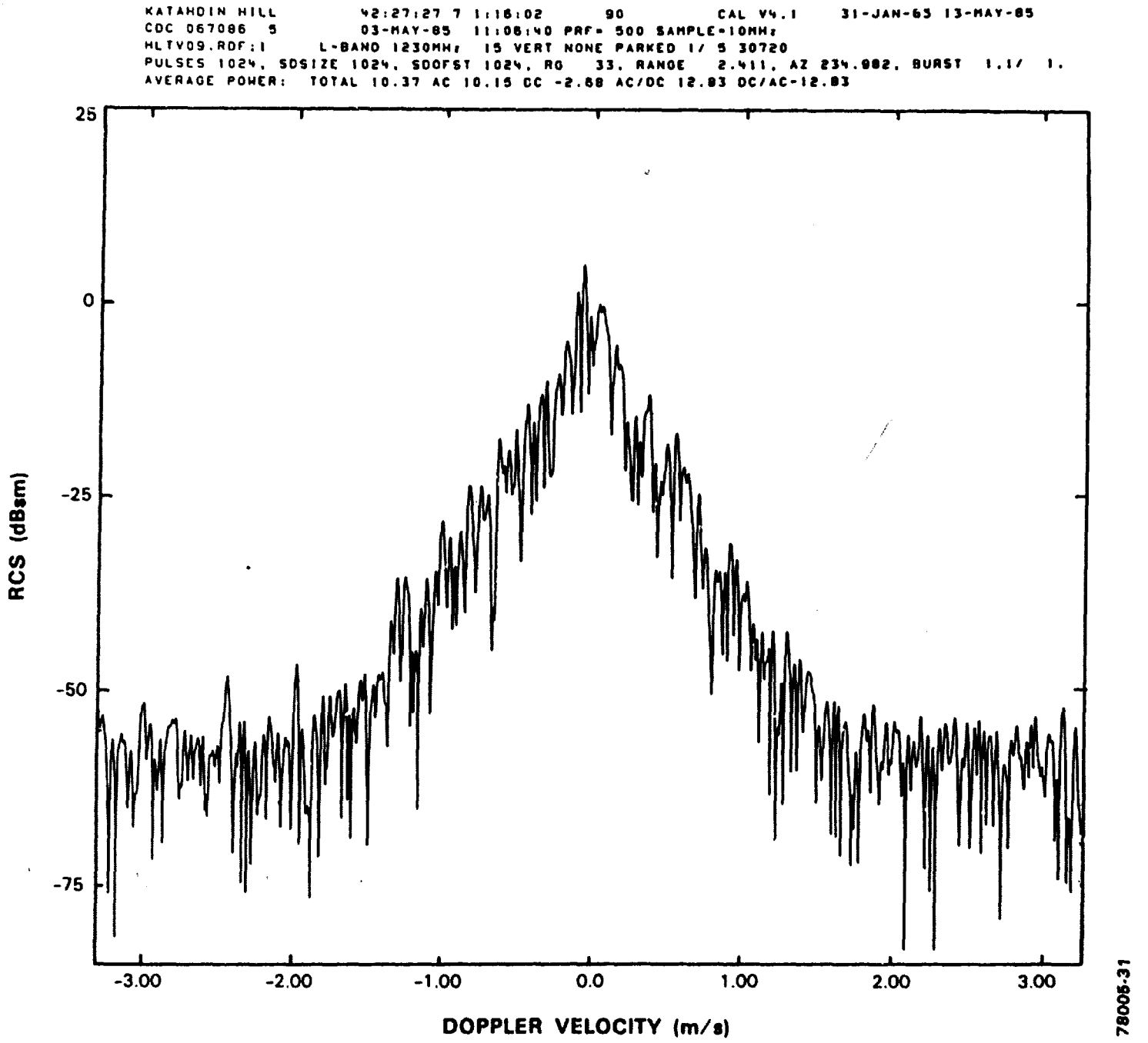

FIG. A.33 INDIVIDUAL SPECTRUM FOR 30TH GROUP OF 1024 PULSES.

ACKNOWLEDGEMENTS

Dr. Seichoong Chang performed an early investigation of ground clutter temporal and spatial correlation characteristics based on Phase One measurements. He has continued his involvement in this current work in a major advisory and consultative role. We cordially acknowledge his important contributions to this effort.

Many people were involved in computer program development and data editing activities throughout the course of this investigation, and we are very appreciative of all of their efforts. In particular, we are pleased to acknowledge Frank Groezinger's efforts in developing our spectral program capabilities, Cheryl Wesinger's work in carefully running the program and providing us with output, Anna Quinn's development of our time history program, and Ken Gregson's daily involvement in overseeing all of these computer related activities.

We are also pleased to acknowledge the skillful typing of the report by Pat DeCuir, and the careful attention to detail by David DesRosiers in drawing many of its figures.

REFERENCES

1. Charles M. Rader, "An Improved Algorithm for High-Speed Autocorrelation with Applications to Spectral Estimation," IEEE Trans. Audio Electroacoustic., vol. AU-18, pp. 439-441, Dec. 1970.

2. V. A. Andrianov, N. A. Armand, and I. N. Kibardina, "Scattering of Radio Waves by an Underlying Surface Covered with Vegetation," Radio Eng. and Electron. Physics (USSR), vol. 21, no. 9, September 1976.

3. Lawrence R. Rabiner and Bernard Gold, Theory and Application of Digital Signal Processing, Prentice-Hall, Inc., Englewood Cliffs, New Jersey, 1975.

4. Fredric J. Harris, "On the Use of Windows for Harmonic Analysis with the Discrete Fourier Transform," Proc. IEEE, vol. 66, no. 1, pp. 51-83, January 1978.

UNCLASSIFIED

SECURITY CLASSIFICATION OF THIS PAGE *(When Data Entered)*

REPORT DOCUMENTATION PAGE		READ INSTRUCTIONS BEFORE COMPLETING FORM
1. REPORT NUMBER ESD-TR-86-153	2. GOVT ACCESSION NO. AD-A179 942	3. RECIPIENT'S CATALOG NUMBER
4. TITLE *(and Subtitle)* Measured Spectral Extent of L- and X-Band Radar Reflections from Wind-Blown Trees		5. TYPE OF REPORT & PERIOD COVERED Project Report 6. PERFORMING ORG. REPORT NUMBER CMT-57
7. AUTHOR(s) J. Barrie Billingsley and John F. Larrabee		8. CONTRACT OR GRANT NUMBER(s) F19628-85-C-0002
9. PERFORMING ORGANIZATION NAME AND ADDRESS Lincoln Laboratory, MIT P.O. Box 73 Lexington, MA 02173-0073		10. PROGRAM ELEMENT, PROJECT, TASK AREA & WORK UNIT NUMBERS Program Element Nos. 62301E and 63003F
11. CONTROLLING OFFICE NAME AND ADDRESS Defense Advanced Research Projects Agency 1400 Wilson Boulevard Arlington, VA 22209		12. REPORT DATE 6 February 1987 13. NUMBER OF PAGES 112
14. MONITORING AGENCY NAME & ADDRESS *(if different from Controlling Office)* Electronic Systems Division Hanscom AFB, MA 01731		15. SECURITY CLASS. *(of this Report)* Unclassified 15a. DECLASSIFICATION DOWNGRADING SCHEDULE

16. DISTRIBUTION STATEMENT *(of this Report)*

Approved for public release; distribution unlimited.

17. DISTRIBUTION STATEMENT *(of the abstract entered in Block 20, if different from Report)*

18. SUPPLEMENTARY NOTES

19. KEY WORDS *(Continue on reverse side if necessary and identify by block number)*

radar ground clutter measurements
power spectra from wind-blown trees
temporal clutter measurements
L-Band
X-Band

20. ABSTRACT *(Continue on reverse side if necessary and identify by block number)*

Measurements of the spectral content of L- and X-band radar reflections from several resolution cells containing wind-blown trees are examined under a wide variety of typical wind conditions. Most of the discernible energy (i.e. within 60 dB of the peak zero-Doppler level) occurs in the spectra at Doppler velocities ususally less than 1.0 m/s, or at most 2.0 m/s on very windy days. The rates of decay of energy with increasing Doppler velocity in the tails of the spectral distributions at spectral off-sets well removed from zero often appear to be approximetely exponential. Estimates of rates of exponential decay in the spectral tails as a function of windspeed are provided in three regimes of windspeed.

DD FORM 1473 1 Jan 73 EDITION OF 1 NOV 65 IS OBSOLETE

UNCLASSIFIED

SECURITY CLASSIFICATION OF THIS PAGE *(When Data Entered)*